GALAXY ANGULAR MOMENTUM

by

Laird Alan Thompson

A Dissertation Submitted to the Faculty of the

DEPARTMENT OF ASTRONOMY

In Partial Fulfillment of the Requirements
For the Degree of

DOCTOR OF PHILOSOPHY

In the Graduate College

THE UNIVERSITY OF ARIZONA

1 9 7 4

GALAXY ANGULAR MOMENTUM

by

Laird Alan Thompson

A Dissertation Submitted to the Faculty of the

DEPARTMENT OF ASTRONOMY

In Partial Fulfillment of the Requirements
For the Degree of

DOCTOR OF PHILOSOPHY

In the Graduate College

THE UNIVERSITY OF ARIZONA

1 9 7 4

THE UNIVERSITY OF ARIZONA

GRADUATE COLLEGE

I hereby recommend that this dissertation prepared under my direction by Laird Alan Thompson

entitled Galaxy Angular Momentum

be accepted as fulfilling the dissertation requirement of the degree of Doctor of Philosophy

Dissertation Director — Date: Nov 4, 1974

After inspection of the final copy of the dissertation, the following members of the Final Examination Committee concur in its approval and recommend its acceptance:*

	Nov 4, 1974
P. A. Strittmatter	"
William J. Cocke	Nov. 5, 1974
	Nov. 5, 1974
T. D. Kinman	Nov. 27, 1974

*This approval and acceptance is contingent on the candidate's adequate performance and defense of this dissertation at the final oral examination. The inclusion of this sheet bound into the library copy of the dissertation is evidence of satisfactory performance at the final examination.

STATEMENT BY AUTHOR

This dissertation has been submitted in partial fulfillment of requirements for an advanced degree at The University of Arizona and is deposited in the University Library to be made available to borrowers under the rules of the Library.

Brief quotations from this dissertation are allowable without special permission, provided that accurate acknowledgment of source is made. Requests for permission for extended quotation from or reproduction of this manuscript in whole or in part may be granted by the head of the major department or the Dean of the Graduate College when in his judgment the proposed use of the material is in the interests of scholarship. In all other instances, however, permission must be obtained from the author.

SIGNED: Laird Alan Thompson

ACKNOWLEDGMENTS

I am grateful to the following individuals for providing me with some measure of assistance during the course of this dissertation analysis: Dr. H. Arp, Dr. J. Harvey, C. Jewsbury, Dr. P.J.E. Peebles, R. Schiff, and S.P. Worden.

I would like to thank the members of my dissertation committee for carefully and critically reading the original version of this work.

And I would like to acknowledge Dr. G.O. Abell for originally stimulating my interest in extragalactic astronomy while I was a student at U.C.L.A. and my graduate advisor Dr. W.G. Tifft for his helpful assistance during the course of this dissertation work.

TABLE OF CONTENTS

TABLE OF CONTENTS--Continued

LIST OF ILLUSTRATIONS

LIST OF ILLUSTRATIONS--Continued

LIST OF TABLES

ABSTRACT

In order to test the theories which purport to explain the origin of galaxy angular momentum, this study presents new data for about 1000 individual galaxies in eight rich clusters. The clusters which are studied include Virgo, A 119, A 400, A 1656 (Coma), A 2147, A 2151 (Hercules), A 2197, and A 2199. Selected samples of these data are used to investigate systematic alignment effects in clusters of galaxies and to investigate the intrinsic ellipticities of E, SO, and spiral galaxies. The following new results are reported:

1. Galaxies in the cluster A 2197 show a significant alignment effect (χ^2 probability < 0.0002), and the preferential direction of alignment corresponds approximately to the major axis of the overall cluster elongation. The galaxies in the core of the cluster are less significantly aligned, consistent with a model of slow dynamic reorientation in the dense cluster core.
2. None of the other seven clusters show any significant alignment trends; this includes A 2199, the cluster for which Rood and Sastry reported a marginal alignment effect (χ^2 probability $\simeq$ 0.02).
3. The spiral galaxy samples in four clusters (Virgo, A 1656, A 2151, and A 2197) were large enough to analyze the number distributions of forward and reverse winding spirals. Very balanced distributions were found in all four cases.

4. Large and small spiral galaxies have identical ellipticity distributions; this result implies that the angular momentum versus mass relation is $L \propto M^{5/3}$, consistent with results reported by Heidmann from rotation curve analyses of spiral galaxies.
5. Large E and SO galaxies tend to be more spherical, and small E and SO galaxies more flattened. For E galaxies the difference is small and might be caused by observational effects; for SO galaxies the difference is more pronounced, but might be caused by morphological classification uncertainties.
6. The intrinsic ellipticities of E, SO, and spiral galaxies are the same for galaxies in the "field" and for galaxies in rich clusters.

Six models of galaxy formation are reviewed, and the major emphasis is placed on how each model explains the origin of galaxy angular momentum. Of the six models it appears that the Peebles' model of tidal acceleration is the least consistent with the data. Two of the models are particularly successful in explaining all observations. These two models, one by Icke and the other by Sunyaev, Zeldovich and Doroskevich, are very similar and both start with a massive protocluster which later fragments into individual galaxies. The other models are less comprehensive and might be consistent with some aspects of the data.

CHAPTER I

INTRODUCTION

The natural philosopher Immanuel Kant was apparently the first person to understand the true extent and nature of the extragalactic universe. In his highly speculative Natural History and Theory of the Heavens of 1775, he not only realized that nebulae were giant star systems (galaxies) seen at a great distance, but he was bold enough to theorize that their origin and evolution followed from Isaac Newton's newly introduced theory of universal gravitation. Even though it took some 180 years to establish that these nebulae were actually extragalactic, today after nearly 220 years the exact nature of their origin and evolution has not been settled. One aspect of this latter problem, the origin of galaxy angular momentum, forms the subject of the present investigation.

A solution to the problem of the origin of galaxy angular momentum will involve fitting the predictions of theoretical models to the observational data. As the problem now stands the greatest portion of labor has been expended on the theoretical side, and in fact there are relatively few observational constraints for any of the models. Where constraints do exist, they depend on observations of the most general type (e.g., mean density of the universe, mean velocity dispersion among "field" galaxies, etc.), and in fitting these models to individual cases the only number specifically quoted is the total angular momentum of our

Milky Way galaxy. Satisfying these general constraints is necessarily of great importance, but to rely upon them exclusively might lead the analysis astray. In the particular case of galaxy formation in and around large density perturbations (i.e., clusters of galaxies), it is important to recognize that the usual cosmological assumptions of homogeneity and isotropy are generally not valid and that local variations are likely to produce important effects on the resulting galaxy angular momenta. The research presented in this dissertation is directed toward the problem of using observations to delineate "local" constraints for models which deal with the origin of galaxy angular momentum in and around rich clusters of galaxies. But before proceeding to that problem, it is important to understand what is known about galaxy angular momentum in general.

The Nature of Galaxy Angular Momentum

Using the simple observation that galaxies are flattened, ellipsoidal stellar systems, it seems natural to suspect that their characteristic shape results from a relaxed state of rotational equilibrium. In fact for the case of a star cluster where the time scale of dynamic relaxation is relatively short, King (1961) has shown that the ellipticity induced by systematic rotation of the star cluster matches the ellipticity of a rigidly rotating, constant density fluid body of equivalent rotational energy. Detailed observational studies of galaxy rotation are rather difficult to obtain, but one important result was reported by Crampin and Hoyle (1964). In an analysis of rotation curves from eight spiral galaxies, it was shown to within a

remarkable degree of accuracy that the rotational angular momentum distribution of each galaxy matches the distribution expected from a uniformly rotating spheroid of constant density. And the ellipticity of this uniformly rotation spheroid is very similar to the intrinsic ellipticity of the observed spiral galaxies ($\epsilon \simeq 7.5$). Because of problems associated with spectroscopy of low surface brightness galaxies rotation studies are available for only a small number of E and SO systems. In the only thorough study of an SO galaxy, Minkowski, Oort, van Houten, and Davis (1971) have shown that the general rotational charactreistics of NGC 3115 are very similar to the observed properties of spiral galaxies. The rotation curve indicates solid body rotation in the central region, a maximum rotational velocity of about 250 $km \cdot s^{-1}$, and following this peak a gradually decreasing rotational velocity indicative of Keplerian motion. Spectroscopic observations of elliptical galaxies provide information only for the high surface brightness nuclear regions. King and Minkowski (1966) and Morton and Chevalier (1973) report that four elliptical galaxies show some form of solid body rotation in thier central regions, but no information is available for rotation in the outer parts of these systems.

Even though the overall rotational properties of elliptical galaxies cannot be obtained directly from radial velocity observations, two indirect methods of analysis provide information on the relation between their angular momentum content and their observed flattening. The first method involves the construction of static numerical model galaxies. The models are static in the sense that the stellar velocity

distribution and overall gravitational potential remain constant in time. The stellar velocity distribution is taken to be Maxwellian leaving the model with two free parameters: the galaxy potential and the total galaxy angular momentum. These two parameters are adjusted to provide a fit to accurately observed elliptical galaxy luminosity profiles. This model is in some ways similar to the one used by King (1961) for analyzing the rotational flattening of star clusters. Successful fits to elliptical galaxies with reasonable values for the rotational angular momentum have been obtained by Prendergast and Tomer (1970). The second method of analysis involves the construction of non-static numerical model galaxies. Using N-body calculations these model galaxies are followed through a simulated gravitational collapse and violent relaxation. Collapsing axisymmetric models with reasonable amounts of initial angular momentum relax after a few crossing times into oblate spheroids with ellipticities directly dependent on the initial "protogalaxy" angular momentum. Four models constructed by Gott (1973), each with different amounts of initial angular momentum, produce relaxed star systems with final ellipticities ranging from 0 to 4.5. Unfortunately these models fail to predict the observed elliptical galaxy luminosity profile, but considering the idealized initial conditions (axisymmetry, sharply bounded initial distribution of mass points, uniform initial density) these deficiencies are perhaps understandable. One general conclusion can be drawn from the two different models described above, namely that the ellipticity of an E galaxy is directly related to its mean angular momentum.

Even though there is this general tendency for the intrinsic galaxy ellipticity to be related to the total galaxy angular momentum, the relation between these two quantities is not simply one to one. Two problems complicate their direct relationship. First, if the mass to light ratio changes over the volume of the galaxy in such a way that the most luminous material feels no gravitational interaction with an excessive amount of low luminosity material, then there is no reason to expect that the ellipticity (which is luminosity weighted) will be a good indicator of the angular momentum (which is mass weighted). Take for example a galaxy embedded in an extended low luminosity halo of the kind recently postulated to insure the stability of thin rotating disk galaxies. The intrinsic flattening of any observed and hence stable disk will give no information on the angular momentum content of the unobserved halo.[1] The second major complication is caused by the variation of intrinsic galaxy ellipticity with radius. For disk type galaxies (spirals and SO's) the effect results from a radial change in the relative contributions of the superposed spheroidal and disk components. Each component has its own ellipticity and radial intensity gradient, so the resulting superposition produces a gradual radial change from the ellipticity of the central spheroidal component to the

---

1. In this context it is interesting to speculate on the angular momentum content of these postulated halos. If our Galaxy is embedded in such a halo, then it seems natural to assume that its rotational properties would be quite similar to the properties of the observed halo component, namely the RR Lyrae stars and globular clusters. For these objects Kinman (1959) has shown that the angular momentum per unit mass of the observed halo component is identical to that of the disk component of the Galaxy.

ellipticity of the flattened disk. For E galaxies the cause of the observed ellipticity change is more subtle. According to detailed surface photometry for a fair number of Virgo Cluster galaxies (Liller 1960, 1966), the ellipticity change for E galaxies follows the same general trend as observed for the disk galaxies, but the changes are less drastic. The central ellipticity is generally the most circular, the ellipticity increases radially to some maximum value, and then it begins to become smaller in the outer low luminosity regions. The two theoretical models of E galaxies which were described above both show a tendency for a radially variable ellipticity. The static model of Prendergast and Tomer (1970) is particularly accurate in matching the observational trends described by Liller, but the theoretical results show an ellipticity change much more drastic than Liller observed. The differences between real galaxies and the models are probably caused by the idealized form of the model and by its incorrectly specified boundry conditions. Galaxies are not totally isolated from their surroundings, and the influences of these surroundings (e.g., tidal shears, infall of matter) were ignored by Prendergast and Tomer. Judged solely on the basis of the two complications described above, it is quite apparent that a fair amount of caution must be used in any attempt to interpret measurements of overall galaxy ellipticity in terms of total galaxy angular momentum.

Since our line of sight to any particular galaxy is fixed, it is impossible to determine observationally the intrinsic ellipticity of any single galaxy (or nearly impossible, cf. Denisyuk and Tumakova 1969).

The intrinsic ellipticity must be determined separately for each morphological type of galaxy by statistically analyzing a large set of each type under the assumption that all galaxies in each set are randomly oriented. For studies of galaxies located in rich clusters, it is very important and interesting in itself to insure that the angular momentum vectors are actually oriented at random and that they are not systematically aligned. The final section of Chapter IV presents a discussion of the most practical methods available for analyzing the orientation properties of galaxies located in rich clusters.

Galaxy angular momentum, like the angular momentum for any object in the universe, remains constant in the absence of external torques. Because our observations of galaxies are confined to the present epoch, it is essential to establish the relative importance of all torques which might disturb a galaxy's "primordial" angular momentum vector. Of primary importance are torques applied during close interactions between individual galaxies. The effect will be strongest in the cores of rich clusters since the frequency of galaxy-galaxy encounters depends strongly on the surrounding galaxy density. Another substantial contribution to the applied torque might come from the conglomerate gravitational influence of the massive cluster core or from the influence of individual supermassive galaxies. Other more violent physical processes might also change a galaxy's angular momentum. One possible process involves the ejection of matter out of galaxy nuclei (e.g., jet of M 87, filaments of NGC 1275, double radio source plasmons). Another violent process involves close disruptive encounters between galaxies. Because

these problems of angular momentum change have received little attention in the literature, the first section of Chapter V presents a brief discussion of their relative effects on galaxy angular momentum.

Theoretical Investigations into the Origin of Galaxy Angular Momentum

The origin of galaxy rotation is clearly tied to the process of galaxy formation. For a succinct review of the numerous contributions to the general field of galaxy formation see Layzer (1964). For the most part all models of galaxy formation can be placed in one of three general categories. In the first category are the gravitational collapse models; these models assume that the early universe was homogeneous and isotropic, and they rely on statistical or thermal perturbations to initiate some form of gravitational collapse. In the second category are the cosmological turbulence models; for these models isotropy and homogeneity are assumed to hold only on the largest scales, whereas the smallest scales are assumed to be in a state of isotropic turbulence. Those turbulent eddies which remain undamped produce density perturbations which initiate the gravitational collapse of galaxies. And the third category contains all other models; these are either models which might work but have not been fully developed, or else they are highly specialized models which rely upon ad hoc initial conditions. In either case the models of the third category are not easily tested with any observational data. Consequently the efforts of this dissertation research are directed toward testing the models in the first two categories. If none of these models fit the

observations, then it will be necessary to move on to the models in the third category.

According to the gravitational collapse models, the density perturbations grow as the universe expands. Whenever a specific perturbation becomes unstable to Jeans collapse, it separates from the uniformly expanding background. Galaxies are purported to gain angular momentum during the collapse process, and the exact mechanism involved depends upon the type of collapse envisioned. Peebles (1969, 1971a) treated the idealized case in which a spherically symmetric protogalaxy collapses in the viscinity of other protogalaxies (which he treats as mass points). During the collapse process angular momentum is transfered from relative protogalaxy "orbital" motion to the rotational motion of individual protogalaxies. The spin-up process involves torques which are applied to a tidally distorted protogalaxies by neighboring "mass points". Another variation was envisioned by Silk and Lea (1973). In their model inelastic collisions between massive gas clouds produce a set of slowly growing mass aglomerations. The final masses of these objects are comparable to the present day masses of individual galaxies. Angular momentum is transfered to these objects during the inelastic collision process. Another set of gravitational collapse models proceeds on the basis that very massive objects (with masses between 10^{15} and $10^{16}\,\mathcal{M}_{\odot}$) collapse first, and in the process of their collapse they fragment into galaxy-sized masses. Sunyaev and Zeldovich (1972) have followed the scenario of a rotating oblate spheroid which collapses into a very thin disk, and subsequently

fragments into individual galaxies. Galaxy rotation is produced during the turbulent collapse of the disk.

The second class of models rely upon turbulent eddies to initiate the gravitational collapse of galaxy-sized masses, and the rotational motion of these eddies naturally explains the rotational motion of the resulting galaxies. The general ideas behind this model were outlined by von Weizsacker (1951), but subsequently objections were raised since the proposed turbulent motions are quickly damped by viscous friction. Recently these models have been revived by the proposals of Ozernoi, Chernin, and their co-workers. They propose that the turbulence is driven during the radiation era by instabilities of a plasma-linked photon gas. Even this type of turbulence is subject to strong damping, and the basis of the recently revived work is still in question. For a general review of the work by Ozernoi and associates see Dallaporta and Lucchin (1972). Jones (1973) presents a very critical analysis of the cosmic turbulence models, and a partial reply to the criticism is given by Harrison (1973). In a third model Icke (1973) proposes that a massive prolate spheroid (mass between 10^{12} and $10^{14} m_\odot$) becomes unstable to gravitational collapse because of large scale turbulent motions, and this massive cloud then collapses and fragments into galaxy-sized masses. In this case the fragmentation process is caused by turbulent motion within the collapsing spheroidal cloud. The second part of Chapter V contains a more detailed discussion of both the cosmic turbulence models and the gravitational collapse models, along with their observational predictions regarding galaxy angular momentum.

Previous Observational Investigations

Three different types of observational data can be used to study galaxy angular momentum. Two of these, galaxy ellipticity and orientation, are used exclusively in this dissertation research. The third type of data are taken from galaxy rotation curves; the rotation curves are of course very informative but difficult and tedious to obtain. Before reviewing galaxy ellipticity and orientation studies, a brief discussion will be given of the results obtained from galaxy rotation curves. The most extensive set of optical data on galaxy rotation was collected by Burbidge and Burbidge (1968), and this optical data is now being supplemented by 21 cm radio observations. The data have been analyzed by a number of workers, and the important results of Crampin and Hoyle (1964) were mentioned above. Their result, that the observations are consistant with the implication that galaxies condensed with little turbulent mixing from uniformly rotating clouds, was also supported in a similar analysis by Innanen (1966). Saslaw (1970, 1971) analyzed data from the central solid body rotation regions of Sb and Sc galaxies and found a relation between the extent of this region and its rate of rotation. Using this result he was able to place an upper limit of a few hundred $km \cdot s^{-1}$ on the turbulent motions which might have once existed in the central regions of these galaxies. Finally N. Heidmann (1969), using observations of spiral galaxies, found that a spiral galaxy's angular momentum L is related to its mass M by the relation $L \propto M^{5/3}$. All of these results are important constraints to any model purporting to explain the origin of galaxy rotation.

All early studies of galaxy ellipticity were reviewed by de Vaucouleurs (1959b). Included in this review are data from Hubble (1926), Reinmuth (1926), and Holmberg (1946), plus additional data from de Vaucouleurs' (1956) Mount Stromlo study. From this analysis it was possible for de Vaucouleurs to obtain the general distribution of ellipticity for spiral and elliptical galaxies, but the data for S0 galaxies was much too sparce for any firm conclusions to be drawn. In order to fill the S0 deficiency Sandage, Freeman, and Stokes (1970) repeated the entire analysis using data from the Bright Galaxy Catalogue of de Vaucouleurs and de Vaucouleurs (1964). The Sandage et al. results are probably the best that are currently available, but their study suffers from two major deficiencies. First, measuring problems exist in the ellipticities which are listed in the Bright Galaxy Catalogue (cf. Sandage et al. 1970). Second, the galaxy sample was haphazardly chosen in a physical sense. Although the analysis is restricted to those galaxies listed in the Shapley-Ames Catalogue (1932), this sample includes many Virgo Cluster galaxies along with local "field" galaxies and galaxies located in small groups. In another study of galaxy ellipticity Rood and Sastry (1967) review the evidence for a possible relation between the size and ellipticity of E type galaxies. Using data for E galaxies from the Bright Galaxy Catalogue and from the Rood and Baum (1967) Coma Cluster study, they conclude (contrary to Edelen 1965) that the ellipticity and diameter are not related to one another for E type galaxies. In detailed studies of the two clusters A 1656 (Coma) and A 2199, Rood and Baum (1967) and Rood and Sastry (1972)

include analyses of galaxy ellipticity. The results for the core of the Coma Cluster appear to conform quite well to the results expected from the Sandage et al. analysis, but the results for A 2199 seem to be very erratic. Both of these clusters are also included in the present dissertation analysis. A short note should be added to recognize the work of Gorbachev (1970). He used the Rood and Baum (1967) data for the core of the Coma Cluster to study the area distribution of galaxies with different ellipticities. Although he shows evidence for some very important trends, the galaxy sample which he used (the very inner core of the Coma Cluster) covers such a small area of the cluster that significant radial changes are nearly impossible to detect.

Studies of galaxy orientation can be divided into two groups: those dealing with random samples of field galaxies, and those dealing with specific cluster samples. The field galaxy data were collected almost entirely by Brown (1939, 1964, 1968, also Wyatt and Brown 1955). Significantly non-random alignment effects were reported for the Horologium region (Brown 1939) and also for the Cetus region (Wyatt and Brown 1955). Both of these areas have been re-examined by other workers. The Cetus region was remeasured by Kristian (1967), and a small portion of the Horologium region was remeasured by Reaves (1958); the alignment effect was not confirmed in either case. Systematic measuring errors might be responsible for these discrepancies. For a succinct but somewhat questionable review of Brown's work see Reinhardt (1972). All of Brown's field galaxy data were globally analyzed by Reinhardt and Roberts (1972) in an attempt to find a relation between galaxy orientation and the equator of the local supercluster (de Vaucouleurs 1960);

a marginally significant relation was found. A similar global analysis was carried out by Holmberg (1946). He too found a slight preferential orientation effect, but the relation between Holmberg's results and the Reinhardt-Roberts results are not clear. Galaxy orientation studies are available for only a small number of rich galaxy clusters. Kristian (1967) presented data for six rich Abell clusters, and no systematic effects were found. Similarly the Rood and Baum (1967) Coma Cluster study showed a smooth (i.e., random) distribution of galaxy position angles. Rood and Sastry (1972) report a marginal position angle alignment effect for the rich cluster A 2199 (χ^2 probability for nonrandomness = 97.5%). Since A 2199 is one of the rich clusters included in the present investigation, this result is checked in the analysis below. And finally Gainullina and Roshjakova (1967) have reported that a certain fraction of the galaxies in the rich clusters A 1656 and A 2065 tend to be aligned in the sense that their major axes are directed toward the center of the cluster.

Cluster Approach

For three major reasons the present analysis is restricted to analyzing galaxies in rich clusters. The first reason is one of observational convenience. Galaxy clusters provide a large sample of nearly equal sized galaxies closely concentrated into a small area of the sky. A single photographic plate of each cluster provides an equivalent set of images for the individual galaxies in each cluster. Troubles with changing plate sensitivity (or spectral response) are thereby avoided, and the analysis can rely upon the accuracy of plate

limited isophotal galaxy diameters and ellipticities. One of the eight clusters included in the current sample is the Virgo Cluster. Even though its large angular diameter (about 12^{o}) makes it impossible to study on a single Sky Survey plate, the Virgo Cluster was included in the analysis for other reasons.

Apart from the observational conveniences, there are two important physical reasons for restricting the galaxy sample to rich clusters. First, differences in the initial conditions and in the time of galaxy formation at a particular site might have a significant influence on the resulting galaxies. For example, marked changes of ellipticity might be expected between field galaxies and galaxies in rich clusters. By analyzing only cluster galaxies, it is possible to eliminate this field-cluster discrepancy, and it becomes possible to test for variations in the initial conditions from cluster to cluster. A cursory glance at the morphological differences between individual clusters (cf., Abell 1965) shows that this cluster comparison technique might hold a great deal of interesting information. The second physical reason for restricting the analysis to rich clusters comes about because of the statistical nature of galaxy formation. The Sandage, Freeman, and Stokes (1970) analysis indicated that all types of galaxies have fairly broad distributions of intrinsic ellipticity. If these broad distributions are produced by the processes involved in the origin of galaxy angular momentum, then it is important to know the exact form of these distributions and how their widths change from cluster to cluster.

Scope of this Project

A sample of eight rich galaxy clusters (Virgo, A 119, A 400, A 1656 (Coma), A 2147, A 2151 (Hercules), A 2197, A 2199) are included in this study. For an average sample of 100 to 150 galaxies in each cluster, data have been collected for galaxy position, morphological type, major axis diameter (face-on), ellipticity, major axis position angle, direction of spiral winding (wherever applicable), and estimated surface brightness. The galaxies which are included in the sample were selected on the basis of their apparent diameters, and the areas covered in this study are limited by cluster diameters derived from the observed cluster redshifts. The data, listed in catalogue form in Appendix I, are taken from the red plate copies of the National Geographic Palomar Sky Survey (from the collection of the Kitt Peak National Observatory). The galaxy major axis position angles and spiral winding directions are analyzed for systematic alignment effects in the eight individual clusters. The ellipticity data for each cluster are presented individually, and then a conglomerate analysis is presented for all of the data. The orientation and ellipticity data are then used to draw conclusions which relate to the origin of galaxy angular momentum.

The chapters which follow include (II) a discussion of the cluster sample, the procedures of the data collection, and application of Holmberg corrections, (III) a presentation and discussion of the galaxy orientation data, (IV) details of the galaxy ellipticity analysis, (V) a theoretical discussion of the origin and evolution of galaxy angular momentum, and finally (VI) an interpretation relating the theoretical and observational aspects of this problem.

CHAPTER II

OBSERVATIONAL DATA

All previous studies of galaxy ellipticity are based on inhomogeneous collections of data. This is especially true of the comprehensive Sandage, Freeman, and Stokes (1970) study which relied totally on measurements listed in the Reference Catalogue of Bright Galaxies by de Vaucouleurs and de Vaucouleurs (1964). The ellipticity data in the de Vaucouleurs' catalogue are taken from a somewhat random collection of plates and secondary references. In collecting the data for the present analysis, a careful effort was made to insure that the observations form a homogeneous sample in both a physical sense and in an observational sense. The following chapter is devoted to a three part discussion of the observational data. The first part briefly outlines the methods by which the cluster and galaxy samples were selected. The second part contains a discussion of the measuring procedures and the accuracy of the data. And the final section contains the details of the diameter and ellipticity correction procedures. For a brief description and tabular listing of the data, see Appendix I. Photographs of all but the Virgo Cluster are given in Appendix I, figures 14 - 20.

Cluster Sample and Galaxy Sample

In selecting the sample of eight clusters, the primary restrictions were determined by the Palomar Sky Survey plates. Since the

nearby clusters have fairly large angular diameters, many of them fall on two or more adjacent sky survey plates. In order to eliminate these multiple plate clusters, every Abell cluster with a measured redshift (Noonan 1973) was assigned an angular radius according to the following relation (cf., Sandage 1972a)

$$R = 90'' \frac{(1 + z)^2}{z}$$

which follows from the assumption that the cosmological constant is zero and that $q_o = +1$; z is of course the observed cluster redshift. This radius corresponds to a metric cluster diameter of approximately 3 Mpc. Comparing this radius with the cluster positions on the sky survey plates (as listed by Sastry and Rood 1971), a list was made of those Abell clusters which fall no closer than R to any boundry of their respective sky survey plate. Next, all clusters at galactic latitudes $|b^{II}| < 40^o$ were eliminated; this restriction makes it unnecessary to correct measured galaxy diameters for absorption effects produced by our own Galaxy. With twenty-five clusters remaining on the list, three additional considerations were used to reduce the sample to seven clusters (not including the Virgo Cluster): (1) the richer clusters were favored over the poorer ones, (2) clusters with smaller redshifts were favored over those with larger redshifts, and (3) where some choice was available an attempt was made to include a variety of cluster types as defined by Bautz and Morgan (1970) and Rood and Sastry (1971). The Virgo Cluster is the eighth member of the sample. Even though Virgo is so nearby that the galaxies are scattered over eight or nine sky survey

plates, this disadvantage is overcome by the relative ease with which each galaxy can be studied. The names and general properties of each cluster are summarized in Appendix I, table 9.

Within each cluster it was necessary to select a specific set of galaxies for detailed analysis. In the absence of galaxy photometry, the next best limiting parameter is face-on galaxy diameter. In order to obtain face-on diameters the apparent diameters must be corrected for projection (i.e., optical depth) effects; this procedure will be discussed in the final section of this chapter. If the diameters are properly corrected, a diameter limited sample should be just as well defined as a magnitude limited sample. This is justified by the fairly good correlation between galaxy luminosity and major axis diameter found by J. Heidmann (1969).

In order to determine the center for each cluster and to select the galaxy sample, it was necessary to survey each of the eight cluster fields to measure major axis diameters for all galaxies. These measurements (as well as all others described below) were made on the 103a-E Palomar Sky Survey plate; the survey diameters were made using a reticle micro-scale at a magnification of 6.7 X. It was found that the eight clusters contained a total of approximately 1000 galaxies with diameters greater than

$$D = \frac{7.5 \text{ kpc}}{h} = 0.\!\!^{\prime}50 \, \frac{(1+z)^2}{z} \qquad (2)$$

where h = Hubble's constant/ 100 $km \cdot s^{-1} \cdot Mpc^{-1}$. This value of D was adopted as the formal survey limit and only galaxies larger than D are included in the final sample. Using this survey data it was also

possible to determine to apparent center of every cluster. In Appendix I, table 10 the coordinates of each cluster center are listed with a brief description of the survey galaxy distribution. The final restriction on the galaxy sample requires that all galaxies fall within a distance R, from equation (1), of the newly defined cluster centers.

Measuring Procedures and Accuracy of the Data

The Kitt Peak National Observatory's two-coordinate measuring engine was used extensively for collecting a large fraction of the data listed in the Appendices. It is one of the few instruments which will accomodate the 14"x 14" glass plates, and it provides two convenient methods of inspecting galaxy images. The first consists of a simple projection system which displays an enlarged image of the plate on a ground glass screen. The system uses a Zeiss lens with a variable focal length allowing enlargements ranging from 10 times to 40 times. It was possible to mount a circular rotating scale immediately in front of this projection screen, and in order to measure each galaxy image the scale was rotated until the galaxy major axis lined up with one of the scales. By reading the angular orientation of the rotated scale, the galaxy's position angle was immediately known. Using the two coordinate movable stage, it was possible to shift the galaxy image relative to the measuring scale, allowing multiple settings and multiple measurements of each galaxy's major and minor axis. The second convenience provided by the Grant measuring machine is its ability to display (on a cathode ray tube) the photographic density profile of any image placed under either of its two perpendicular slits. This density profile display

was used to estimate the relative surface brightnesses of all galaxies in this survey (both maximum and average surface brightness are listed). The density profile was used to estimate each galaxy's surface brightness gradient, i.e., the rate at which the galaxy image fades into the plate background. This quantity is important in determining the proper Holmberg measuring corrections (discussed more fully below). The galaxy density profile trace can also be used to estimate galaxy morphological types. It became quite easy to recognize that a spiral or S0 galaxy nearly always would show a break in the density profile corresponding to the transition between the spherical component and the disk component. By simultaneously viewing the enlarged galaxy image and its density profile trace, it was very easy to accurately estimate galaxy morphological types (within the limits of the plate material). As a final point it should be mentioned that the Grant measuring engine is interfaced with a punch card output device; all the measurements of galaxy diameter, morphological type, etc. were numerically coded and then automatically punched onto computer cards for easy data reduction.

The Grant measuring engine was also used to measure accurate X, Y positions for every survey galaxy in the study. For each cluster the positions of 5 to 24 standard stars from the S.A.O. Star Catalogue (Whipple 1966) were measured along with the galaxies, and using the method of dependences (Konig 1962) the galaxies' X, Y positions were converted to right ascensions and declinations (epoch 1950.0). Appendix I table 4 lists the standard stars used for each cluster. By intercomparing the relative positions of the S.A.O. standard stars,

the accuracy of these galaxy positions are estimated to be better than ± 1.0 arc second (1σ). The galaxy positions refer to the nucleus or to the centroid of the galaxy's image on the red Palomar Sky Survey plate. Virgo Cluster galaxies were not measured because a sufficiently accurate set of positions are given by Zwicky and Herzog (1963).

To reduce the errors in all measurements of galaxy major axis, minor axis, and position angle, two totally independent sets of data were collected for each cluster sample. In the first run the plate was oriented with the north-south direction appearing on the projection screen in the vertical direction. For the second run the plate was placed in a new orientation with the north-south line 112° from the vertical. This angle was chosen so that systematic position angle measuring effects would cancel out in the average to the two independent measures. There have been numerous suggestions that a physiological bias is incorporated in any position angle measurement (Hawley and Peebles 1972, Opik 1968, Reinhardt 1972). The preferential bias generally occurs at angles which are multiples of 45°. The 112° plate rotation was chosen to cancel any systematic effect , and it appears to have been quite successful (cf., figure 2 in Chapter III). After completing the two measuring runs, the two sets of data were intercompared. If any galaxy's diameter or position angle measurements were highly discrepant, the galaxy was remeasured a third time. It was necessary to remeasure one or all three quantities for approximately 10% to 15% of the galaxies. The errors occurred almost invariably in position angle measurements of nearly circular galaxies or in the diameters

of galaxies with very flat density profiles. The estimated accuracy of the position angles depends on the galaxy ellipticity. For ellipticities greater than 5, the errors are no more that $\pm 2^{\circ}$ (1σ). For galaxies with ellipticities around 2, this error might increase to $\pm 6^{\circ}$ (1σ). The diameter measurements are not a critical part of this analysis, and more attention was given to the ellipticity measurements. For certain galaxies, the diameter measurements between the two runs might have differed by 10% to 15%, but the ellipticity (which depends on the ratio of the major and minor diameters) would change very little. The ellipticity errors were found to be $\approx \pm$ 0.2 (1σ), where the ellipticity ranges between 0 and 10. For the flatter galaxies, the ellipticity depends critically on the minor axis diameter. Consequently, for ellipticities greater than 7, the errors are generally $\approx \pm$ 0.4 (1σ).

As described above, galaxy morphological types were initially estimated from the enlarged galaxy images and the galaxy density profile. By using galaxy morphological types obtained from 200" plate material (Coma Cluster data published by Rood and Baum 1967, and Hercules Cluster data from a deeply exposed IIIa-J plate kindly loaned to me for an afternoon by Dr. H. Arp), it was found that for some galaxies the Palomar Sky Survey plate material was inadequate for determining accurate morphological types. In many cases individual galaxies could unequivocally be placed in a single class, but in other cases this was impossible. In order to accomodate this deficiency the following morphological classification system was adopted: E , E/S0, S0, S0/S, S , S/Irr, Pec. Galaxies were placed in the singular classes

only if they were definitely a member of that class. The intermediate classes were used for galaxies of less certain type.

Because galaxy morphological types have been traditionally estimated from blue sensitive plates, the morphological types were estimated a second time (after the initial Grant machine estimate) using both the red and blue plates on the Kitt Peak National Observatory's plate blink machine (at a magnification of 6.7 X). By consecutively viewing two images of the same galaxy, it is possible to visually eliminate many plate grain effects which might influence the morphological type estimates. Combining the priorly obtained Grant machine classifications with those from the red and blue plate blinking, the reliability was increased. These data were combined with the previously mentioned 200" plate classifications whenever the samples overlapped. While classifying galaxies with the plate blink, it was possible to estimate the relative dendities of the red adn blue galaxy images. The relative colors obtained in this way are included in the final data list.

Data Correction Procedures

Galaxy diameter measurements are subject to three inaccuracies which must be corrected in order to obtain a consistent and homogeneous set of data. First, if the photographic plate sensitivity changes across the cluster area, all galaxy measurements must be reduced to a uniform system. Second, to obtain isophotal-like galaxy dimensions, so called Holmberg corrections must be applied to the visual measurements. And third, galaxy diameters must be corrected to face-on values in order

to correct for optical depth projection effects which cause an edge-on galaxy to appear larger than an identical galaxy seen face-on. Each of these three corrections are discussed in turn.

The first correction is important only for the Virgo Cluster. Although the plate sensitivity might change slightly in the fields of the other seven clusters, the effects on galaxy diameters should be small. But in the Virgo Cluster the galaxies are scattered over eight Palomar Sky Survey plates, and those galaxies which fall in the overlapping plate areas show significant image diameter differences from plate to plate. Using the relative image sizes for these overlap galaxies, it was possible to construct a rough empirical diameter transfer relation. The Virgo Cluster is centered on the Palomar Sky Survey plate $12^h24^m+12^o$. Because this plate contains the majority of the cluster galaxies, no alterations were made to these galaxy diameters. The transfer relations were used to reduce all other galaxy diameters to a system consistent with the central plate. The details of the correction procedure are presented in Appendix II, page 173. Although there are certainly small inaccuracies in this transfer process the galaxy diameters do not play a critical role in the following data analysis. And out of the final sample of about 1000 galaxies, only 30 are from the outlying areas of the Virgo Cluster where diameter corrections were necessary.

The second set of correction factors are generally known as Holmberg corrections. Holmberg (1946) found that galaxy diameters which were measured visually do not always agree with isophotal measurements.

In extensive tests with a number of observers, Holmberg found two systematic measuring effects. First, visual measurements of galaxy image diameters were generally underestimated if the galaxy image density profile was very flat, whereas for images with steep density profiles the visual measurements correspond very closely to plate limited isophotal measurements. And second, minor axis diameters were generally underestimated for the highly flattened galaxies. The magnitudes of each correction effect change from one observer to the next, and although each individual observer has his own systematic biases, Holmberg found that all correction factors can be accurately determined. Furthermore, these corrections remain constant for each observer over periods as long as five to ten years. In order to determine the Holmberg correction factors for the present investigation, isodensity tracings were obtained for 25 Coma Cluster galaxies from the general survey sample. By directly comparing the isodensity galaxy dimensions with the visual measurements, the necessary correction factors were obtained. The two sets of data and the details of the calculations are given in Appendix II, part 2. The results indicate that only minor corrections are needed for the galaxy major axis measurements, but a more significant correction is required for the galaxy ellipticities. A similar result was found for one of the observers tested in Holmberg's original study.

The third correction is necessary for converting apparent galaxy diameters to face-on values. Because (dust free) galaxies are optically thin flattened spheroids, a galaxy seen edge-on will generally have a

higher surface brightness and a larger diameter than a similar galaxy seen face-on. In order to obtain a well defined diameter limited galaxy sample, apparent diameters must be converted to face-on values. One of the most complete early discussions of this effect was given by Holmberg (1946). From a large sample of field galaxies Holmberg found the following empirical relation for correcting apparent galaxy diameters to face-on values:

$$D(0) = \frac{D}{(a/b)^n} \qquad (3)$$

where D(0), D, and a/b are the galaxy face-on diameter, apparent diameter, and apparent axis ratio, respectively. n is a constant which falls between the limits $\frac{1}{4} \geq n \geq \frac{1}{10}$; Holmberg decided that n= 1/6 was the prefered value. A similar relation was derived theoretically by de Vaucouleurs (1972). Using the assumption that a galaxy's volume emissivity follows the relation

$$E(r) \propto r^{-\alpha}$$

where r is a radial coordinate, de Vaucouleurs successfully derives equation (3) and finds that $n = 1/(\alpha - 1)$. The factor α depends somewhat on galaxy morphological type, but de Vaucouleurs suggests that $\alpha = 6$ or $\alpha = 7$. Using the empirical method of Holmberg with the data listed in the Appendix, the preferred value of n appears to be $n = 0.15$ with an error of ± 0.03 . All of the diameter data were corrected by equation (3) with $n = 0.15$.

As a final note, the diameter data were also corrected for "seeing" effects. If D_A is the apparent galaxy diameter (either major or minor axis) then

$$D_A = D_I + D_S$$

where D_I is the intrinsic galaxy diameter and D_S is the "seeing" diameter. The values of D_S for the individual Palomar Sky Survey plates are listed in Appendix I, table 9 .

CHAPTER III

GALAXY ORIENTATION

To fully define a galaxy's angular momentum vector, four quantities are needed.[1] In this chapter major emphasis is placed on analyzing and interpreting two of these, galaxy position angle and the direction of spiral winding. Although the apparent ellipticity data can be used to estimate each galaxy's inclination to the line of sight, an accurate estimate depends on knowing the intrinsic ellipticity of each galaxy. The broad distributions of intrinsic ellipticity for E and SO galaxies (cf., Chapter IV) and uncertainties in determining individual galaxy morphological types, make the ellipticity data unsuitable for an accurate orientation study. Unfortunately the position angle analysis will detect a preferential alignment effect only if the plane of alignment and the plane of the sky intersect at an angle near 90°. By arguing on a simple geometric basis, the probability of detecting preferential alignment with only position angle data is about 2/3. If the preferential plane is parallel to the plane of the sky then the ellipticity distribution should look very peculiar with an excess of face-on galaxies. This effect will be checked in the next chapter.

---

1. The four quantities (3 Euler angles plus the direction of rotation) can be determined using (1) major axis position angle, (2) inclination to the line of sight derrived from the apparent ellipticity and the intrinsic ellipticity, (3) distinction between the near side and far side of a galaxy (cf., de Vaucouleurs 1959b), and (4) the direction of rotation from the spiral winding appearance or from spectral analysis.

Major Axis Position Angle Data

The following position angle analysis includes only those galaxies with ellipticities greater than or equal to 2. By dropping the more circular galaxies, all individual position angle measurements are certain to have an accuracy of $\pm 4^{\circ}$ (1σ). The remaining sample is also limited to the homogeneous set of galaxies with face-on major axis diameters $D(0) \geq 7.5$ kpc/h.

For each of the eight individual cluster samples, the position angle data are presented in Table 1 and Figure 1. Table 1 also contains a summary of the χ^2 calculations useful in checking the observed distributions for non-random effects. If all galaxies in each cluster were oriented at random, then each of the twelve position angle bins should contain $N/12$ galaxies (where N is the total number of galaxies in the position angle sample of a particular cluster). If n_i = the number of galaxies observed in the i-th position angle bin, then

$$\chi^2 = \sum_{i=1}^{12} \frac{(n_i - N/12)^2}{N/12}$$

Using tables by Pearson and Hartley (1966) the χ^2 values (with n-1 = 11 degrees of freedom) were translated into probabilities of random occurrence, and these probabilities are also listed in Table 1.

Among the more obvious results, cluster A 2197 shows a remarkable alignment effect; this position angle distribution is non-random at the 0.018% level, equivalent to a 1 in 5000 random occurrence. Because only eight clusters were tested, the result appears to be quite significant. Furthermore, the χ^2 test only measures the deviation of

Table 1. Position Angle Distributions

Cluster	0°	15°	30°	45°	60°	75°	90°	105°	120°	135°	150°	165°	Σ	Ave.	σ	$\sqrt{\frac{\Sigma}{12}}$	χ^2	Prob.
Virgo	5	8	2	1	1	8	2	5	0	5	9	3	49	4.08	3.06	2.02	25.204	0.9%
A 119	9	6	8	4	8	9	9	6	4	7	3	2	75	6.25	2.49	2.50	10.920	45.0%
A 400	8	4	6	6	6	7	5	6	3	5	5	5	66	5.50	1.31	2.35	3.455	98.3%
A 1656	14	7	10	11	9	12	12	8	10	7	11	10	121	10.08	2.11	3.18	4.851	93.8%
A 2147	5	5	8	8	4	7	10	10	11	8	12	11	99	8.25	2.63	2.87	9.242	58.1%
A 2151	11	10	7	6	12	11	5	14	10	10	10	9	115	9.58	2.54	3.10	7.400	76.6%
A 2197	4	8	7	6	17	15	20	9	4	12	2	10	114	9.50	5.57	3.08	35.895	.018%
A 2199	6	9	10	6	9	14	10	15	8	11	15	13	126	10.50	3.18	3.24	10.571	48.0%
Total Sample - A 2197	58	49	51	42	49	68	53	64	46	53	65	53	651	54.25	7.99	7.37	1.177	99.9%
Virgo Suppl.	6	14	8	3	3	11	5	9	4	10	12	5	90	7.50	3.71	2.74	20.133	4.4%

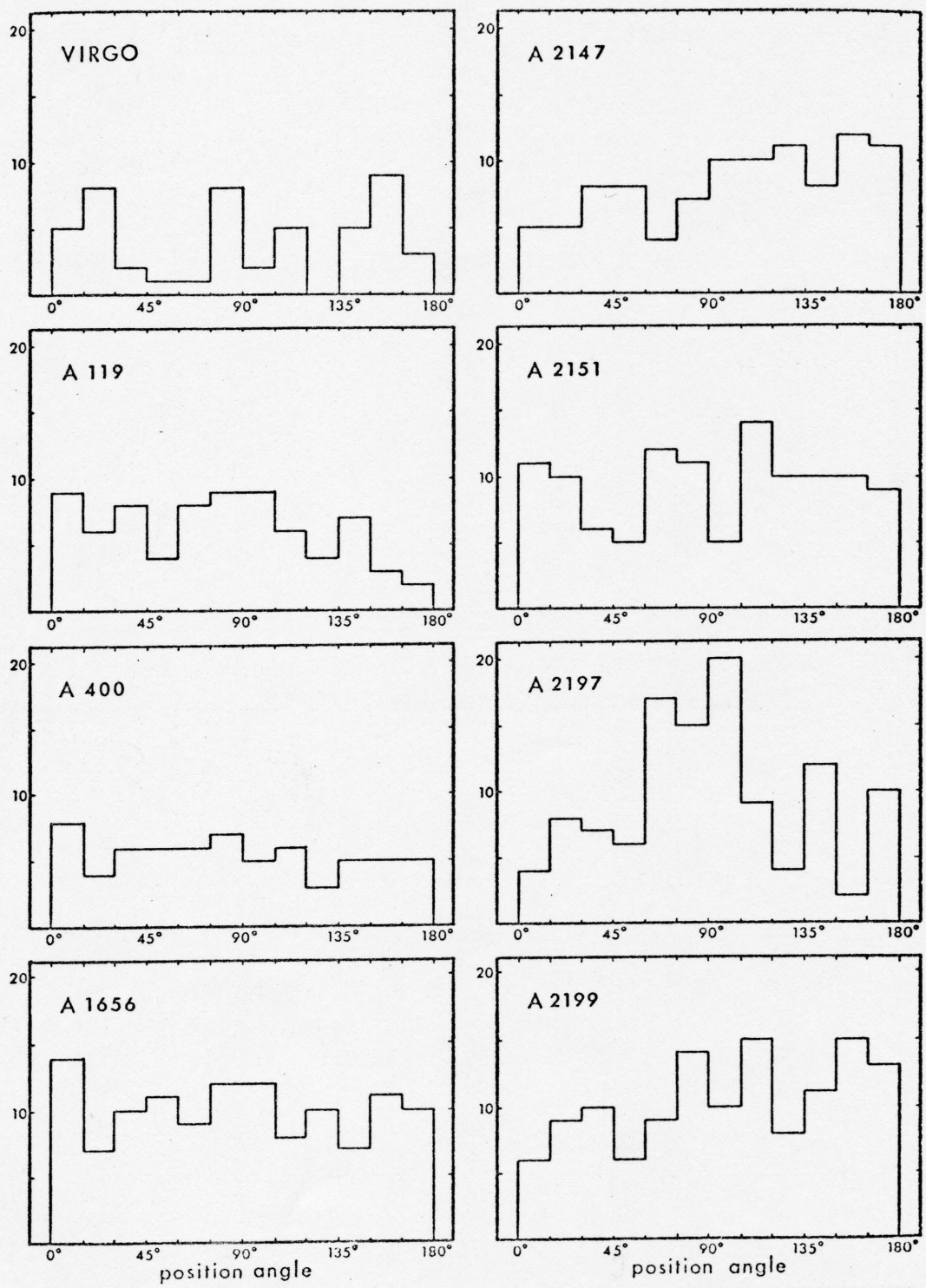

Figure 1. Position Angle Distributions for Each Cluster

Histogram plots of the number of galaxies in position angle bins 15° wide for each of the eight clusters studied.

each bin count from the expected mean value, and no sequential information is included in the probability calculation. The three bins with the highest counts are all adjacent to one another, and this increases the unlikelyhood that the distribution would occur at random. A more detailed discussion of this cluster will be given below. The position angle distributions for two other clusters (A 400 and A 1656) are very flat and contain neither significant peaks nor dips; the distributions are even flatter than might be expected from statistical $\sqrt{N}$ effects. The other five clusters fall between these two extremes. The Virgo Cluster distribution appears to have three separate peaks, but the sample is too small for reliable statistical testing. Besides the 49 galaxies in the homogeneous sample, accurate position angles were obtained for 41 other Virgo Cluster galaxies which fall below the $D(0) = 7.5$ kpc/h limit. This total sample of 90 galaxies (data summarized in Table 1 as Virgo Supplement) is distributed in nearly the same way as the smaller 49 galaxy sample. A χ^2 test indicates that this larger sample is marginally non-random with a χ^2 probability of 4.4%.

Because position angle measurements are subject to measuring errors, it is important to check this set of data for preferential measuring bias. The check can be made most easily by combining all position angle data into a single distribution; any preferential effects should show up as deviations (from the mean) larger than the expected $\sqrt{N}$ errors. The data for the cluster A 2197 will not be included in the test sample because of its obvious internal

non-randomness. The total position angle distribution for the other seven clusters is shown in Figure 2. The distribution is apparently quite flat and the largest deviation from the mean is $1.8\,\sigma$. There is a 99.9% χ^2 probability that the variations in this seven cluster sample are the result of random sampling error.

The two clusters A 2197 and A 2199 are close companions of one another. The angular separation between the cluster centers is only 1.3 degrees, and their redshifts are nearly identical ($z = 0.0303$ and $z = 0.0312$). Because A 2197 shows an unusual alignment effect, it is rather interesting that Rood and Sastry (1972) report a non-random galaxy alignment effect for the cluster A 2199. Rood and Sastry's position angle distribution is non-random at the χ^2 probability level of 2.5%, and they claim that the galaxies in A 2199 are concentrated in two peaks, one parallel and the other perpendicular to the position angle of the giant cD galaxy N 6166 (position angle about 40°). Judging from the position angle data for A 2199 presented in Figure 1, the present study does not confirm the Rood and Sastry analysis; this is not terribly surprising since the probability level of 2.5% is just marginally significant. And besides, the galaxy samples used in the two studies are not identical. The Rood and Sastry sample includes all galaxies with diameters larger than 8 arc seconds on a relatively short (20 minutes) 48" Schmidt plate in the V pass-band. The sample used for the present analysis includes all galaxies with diameters larger than 20 arc seconds on a relatively long exposure (45 minutes) 48" Schmidt plate through a broad red filter (cf., Minkowski and Abell 1963). The

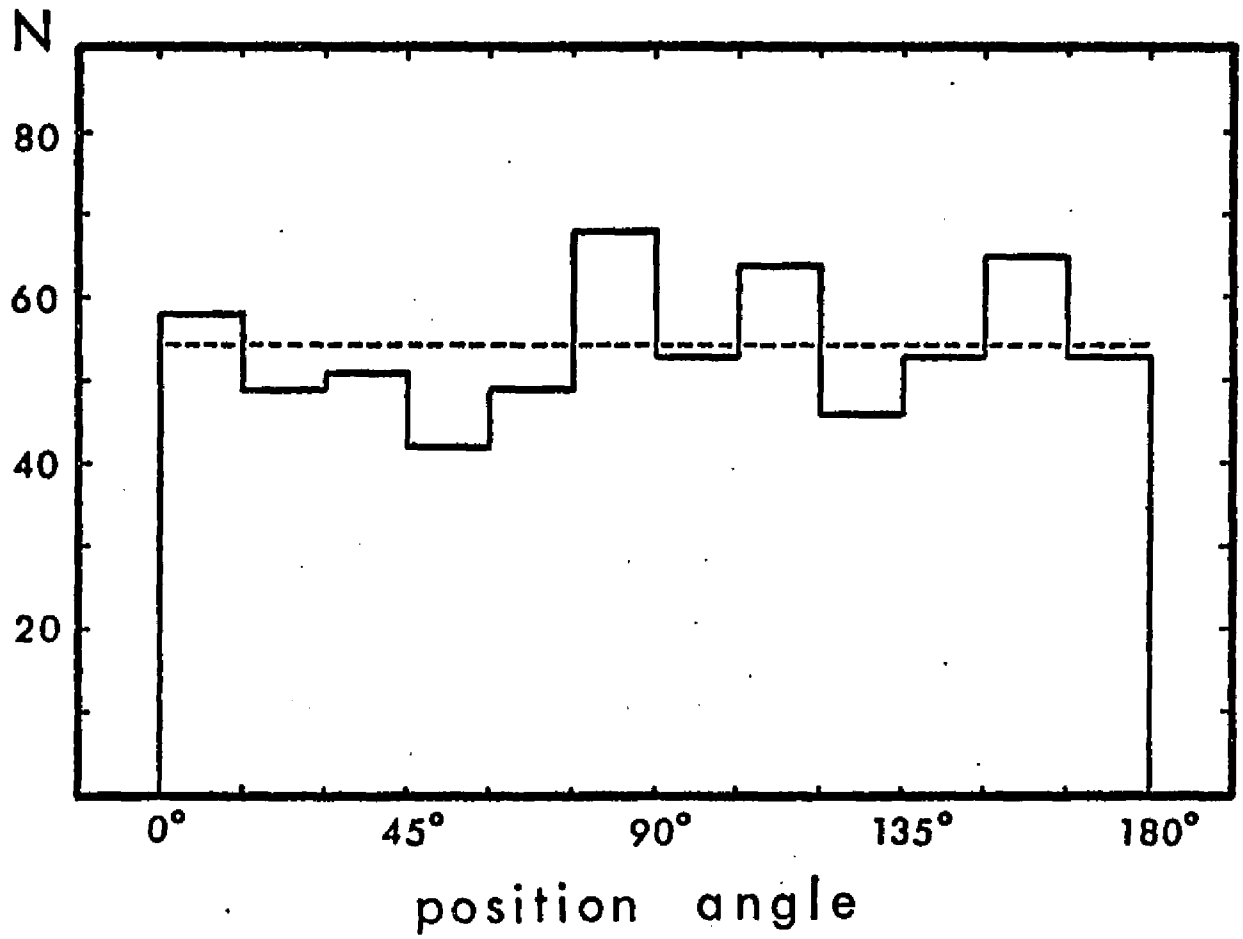

Figure 2. Position Angle Distribution for Total Sample without A 2197

most direct comparison can be made by limiting both studies to the same cluster area (radius = 47.5 minutes of arc centered on NGC 6166), and following the Rood and Sastry technique, summing the data in bins 20° wide. For comparison the two position angle distributions are shown in Figure 3, the top panel from the Rood and Sastry study and the bottom panel from the present study. The 142 galaxy Rood and Sastry sample has $\chi^2 = 17.59$ implying a random probability of occurrence = 2.5%. The 116 galaxy sample from the present study has $\chi^2 = 6.23$ which gives a probability = 62%. Suspecting that the discrepancy might be caused by measuring errors, a direct comparison was made of the individual position angle measurements. For the 103 galaxies which overlap both studies, 65 have position angle differences less than 10°, 85 have differences less than 20°, and the other 18 are more discrepant. In most cases these position angle differences are larger than the claimed measuring errors, so it appears likely that there might be slight but significantly important position angle changes which depend on a photograph's color sensitivity or depth of exposure. There is some possibility that the extra 30 Rood and Sastry galaxies are those contributing to the anisotropy, but a more extensive investigation is needed to explain the discrepancy.

To investigate A 2197 in more detail, a comparitive analysis was made for two sub-samples of galaxies: those falling in the position angle peak ($60^{\circ} \leq PA < 105^{\circ}$) and those falling outside the peak. It became quite obvious that the galaxies in the position angle peak tended to fall in the cluster halo, that they were most often spirals, and that

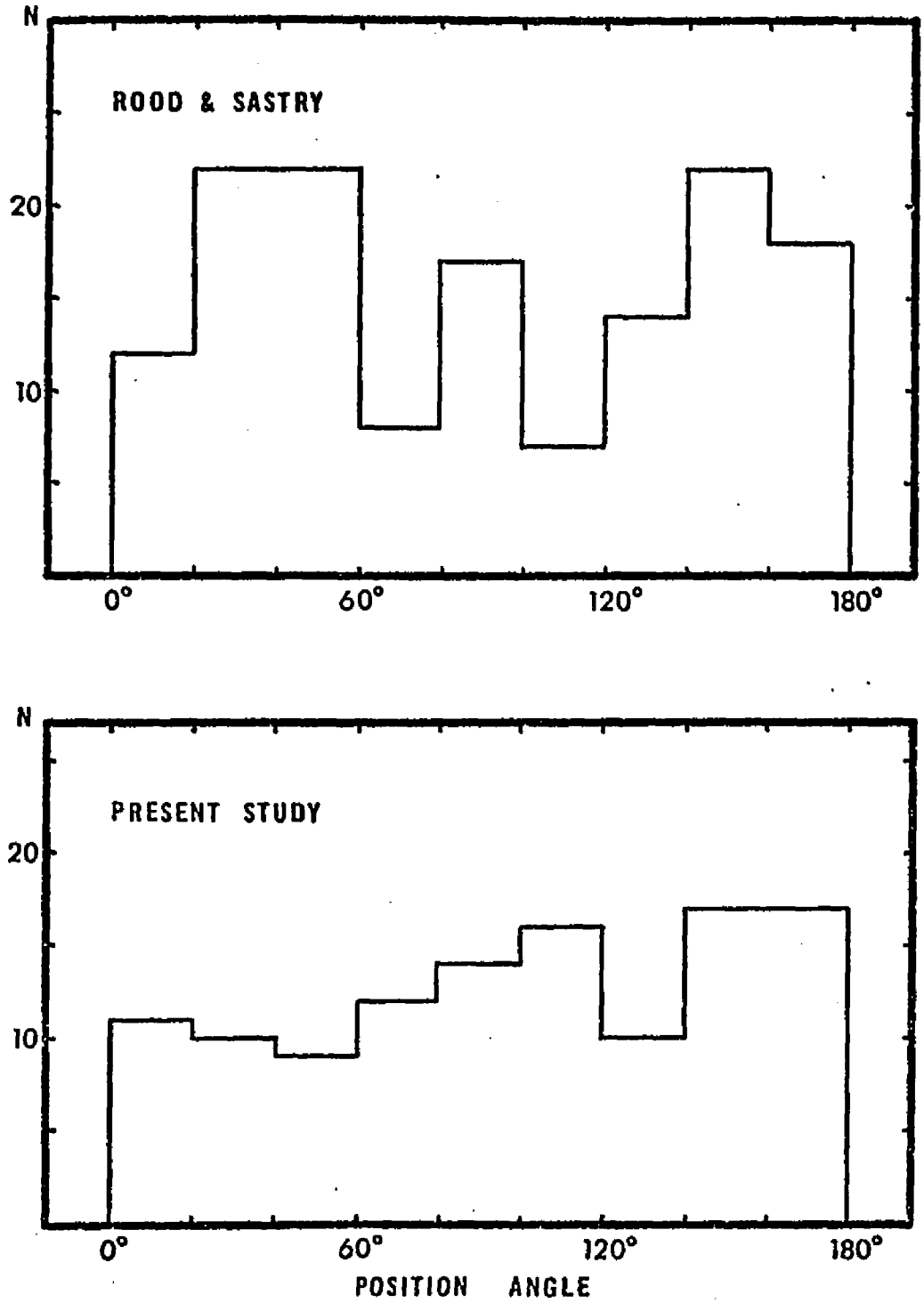

Figure 3. Position Angle Distributions for A 2199

Comparison between two independent galaxy position angle studies for the cluster A 2199. The distribution plotted in the lower panel is the same as that shown in figure 1 for A 2199, but here the position angle bins are 20° wide rather than 15° wide.

they were somewhat bluer than the other galaxies. To make the analysis more quantitative the cluster was divided into twelve radial zones, each of equal width; the galaxies within the inner five zones were taken to be the core sample and those in the outer seven zones the halo sample. The two separate position angle distributions are shown in Figure 4. Quite obviously the position angle peak is contributed almost entirely by the cluster halo population. One possible explanation for this effect, dynamic realignment of galaxies in the dense cluster core, will be discussed in Chapter V. The halo and core samples also have very different morphological type distributions:

core sample:	24% E's,	44% S0's,	32% Spirals
halo sample:	10% E's,	20% S0's,	70% Spirals

The same general trend is observed in nearly all rich galaxy clusters, so this result is not necessarily related to the position angle alignment effect. Consistent with the morphological type distribution, the halo galaxies tend to be bluer than the core galaxies. Using the color system described in Appendix I (7 = very red, ..., 4 = neutral, ..., 1 = very blue) the halo sample galaxies have a mean color of 4.1, whereas the core galaxies have a mean color of 5.1 .

The position angle data were also used to check for radial position angle (RPA) alignment. Gainullina and Roshjakova (1967) have reported that a significant fraction of the galaxies in A 1656 and A 2065 point toward the cluster center. RPA will be defined as the angle between a galaxy's major axis and the line connecting the galaxy's

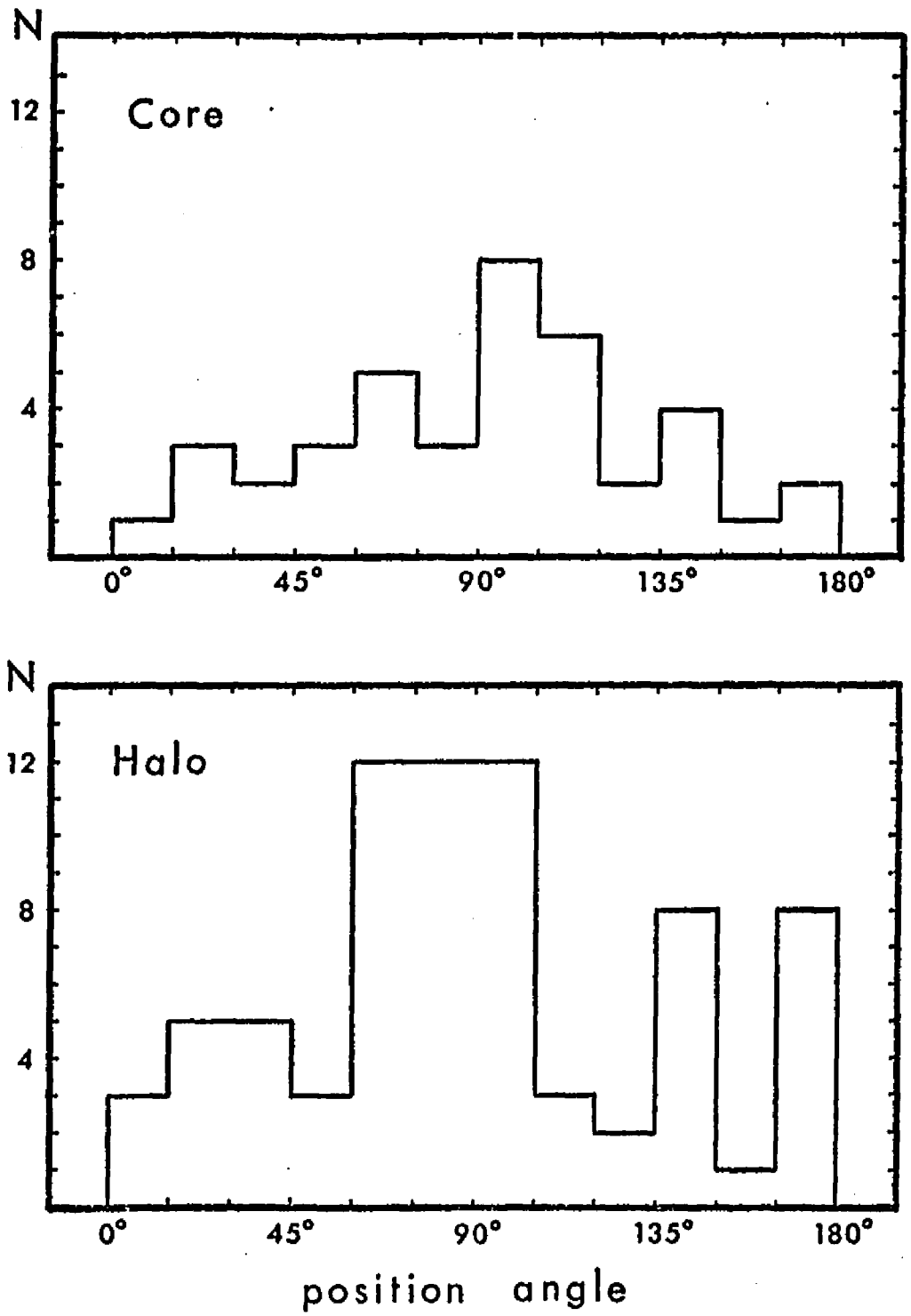

Figure 4. Position Angle Distributions for Core and Halo Samples of A 2197

center with the cluster center, e.g., RPA = 0^{o} if the galaxy major axis points toward the center of the cluster. The RPA distributions for seven of the eight clusters are totally flat, but for A 1656 (Coma) the distribution is definitely skewed. The Coma Cluster distribution is shown in Figure 5. To test the non-randomness of the data, the distribution was divided into two halves at RPA = 45^{o}. The excess in the small RPA section has a random probability of occurrence = 4.1% (χ^2 test). This result is not very strong statistically, but it is interesting that the two clusters which show the effect (A 1656 and A 2065) are both very symmetrical regular clusters. Calculations presented in Chapter V indicate that if a galaxy on a radial orbit is disrupted only in its direction of motion, then the core of the Coma Cluster is just dense enough to cause a significant amount of disruption. The other clusters with cores of lower density might never show this effect.

Spiral Winding Data

The direction of spiral winding is the second easily obtainable parameter which can be used for statistical studies of galaxy angular momentum. The analysis depends on the single assumption that spiral arms always rotate in a consistant way; either they are always trailing or they are always leading. Then by simply determining whether the spiral arms appear as a forward S or as a reversed S , it is possible to decide whether the angular momentum vector points into or out of the plane of the sky. The analysis is limited mainly by the small numbers of spiral galaxies which occur in rich clusters. A sufficient number of

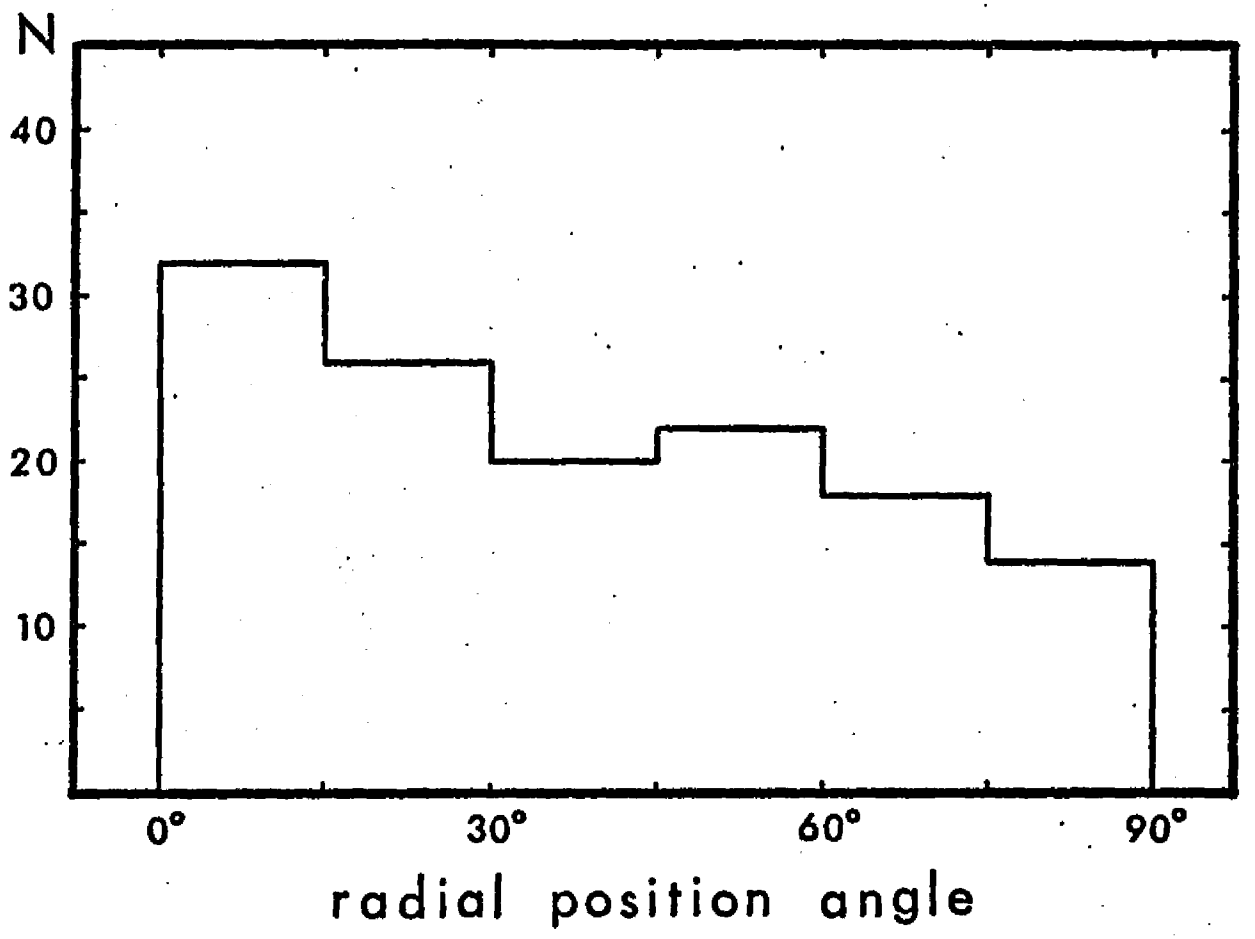

Figure 5. Radial Position Angle Distribution for Cluster A 1656

Radial position angle is defined to be 0° if the galaxy's major axis is directed toward the cluster core, and 90° if the major axis is perpendicular to the radius vector connecting the galaxy and the cluster core.

spiral galaxies were found in four clusters. The data are summarized in Table 2. For each cluster the numbers of spirals are quite small, but in every case the distributions are well balanced. Only for the Hercules Cluster (A 2151) is the sample large enough to analyze the area distribution of the spiral winding directions. No area of the cluster has an excess of one winding direction or the other. In another analysis (Thompson 1973) the Virgo Cluster was analyzed in more detail by including every spiral galaxy appearing on the Palomar Schmidt plates in the cluster area (i.e., not limited by the face-on galaxy diameter $D(0) \geq 7.5$ kpc/h). The Virgo Cluster sample is quite large (101 galaxies), and the balance is still very well maintained in the main body of the cluster. An interesting but marginally significant alignment effect was observed in a concentration of galaxies on the south side of the cluster, in the "Southern Wing". Another interesting effect, the distance modulus separation between the galaxies in the two oppositely winding classes, was just marginally significant; this effect is mentioned only because it has some application to the models of galaxy formation.

Table 2. Spiral Winding Analysis

Cluster	S	Z
Virgo	14	12
A 1656	15	10
A 2151	22	24
A 2197	9	9

CHAPTER IV

GALAXY ELLIPITICITY

The galaxy ellipticity data can be used to answer four questions which are important to the origin of galaxy angular momentum. First, what are the intrinsic ellipticities of the various morphological types of galaxies? Second, are there significant changes in the ellipticity distributions from cluster to cluster? Third, do large and small galaxies of the same morphological type have identical ellipticity distributions? And fourth, is there a significant variation of galaxy ellipticity from the core to the halo of the cluster? The galaxy sample used in the following analysis is restricted to the data listed in Appendix I, Table 8. From this sample only galaxies with face-on diameters $D(0) \geqslant 7.5$ kpc/h are included. And because the assumption of random orientation is important in the conversion from the observed ellipticity distribution to the intrinsic one, the galaxies in the cluster A 2197 are not included in the following analysis. The remaining sample from the other seven clusters contains a total of 813 galaxies; this is the total sample analyzed below.

Morphological Type - Ellipticity Analysis

By separating the galaxies into their respective morphological classes, it is possible to obtain the apparent ellipticity distribution for each of the galaxy types. Table 3 presents a summary of the data,

Table 3. Ellipticity Distribution for Each Morphological Type

Number Distribution

Ellip.	E	E/SO	SO	SO/S	S	S/Irr	Irr	Pec.	Total
0	25	7	29	7	21	0	1	0	90
1	14	7	25	5	17	1	2	0	71
2	18	19	36	12	34	3	4	2	128
3	11	15	33	14	29	4	3	2	111
4	8	6	20	19	32	6	4	0	95
5	1	2	19	28	48	5	2	0	105
6	0	1	24	41	70	6	3	1	146
7	0	0	4	7	49	2	2	1	65
8	0	0	0	0	2	0	0	0	2
Total	77	57	190	133	302	27	21	6	813

Frequency Distribution

Ellip.	E	E/SO	SO	SO/S	S	S/Irr	Irr	Pec.	Total
0	32.5	12.3	15.3	5.3	7.0	0	4.8	0	11.1
1	18.2	12.3	13.2	3.8	5.6	3.7	9.5	0	8.7
2	23.4	33.3	18.9	9.0	11.3	11.1	19.0	33.3	15.7
3	14.3	26.3	17.4	10.5	9.6	14.8	14.3	33.3	13.7
4	10.4	10.5	10.5	14.3	10.6	22.2	19.0	0	11.7
5	1.3	3.5	10.0	21.1	15.9	18.5	9.5	0	12.9
6	0	1.8	12.6	30.8	23.2	22.2	14.3	16.7	18.0
7	0	0	2.1	5.3	16.2	7.4	9.5	16.7	8.0
8	0	0	0	0	0.7	0	0	0	0.2

and the six most important distributions are plotted in Figure 6. The ultimate goal is to obtain the intrinsic ellipticity distribution from the apparent distribution for each of the galaxy types. But before proceeding to that problem, it is important to briefly discuss the accuracy of the morphological type data. Because galaxies seem to fall into a continuous and smooth morphological sequence (de Vaucouleurs 1959a, Sandage 1961), accurate galaxy morphological types are sometimes difficult to estimate even with the best plate material. In the present study, low scale (Palomar Sky Survey) plates were used in estimating galaxy types, and because the morphological type of each galaxy is slightly uncertain, the morphological classes tend to overlap one another more than usual. In order to minimize the inaccuracies of the data, the only galaxies placed in the singular E, SO, S and Irr classes were those galaxies which definitely belonged to a specific morphological class. The remaining galaxies had less certain morphological classifications, and for these galaxies the appropriate intermediate class (E/SO, SO/S, S/Irr) was used. By following this procedure the galaxies in the singular classes (E, SO, S and Irr) became more useful and reliable at the expense of the galaxies which fell in the intermediate classes.

If galaxies in each sample are randomly oriented, a unique intrinsic ellipticity distribution can be obtained from any observed ellipticity distribution. The following summary outlines the method of converting an apparent distribution into an intrinsic distribution:

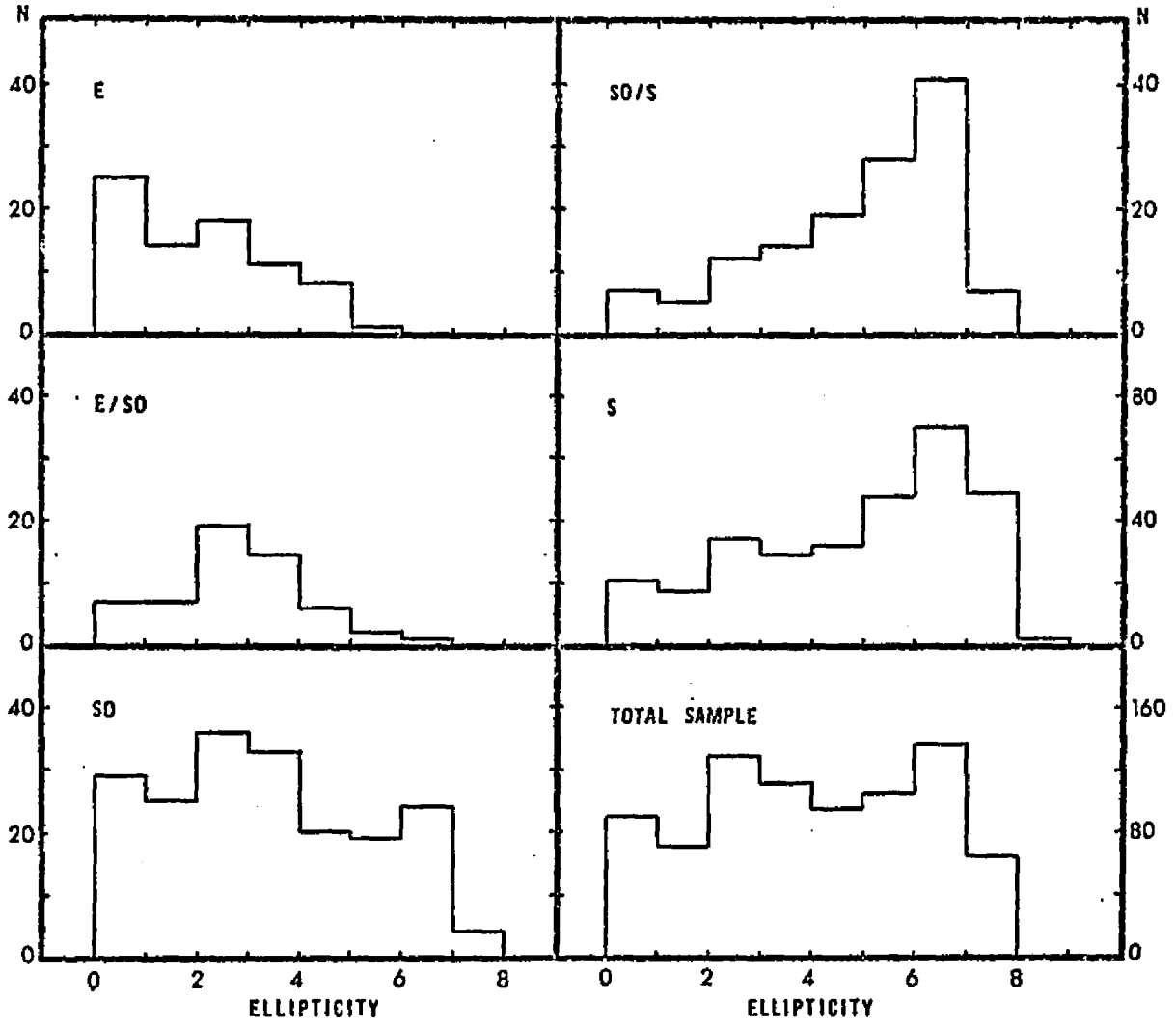

Figure 6. Apparent Ellipticity Distributions for Various Morphological Types

(1) Assume that all galaxies in the highest ellipticity class are seen exactly edge-on so their intrinsic ellipticity equals their apparent ellipticity. Using the number of galaxies observed in this highest ellipticity class, calculate the number of galaxies in this intrinsic class which fall at lower apparent ellipticities (cf., Appendix II, page 179).

(2) Subtract from the apparent distribution the contribution of the previously calculated intrinsic ellipticity sample (smoothed over all orientations).

(3) The remaining apparent ellipticity distribution ends one ellipticity class lower than the original sample. Treat this reduced sample as before, and find the intrinsic frequency for the next highest ellipticity class.

(4) Repeat this process until all of the apparent ellipticity classes are accounted for.

There is one deficiency involved in this procedure. Statistical errors in the data at high ellipticity are translated down the sequence so the reconstruction becomes less reliable at low intrinsic ellipticities.

In fitting an intrinsic distribution to the spiral galaxy data, it became immediately apparent that there was an excess of edge-on galaxies relative to the number of face-on galaxies. This effect might be produced either by (1) poor determinations of morphological types for certain galaxy orientations, or (2) inaccuracies in the correction from apparent to face-on galaxy diameters (cf., discussion of equation 3 in

Chapter II). Because this same deficiency shows up in the analysis of the "total sample" distribution, where problems with morphological classification are not involved, explanation (1) seems less plausible. The effect is most easily explained in terms of a slight inaccuracy of the face-on diameter correction for spiral galaxies. Note that equation 3 depends on the index n which probably changes from one galaxy type to another. The value $n = 6$ was applied to all the data independent of morphological type, and the spiral galaxy data probably require a value of $n = 7$ or $n = 8$.

The intrinsic ellipticity distributions for E, SO, S, and "total sample" are presented as histograms in Figure 7. Superimposed over the E and S distributions are curves representing the results of an analysis by Sandage, Freeman, and Stokes (1970). The two studies obviously agree very well for E and S galaxies. But Sandage et al. find that for SO galaxies the intrinsic distribution is identical to the smoothed curve shown for spirals. This is obviously not the case for the SO galaxy data shown in Figure 7. A closer investigation of the Sandage et al. analysis indicates that the intrinsic distribution found here for SO galaxies might also be consistant with their data. Both of the studies show that the SO apparent ellipticity distributions have peaks at $\epsilon = 3$ and $\epsilon = 7$. In the Sandage et al. analysis the peak at $\epsilon = 3$ is ignored and it is claimed that the SO distribution agrees (within $\sqrt{N}$ errors) with the single peak intrinsic $\epsilon = 7$ distribution. This conclusion looks reasonable only because of the large apparent errors present in the Sandage et al. data, judged from the poor quality of the spiral galaxy

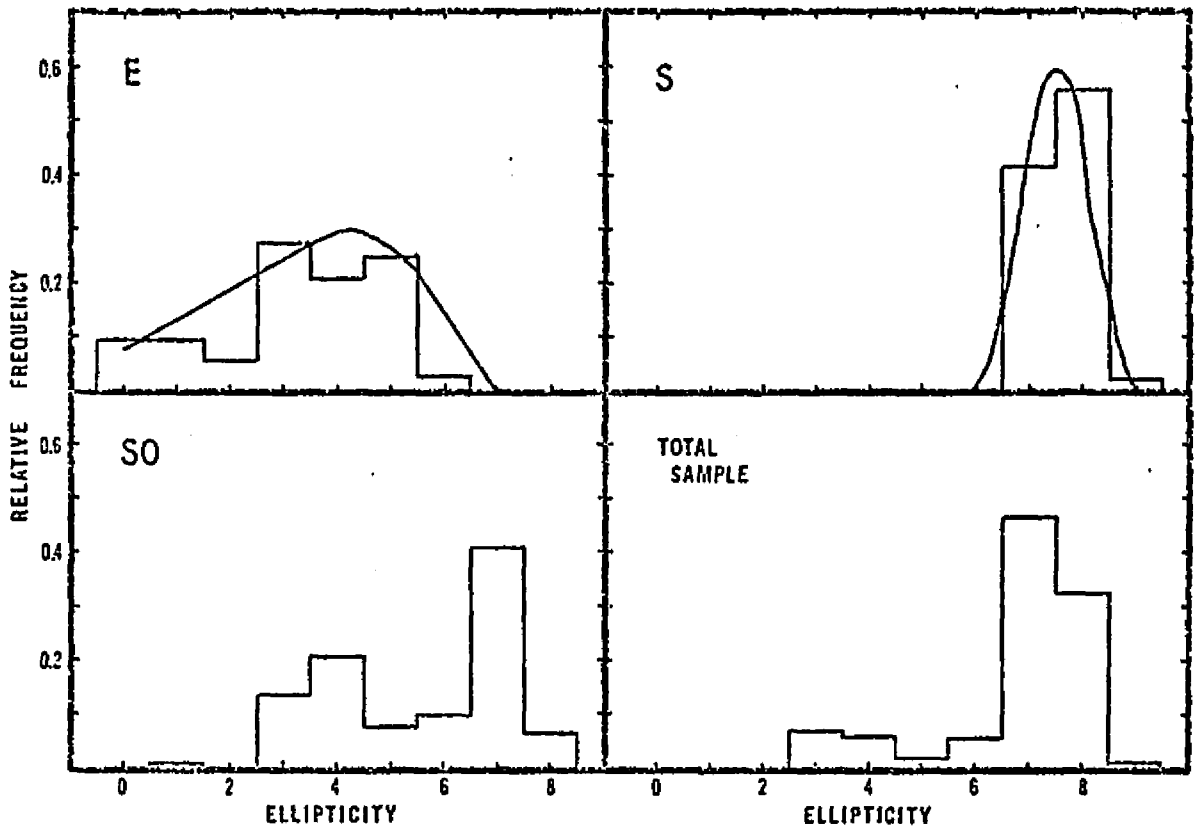

Figure 7. Intrinsic Ellipticity Distributions for E, SO, S, and Total Sample

The histogram plots show the distribution of intrinsic ellipticity reconstructed from the apparent ellipticity distributions in figure 6; the reconstruction process introduces errors which become cumulatively larger at low ellipticity. The smooth curves are from the analysis of Sandage, Freeman, and Stokes (1970).

distribution. In the present analysis the spiral galaxy distribution closely matches the intrinsic ellipticity 7 distribution found in other investigations (cf., de Vaucouleurs 1959b). So it seems that the errors in the present analysis are considerably smaller and that the SO ellipticity distribution might actually have two intrinsic ellipticity peaks.

Also note that the "total sample" analysis shows the bias for edge-on galaxies found in the spiral galaxy analysis. In order to be consistent with the relative fractions of E and S galaxies actually in this sample, the peak at ellipticity 7.5 is much too strong with respect to the peak at ellipticity 4 . Furthermore, the "total sample" distribution shows no contribution for ellipticities between 0 and 2, even though the E galaxy distribution indicates that there should be galaxies contributing in this interval. The deficiency is not real but is caused by the method of reconstructing the intrinsic ellipticity distribution from the observed distribution. The errors associated with the lowest intrinsic ellipticity classes are actually quite large.

The following concluding remarks should be made. First, E galaxies appear to have a skewed ellipticity distribution which peaks at an intrinsic ellipticity of 4.5 ; there are relatively few low ellipticity E galaxies. Second, spiral galaxies have a narrow intrinsic ellipticity distribution centered at 7.5 . Third, SO galaxies are intermediate between these two extremes; the intrinsic ellipticity distribution suggests that there are two ellipticity peaks, one at ellipticity 3 and another at ellipticity 7. This last conclusion depends on the accuracy

of the morphological type determinations. And finally the most important conclusion, the intrinsic ellipticity distributions appear to be identical for galaxies located in clusters (the present study) when compared to galaxies located in the general field (the Sandage et al. study).

Individual Cluster Ellipticity Distributions

Figure 8 presents eight separate ellipticity distributions, one for each of the eight individual clusters. The distributions which are shown were normalized to a total sample of 100 . Table 4 contains the numerical data in both the original form and in the normalized form. Although there are marked differences between the individual ellipticity distributions, these differences might not be physically significant. There are two major complications in interpreting the data. First, ramdom statistical errors could be large because all the samples are very small. Second, foreground and background contamination might significantly change each apparent ellipticity distribution. The latter complication is the most troublesome, because for each cluster there appears to be a radial change in the relative numbers of E, SO, and spiral galaxies (see discussion below). The strength of the halo contamination varies from one cluster to another, ranging between 30% and 50% (see Table 9 in Appendix I). Without eliminating this halo component and knowing which portion of the ellipticity sample actually belongs to the cluster core, only qualitative results can be obtained.

Among the eight clusters, A 400 appears to have the most unusual ellipticity distribution. Although the galaxies in the cluster have a

Table 4. Ellipticity Distributions for Each Cluster Sample

Number Distributions

Cluster	0.	1.	2.	3.	4.	5.	6.	7.	8.	Total
Virgo	4	11	10	6	11	7	11	5	0	65
A 119	12	9	13	12	12	16	20	2	0	96
A 400	6	7	16	15	12	11	11	1	0	79
A 1656	15	16	20	22	18	10	31	18	2	152
A 2147	13	6	21	21	8	14	21	14	0	118
A 2151	16	11	22	11	17	25	21	19	0	142
A 2197	26	12	12	24	20	25	29	4	0	152
A 2199	24	11	26	24	17	22	31	6	0	161

Normalized to $\Sigma = 100$

Cluster	0.	1.	2.	3.	4.	5.	6.	7.	8.	Total
Virgo	6.2	16.9	15.4	9.2	16.9	10.8	16.9	7.7	0	100
A 119	12.5	9.4	13.5	12.5	12.5	16.7	20.8	2.1	0	100
A 400	7.6	8.9	20.3	19.0	15.2	13.9	13.9	1.3	0	100
A 1656	9.9	10.5	13.2	14.5	11.8	6.6	20.4	11.8	1.3	100
A 2147	11.0	5.1	17.8	17.8	6.8	11.9	17.8	11.9	0	100
A 2151	11.3	7.7	15.5	7.7	12.0	17.6	14.8	13.4	0	100
A 2197	17.1	7.9	7.9	15.8	13.2	16.4	19.1	2.6	0	100
A 2199	14.9	6.8	16.1	14.9	10.6	13.7	19.3	3.7	0	100

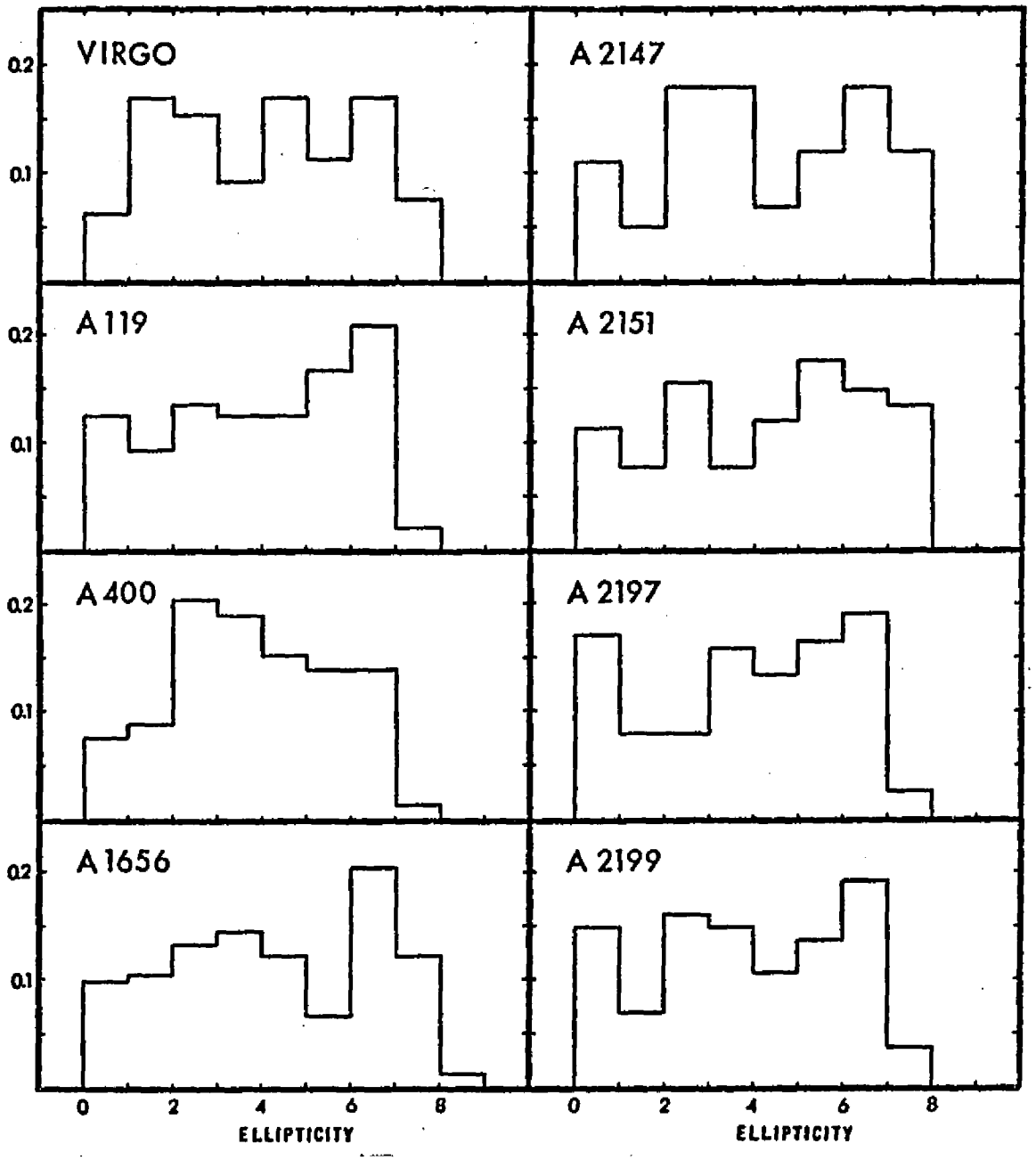

Figure 8. Apparent Ellipticity Distributions for the Eight Clusters

Histograms show the relative frequency distributions of galaxy ellipticity.

very typical morphological type distribution (see Appendix I, Table 9), the ellipticity distribution looks abnormal. This cluster deserves further investigation because the unusual distribution might be caused by a preferential alignment of galaxies.

Ellipticity Distributions for Large and Small Galaxies

The relation between galaxy mass and angular momentum can be checked very easily by comparing the ellipticity distributions for large and small galaxies. For example, if galaxies of all sizes (i.e., all masses) have identical ellipticity distributions, then $L \propto M^{5/3}$. A derivation of this relation will be presented in the final chapter; in this section the major emphasis will be placed on presenting the ellipticity data. By dividing the galaxies according to the face-on galaxy diameter, D(0), two samples of comparable size were obtained for each of the galaxy types E, SO, and S. One sample contains all galaxies with $7.5 \text{ kpc/h} \leq D(0) \leq 12 \text{ kpc/h}$, and the other sample contains all galaxies with $D(0) > 12 \text{ kpc/h}$. The data are presented in Table 5 and in Figure 9. In the figure the solid line corresponds to the large galaxy sample and the dashed line to the small galaxy sample.

It is quite obvious that the large and small spiral galaxies have identical ellipticity distributions. This is not the case for the E and SO galaxies. The slight difference between the two E galaxy distributions might be caused by an observational effect which can be explained as follows. Because E galaxies are known to have a radially changing intrinsic ellipticity (Liller 1960, 1966), any systematic bias in the diameter measurements will be reflected in the ellipticity data.

Table 5. Diameter Separation of Galaxy Ellipticity

Number Distributions

Ellip.	Sm.E	Lg.E	Tot.E	Sm.SO	Lg.SO	Tot.SO	Sm.S	Lg.S	Tot.S
0	14	11	25	12	17	29	12	9	21
1	4	10	14	8	17	25	7	10	17
2	9	9	18	14	22	36	16	18	34
3	8	3	11	20	13	33	20	9	29
4	6	-	8	15	5	20	17	15	32
5	1	-	1	13	6	19	26	22	48
6	-	-	-	18	6	24	37	33	70
7	-	-	-	2	2	4	25	24	49
8	-	-	-	-	-	-	1	1	2
Total	42	35	77	102	88	190	161	141	302

Frequency Distributions

Ellip.	Sm.E	Lg.E	Tot.E	Sm.SO	Lg.SO	Tot.SO	Sm.S	Lg.S	Tot.S
0	33.3	31.4	32.5	11.8	19.3	15.3	7.5	6.4	7.0
1	9.5	28.6	18.2	7.8	19.3	13.2	4.3	7.1	5.6
2	21.4	25.7	23.4	13.7	25.0	18.9	9.9	12.8	11.3
3	19.0	8.6	14.3	19.6	14.8	17.4	12.4	6.4	9.6
4	14.3	5.7	10.4	14.7	5.7	10.5	10.6	10.6	10.6
5	2.4	-	1.3	12.7	6.8	10.0	16.1	15.6	15.9
6	-	-	-	17.6	6.8	12.6	23.0	23.4	23.2
7	-	-	-	2.0	2.3	2.1	15.5	17.0	16.2
8	-	-	-	-	-	-	0.6	0.7	0.7

Figure 9. Apparent Ellipticity Distributions for Large and Small E, SO, and S Galaxies

Histogram plots show the relative frequency distributions for large (solid line) and small (dashed line) galaxies of three different morphological types.

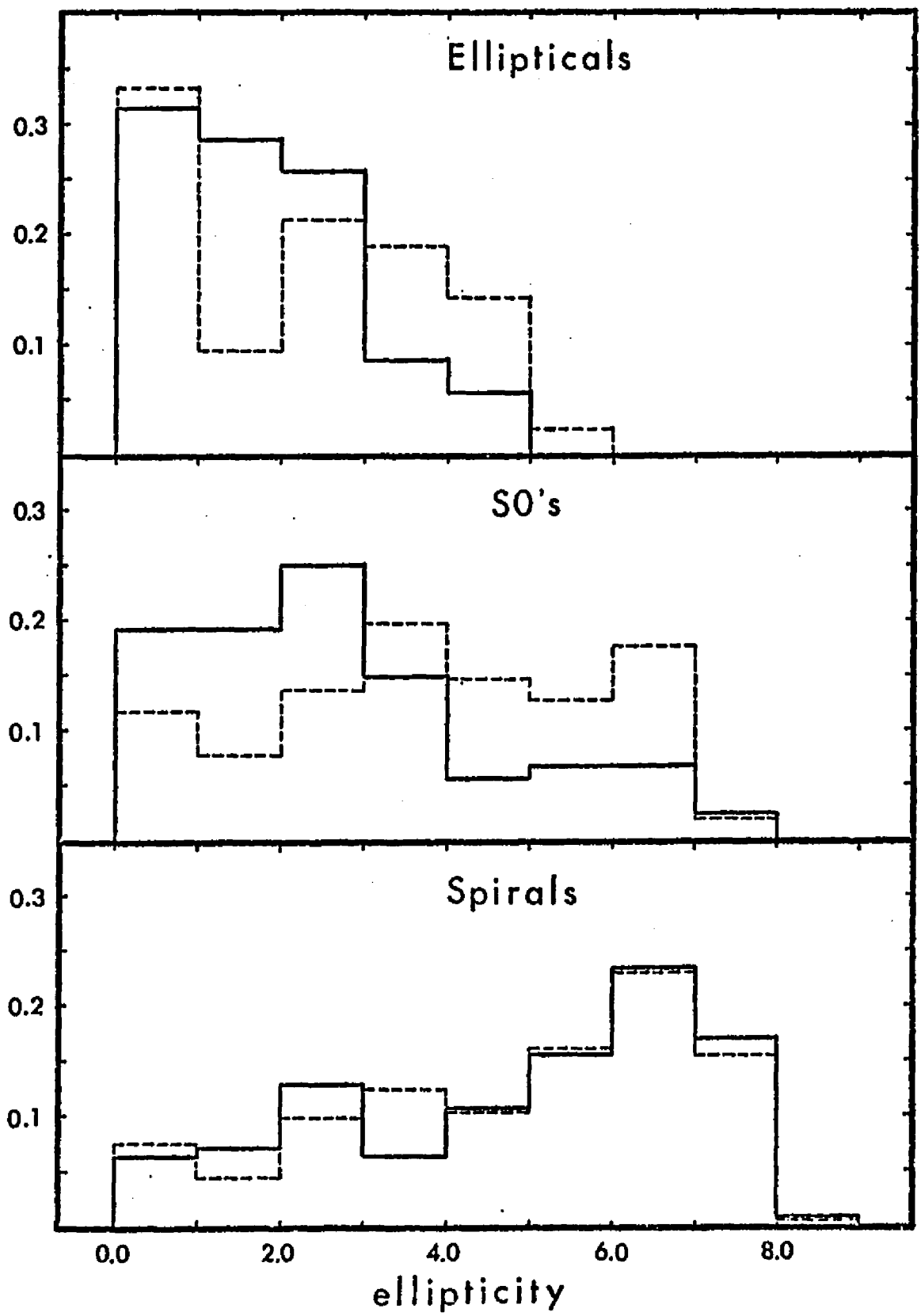

Figure 9. Apparent Ellipticity Distributions for Large and Small E, S0, and S Galaxies

The diameter measurements used in this study are isophotal-like dimensions limited at a specific surface brightness level (i.e., the plate limit). If all E galaxies have similar stellar densities and mass to light ratios, then the plate limited surface brightness will correspond to a constant galaxy thickness ℓ. Figure 10 illustrates the effect for large and small galaxies. For the larger galaxy the chord length ℓ falls in the outer halo of the galaxy where the ellpticity is lowest. For the smaller galaxy the chord length ℓ falls nearer to the nucleus where the ellipticity is larger.

The difference between the two SO ellipticity distributions is more definite, and there is no easy way to account for the difference. Using the technique described earlier in this chapter, the two SO ellipticity distributions were converted into intrinsic distributions; the results are shown in Figure 11. The small SO galaxies are nearly all high ellipticity objects whereas the large SO galaxies have two intrinsic ellipticity peaks, one at $\epsilon = 3$ and the other at $\epsilon = 7$. Because the large and small galaxy ellipticity distributions are nearly identical for the E and S galaxies, it is difficult to argue that the SO distributions are really as different as the data indicate. The low scale plate material might lead to confusion in determining galaxy morphological types. An investigation with better plate scale is needed to clarify this point.

Morphological Type Separation

It is generally recognized that the cores of rich clusters are dominated by E and SO galaxies, and that spiral galaxies are associated

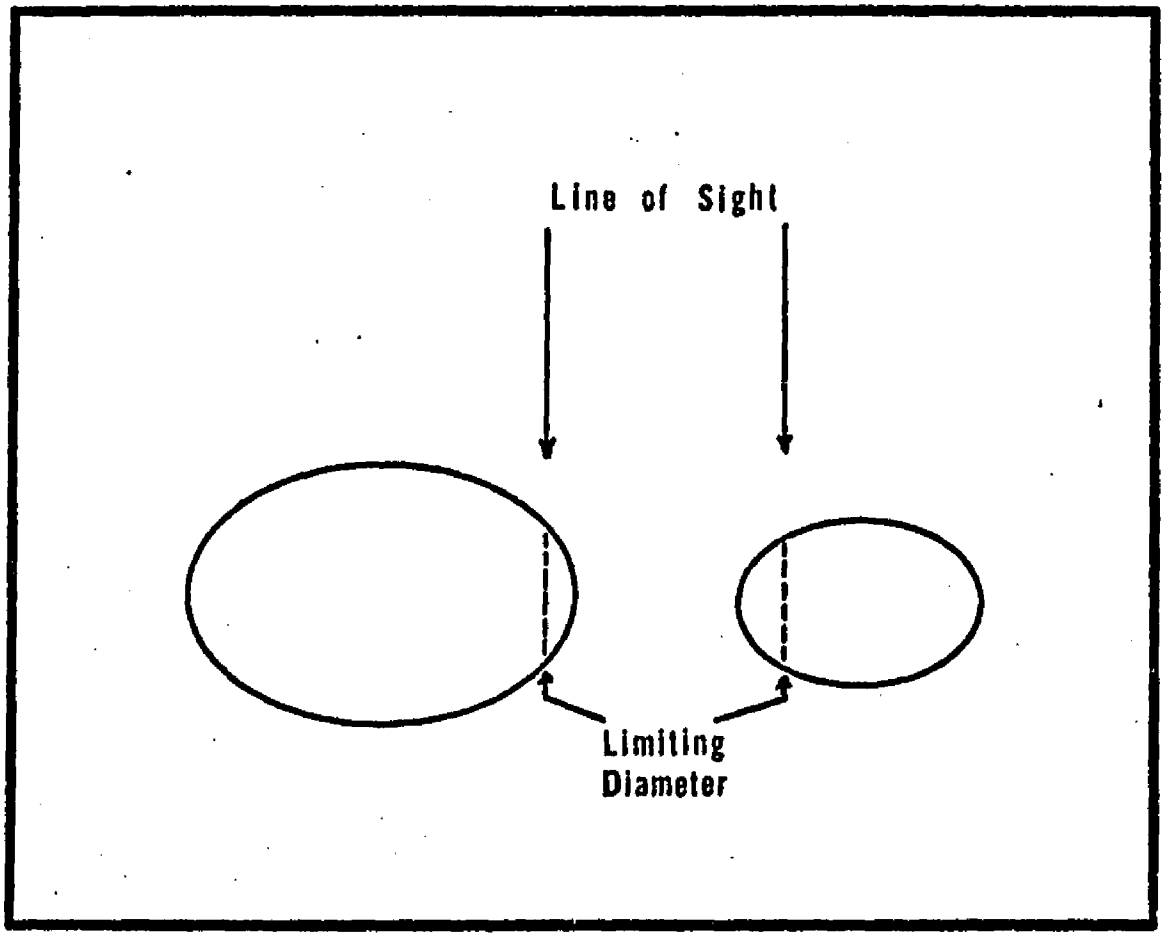

Figure 10. Line of Sight-Optical Depth Effect

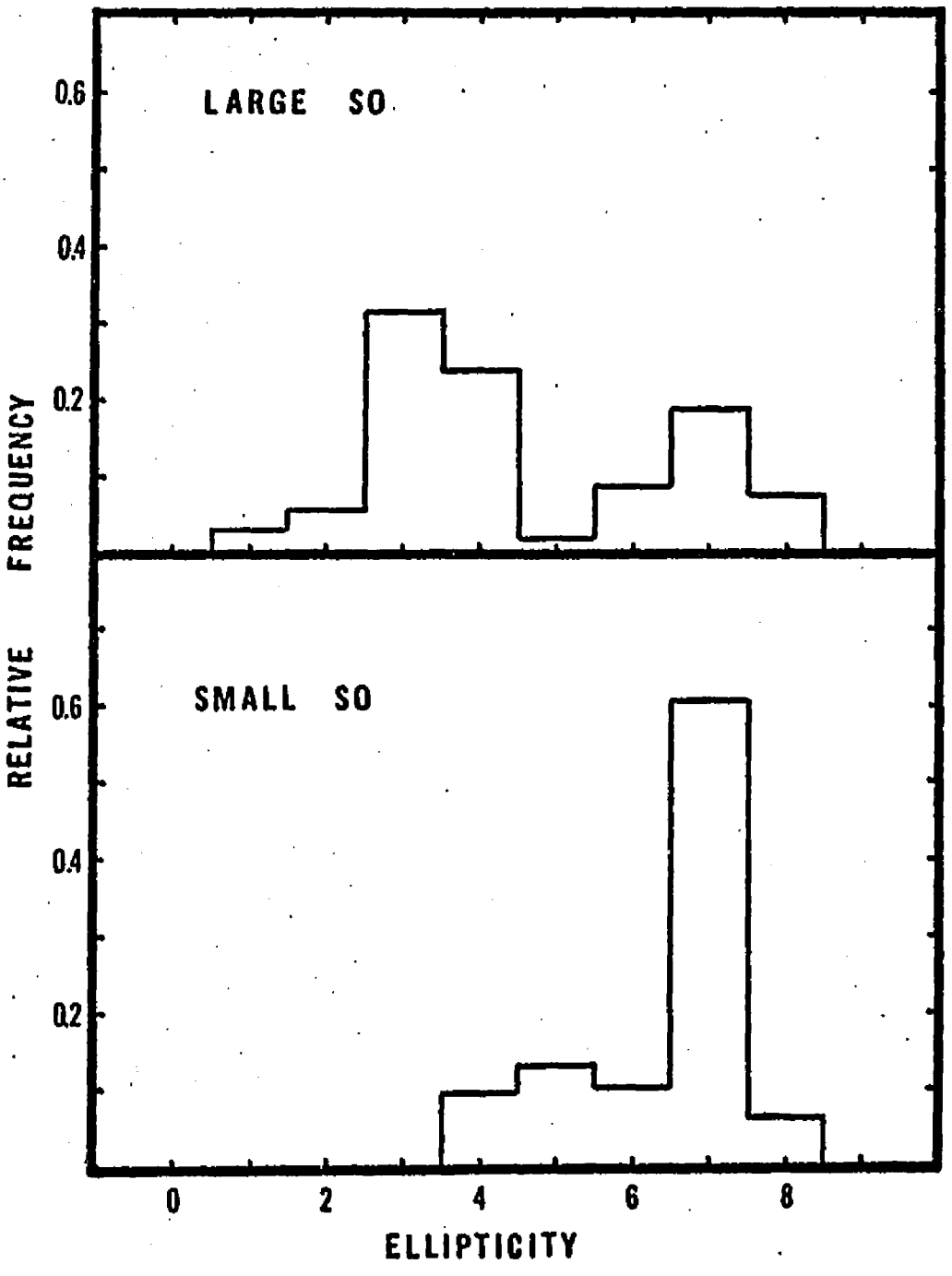

Figure 11. Intrinsic Ellipticity Distributions for Large and Small SO Galaxies

with the "field" population. If this separation is related to the formation of the clusters or to the formation of the individual galaxies, it has interesting implications for the origin of galaxy angular momentum. It would be ideal to compare the intrinsic ellipticity distributions for the cluster core and halo samples, but these are very difficult to obtain. The greatest difficulty is removing foreground and background halo contamination from the nine different ellipticity groups for the cluster core sample. The best alternative is to analyze the galaxy morphology distributions within a single composite cluster produced by combining all data from each of the eight individual clusters. This will reduce the problems of $\sqrt{N}$ errors caused by the small sample distributions, and will produce results for what might be called an "average" cluster. As described below the background contamination can be eliminated by analyzing the data in radial zones. And then the intrinsic ellipticity distributions for the various morphological types can be used to reconstruct the core and halo ellipticity distributions. This final step is not really necessary so only the morphological type distributions will be presented here.

The sample of data used in this analysis includes every galaxy with a face-on diameter $D(0) \geq 7.5$ kpc/h. The galaxies with intermediate morphological types (i.e., E/SO, SO/S, S/Irr) were split equally between the singular morphological classes. Each cluster was divided into twelve radial zones (each of equal width), and the final composite sample was obtained by adding the counts in each of the twelve respective zones. The data are presented in the first part of Table 6 and

Table 6. Radial Distribution of Morphological Types within Clusters

Radial Zone	E	SO	S	Irr
1	14	22	9	1
2	11	31.5	20.5	1
3	16	34	29	0
4	8	26	36.5	0.5
5	15.5	31	40	3.5
6	11	28	42.5	3.5
7	14	35	47	5
8	8	32.5	51	2.5
9	13.5	18	49.5	6
10	4.5	30	44	4.5
11	3	29.5	44.5	4
12	6.5	14	41	6.5

	Morphological Separation			
Radial Zone	E	SO	S	Irr
Cluster only 1 + 2	24%	53%	23%	0
Cluster only 6 + 7	18%	38%	44%	0
Field only 12	7%	25%	59%	9%

then graphed in Figure 12. The dashed lines in the figure represent the uniform background or foreground contamination. Any galaxy falling above this line is a member of the cluster population, and any galaxy falling below the line is a member of the "field" population. This method of analysis is described more fully by Yahil (1974). The results are summarized in the second part of Table 6. Three samples are presented: core (zones 1 and 2), intermediate cluster area (zones 6 and 7), and the "field" population (zone 12). The following conclusions can be drawn from the numbers in the table:

(1) Nearly all E galaxies are members of rich clusters.

(2) Of the three types of galaxies, the SO galaxies dominate the cluster core sample.

(3) The "field" population is dominated by spiral galaxies.

(4) Irregular galaxies are not cluster members.

On the basis of point (1) above, it can be concluded that the intrinsic ellipticity distribution of the cluster core sample will be different from the ellipticity distribution of the "field" sample, in the sense that the core sample will contain more galaxies in the low ellipticity range.

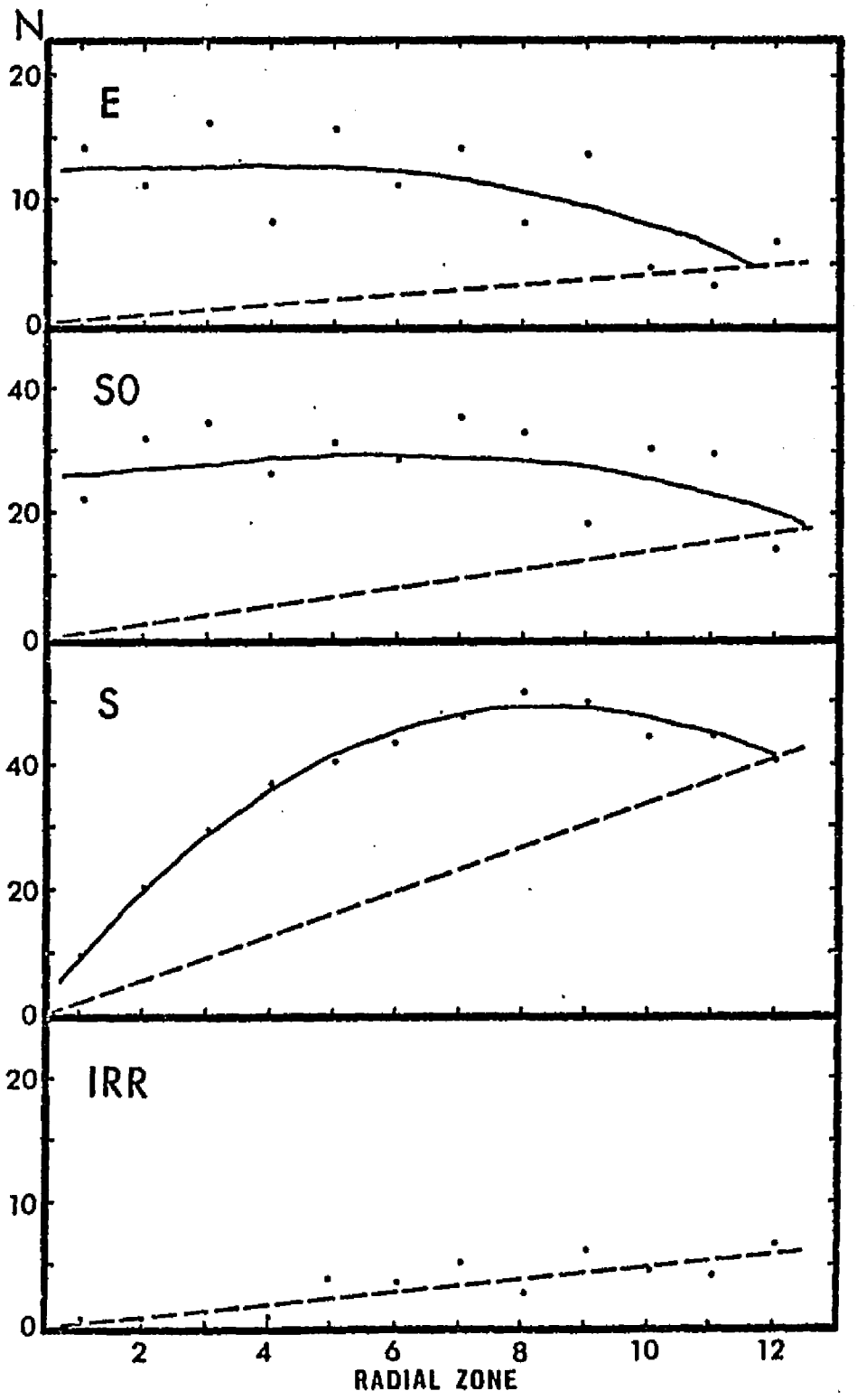

Figure 12. Radial Distribution of Morphological Types

All eight clusters are shown together in a composite analysis. The dots represent galaxy counts in radial zones of equal width and the solid line is the smoothed galaxy distribution; the dashed line represents the contamination by a uniform background.

CHAPTER V

ORIGIN AND EVOLUTION OF GALAXY ANGULAR MOMENTUM

In this chapter two general topics will be discussed. Both are directed to answering the question: What physical effects are responsible for the origin of galaxy angular momentum? The first section deals with those mechanisms which might change a galaxy's angular momentum during the entire period of time following galaxy formation. The second deals solely with the mechanisms which might explain the original source of the angular momentum. Six different models of galaxy formation are reviewed, and particular attention is given to four observationally testable predictions. Whenever the published version of the model ignors any of these four tests, an attempt is made to extend the details of the model to include all of them. Table 7 (which is on p.102 at the end of this chapter) contains a concise summary of the theoretical predictions made by all six models. In the following review the published version of each model is taken at face value; critical remarks are reserved for the discussion in the final chapter where the theoretical predictions are compared with the observations.

Evolution of Galaxy Angular Momentum

Galaxy Collapse Process

In most models of galaxy formation angular momentum is transferred to the developing protogalaxy during the pre-stellar gaseous

phase. It is important to know whether a gaseous protogalaxy is apt to loose a significant fraction of its initial angular momentum during the process of collapse and star formation. Because the loss of angular momentum should proceed more rapidly in the more dense central parts of a galaxy, it is interesting to recall the results of Crampin and Hoyle (1964). They concluded that galaxy rotation curves are consistent with the hypothesis that galaxies collapsed from uniformly rotating clouds. This would seem to indicate that no dissipation takes place during the collapse process. Mestel (1963) presented a very straight-forward theoretical argument which supports the same conclusion. By comparing the collapse time $t_{coll} = (G\rho)^{-\frac{1}{2}}$ with the time it would take for turbulent friction to destroy a gradient of angular velocity, t_{turb}, Mestel concluded that

$$\frac{t_{turb}}{t_{coll}} = \left(\frac{a}{b}\right)\left(\frac{a}{\lambda}\right) \qquad (4)$$

where a = galaxy's instantaneous major axis, b = galaxy's instantaneous minor axis, and λ = mean eddy size of turbulent viscosity. Since $\lambda \lesssim b$ the equation (4) is always greater than 1. Consequently a protogalaxy should collapse and fragment into stars long before any turbulent processes have a chance to redistribute the protogalaxy angular momentum.

Although Mestel (1963) did not include a discussion of magnetic effects in his analysis of galaxy collapse, an account of these effects can be found in an article by Harrison (1973). In analogy with the

turbulent dissipation discussion above, the dissipation produced by magnetic effects might be quite large. But again the results of Crampin and Hoyle (1964) are useful in placing observational limits on these effects (at least for spiral galaxies). In a different context the strength and overall configuration of a protogalaxy's magnetic field might be important in determining the overall extent of a galaxy's collapse. In models of galaxy formation by Piddington (1972), a galaxy's morphological type is determined by the large scale magnetic field of the protogalaxy. For example, according to Piddington's model magnetic pressure perpendicular to the protogalaxy's rotation axis prevents elliptical galaxies from collapsing into disk systems before star formation occurs. But in protogalaxies which eventually turn into SO's or spirals, the magnetic pressure perpendicular to the rotation axis must be small enough to allow the protogalaxy to collapse into a disk.

Tidal Interactions

Tidal interactions among galaxies might also alter the primordial angular momentum of a galaxy. In fact Peebles (1969, 1971a) argues that tidal interactions in a homogeneous medium can entirely explain the origin of galaxy angular momentum. Because a detailed discussion of Peebles' model will be given in the second part of this chapter, in this section the calculations will be restricted to one special problem not discussed by Peebles: If a galaxy is in orbit around a dense cluster core, can tidal interactions with the cluster core efficiently convert galaxy spin angular momentum into orbital angular momentum, or vice

versa? To calculate an upper limit to this effect, assume that galaxies act as viscous fluid bodies when deformed by tidal forces. In the real case the efficiency of angular momentum transfer will be much lower because the galaxy "viscosity" depends on the collective gravitational interaction of all the stars in the galaxy. Notice that a particular galaxy will be systematically decelerated or accelerated depending on whether the tidal bulge leads or lags in phase as the galaxy orbits the cluster core; the geometry and relative angular velocities (orbital versus rotational) will determine whether the galaxy is accelerated or decelerated. To estimate the maximum influence in the calculations below, it will be assumed that this phase lag always remains constant at the maximum value. Expressing the change in angular momentum ΔL as the torque integrated over all time then

$$\Delta L = \frac{3}{4} \cdot \frac{G\, M_{cl}}{r^3_{ORBIT}} \cdot \sin 2\theta \left[\frac{2}{5} \cdot M \cdot (a^2 - b^2)\right] \times t \qquad (5)$$

where M_{cl} = cluster mass, M = galaxy mass, a = galaxy semimajor axis, and b = galaxy semiminor axis. Taking the phase lag $\theta = \pi/4$ and defining the cluster density within the galaxy's orbit as

$$\rho_{cl} = \frac{M_{cl}}{\frac{4}{3}\pi r^3_{ORBIT}}$$

then $\Delta L = \frac{2}{5} \cdot \pi \cdot G \cdot \rho_{cl} \cdot M \cdot (a^2 - b^2) \times t$. To estimate a reasonable value for ΔL let

$$t = \frac{1}{h} \times 10^{10} \text{ years}$$

$$\rho_{cl} = 1.4 \times 10^{-25}\ h^2 \ \ g \cdot cm^{-3}$$

$$M = 10^{11} m_{\odot}$$

$$a = 10 \text{ kpc}$$

$$b = 0.3 \times a$$

and comparing ΔL with our Galaxy's angular momentum (Innanen 1966)

$$L_{GAL} = 1.5 \times 10^{75} \quad g \cdot cm^2 \cdot s^{-1}$$

gives $$\frac{\Delta L}{L_{GAL}} = h \times 0.4$$

where $0.5 \leq h \leq 1$. Although it appears that ΔL is just large enough to be significant, this value should be viewed only as an upper limit. Recall that three factors were over-estimated: (1) average phase lag factor $\sin 2\theta$, (2) cluster density ρ_{cl} , and (3) the viscous response of a galaxy. The last factor alone could reduce ΔL by a factor of 10 to 100. So in general, tidal interactions with dense cluster cores should have relatively little influence on a galaxy's angular momentum.

Radio Source Ejection

Next consider what effects a galaxy might suffer if its nucleus ejects massive objects, e.g., compact radio sources or jets. Two different cases will be discussed: (1) the ejection process is symmetrical and the galaxy only suffers from mass loss in the nucleus, or (2) the ejection process is asymmetrical and the galaxy nucleus absorbs the recoil. In the first case the dynamic effects of the moving compact objects can be ignored since they are in or near the galaxy only for a very short time. It is generally agreed that the ejection speed of radio source lobes is on the order of $0.01 \cdot c$. This means that their travel time through the galaxy takes only 1/25 of a typical galaxy's

rotation period. The only influence which the galaxy will feel is that caused by the loss of nuclear mass. To find how this mass loss affects the structure of the galaxy, consider the motion of an individual star. For a star of mass = m , velocity = v , and distance = r from the galaxy's center

$$L = m \cdot v \cdot r$$

Because the star in its orbit will have an unchanging mass = m and angular momentum = L , then

$$dL = 0 = m \cdot dv \cdot r + m \cdot v \cdot dr$$

so

$$\frac{dv}{v} = - \frac{dr}{r} \quad . \tag{6}$$

If M_r is the mass of the galaxy interior to a radius r , then for the star of mass m

$$\frac{G \cdot M_r \cdot m}{r} = \tfrac{1}{2} \cdot m \cdot v^2 \tag{7}$$

and differentiating equation (7) and dividing both sides by m

gives

$$\frac{G \cdot dM_r}{r} - \frac{G \cdot M_r \cdot dr}{r^2} = v \cdot dv = v^2 \cdot \frac{dv}{v} = \frac{dv}{v} \frac{2 \cdot G \cdot M_r}{r}$$

where the last step follows from equation (7). So

$$\frac{dM_r}{M_r} = \frac{dr}{r} + 2 \frac{dv}{v} = - \frac{dr}{r}$$

If a galaxy nucleus ejects 10% of its mass, then the stars in the vicinity of the nucleus expand into orbits with 10% greater radii.

The outer parts of the galaxy will be affected to a lesser extent because the relative change in r scales inversely with M_r, the total mass interior to r. In conclusion, if massive objects are ejected from the nucleus of a galaxy in a symmetrical way, the overall galaxy structure will change very little. The outer parts of the galaxy will feel only a slight effect and the disturbed inner parts will recover after a few stellar crossing times.

For the second case the ejection process is asymmetrical, and the galaxy nucleus absorbs the recoil. If the nucleus is able to escape from the galaxy, the remaining stars will take on some peculiar or ring shape at first, but then the system will relax into a more stable configuration with the angular momentum redistributed. If the nucleus does not manage to escape but still recoils substantially, the galaxy will again be disrupted and the angular momentum will be redistributed. Although it is difficult to estimate the overall importance of this effect, at least two galaxies included in this study (#91 in cluster A 2151 which is IC 1182 and also #42 in Virgo which is NGC 4486 = M87) are suffering from some type of ejection from their respective nuclei.

Galaxy Precession

Next consider the gravitational interactions which might change a galaxy's orientation. First, close disruptive encounters between individual galaxies might drastically alter the orientation of both galaxies; a discussion of close collisions is given in the next section. Second, moderately close but non-disruptive galaxy-galaxy encounters might cause the individual galaxies to precess and thus

change their orientations. And third, a galaxy orbiting a massive cluster core will feel a long term tidal torque which will also cause the galaxy to slowly precess. Because cluster galaxies have such high relative velocities (judging from the observed cluster velocity dispersions) the second process has very little time to be effective, and the third process is the dominant one. Consequently in the following calculations only the thrid process is considered.

Take any galaxy which is in orbit around a massive cluster core. Assume that the galaxy is rotating and that it has a non-spherical mass distribution. The gravitational force of the cluster core will produce a torque on the freely rotating galaxy. If the galaxy were a solid body or a viscous fluid, it would respond by simply precessing around its original rotation axis. Because the galaxy is not rigid, the precession must be slow enough to allow the galaxy time to react as a single system. Taking the galaxy's characteristic reaction time to be on the order of its rotation period (i.e., around 2×10^8 years), then the calculations given below show that the precession is slow enough for the galaxy to respond as a whole. For a flattened galaxy the halo and disk components might react separately and on different time scales, causing the two components to precess independently of one another. If this occurs the rate of precession for each sub-system will depend on its moment of inertia tensor I_{ii} .

The angular velocity of precession is given by (cf., Danby 1962)

$$\omega = \frac{3 \cdot G \cdot P}{4\pi} \left[\frac{I_{11} - I_{33}}{I_{11}} \right] \frac{M}{r^3} \cdot \cos \theta$$

where G = gravitational constant

P = rotational period of galaxy

$I_{11} = \frac{2}{5} \cdot m \cdot a^2$

$I_{33} = \frac{m}{5}(a^2 + b^2)$

The I_{ii} are the moment of inertia components for an ellipsoidal galaxy of mass m and axis ratio b/a . Also

M = mass of the cluster core

r = radius of the galaxy's orbit

θ = angle between the plane of the orbit and the galaxy's angular momentum vector

Reducing the moment of inertia terms to a simpler form and also using the relation

$$\rho_r = \frac{M}{\frac{4}{3}\pi r^3}$$

then $$\omega = G \cdot \rho_r \cdot P \left(1 - \frac{b^2}{a^2}\right) \cdot \cos\theta$$

Now to estimate the number of precession cycles a galaxy will complete during its entire lifetime (say $\frac{1}{h} \times 10^{10}$ years), take the rotation period of the galaxy to be the same as for our galaxy, $P = 2 \times 10^8$ years

then $$N = \frac{1}{h} \times 10^{10} \text{ yrs} \times \frac{\omega}{2} = \frac{2.1}{h} \times 10^{25} \cdot \rho_r \cdot \left(1 - \frac{b^2}{a^2}\right) \cdot \cos\theta$$

The factor $\left(1 - \frac{b^2}{a^2}\right)$ should range from 0.88 for spirals to 0.50 for ellipticals; take 0.70 as a mean value. The factor $\cos\theta$ is constant

for any particular galaxy, but it must fall in the range from 0 to 1 ; for galaxies which spin in their orbital plane $\cos\left(\frac{\pi}{2}\right) = 0$ and they feel no precessional torque. Since forward and reverse precession will be indistinguishable, an average for all galaxies is $\langle|\cos\theta|\rangle = \frac{1}{2}$ and hence

$$N = \frac{7.5}{h} \times 10^{+26} \cdot \rho_r \quad .$$

ρ_r (in $g \cdot cm^{-3}$) should represent the density of matter interior to an average orbital radius r . Consider three different values of ρ_r using the Coma Cluster as an example; all values of ρ_r depend on the cluster's dynamic mass through the observed galaxy velocity dispersion (from Peebles 1971b)

(1) maximum central density $\rho_1 = 4.8 \times 10^{-25}\ h^2\ g \cdot cm^{-3}$

(2) cluster core density $\rho_2 = 1.4 \times 10^{-25}\ h^2\ g \cdot cm^{-3}$

(3) cluster density within $\frac{2\ Mpc}{h}$ $\rho_3 = 5.8 \times 10^{-26}\ h^2\ g \cdot cm^{-3}$

then

$$N_1 = 3.6 \times h$$
$$N_2 = 1.1 \times h$$
$$N_3 = 0.5 \times h$$

Because the Hubble constant has a value between 50 and 100 $km \cdot s^{-1} \cdot Mpc^{-1}$ the value of h falls in the range from 0.50 to 1 . It should be remarked that the core of the Coma Cluster is very likely above average since it appears to be one of the most relaxed clusters in the sample. Judging from the value of N_3 it appears that galaxies in the extreme

outer parts of the clusters should maintain their primordial orientation, and from the value of N_1 that galaxies in the cores of clusters will loose their original orientation. This result will depend somewhat on the central density of each particular cluster.

Disruptive Collisions

Sastry and Alladin (1970) have described the disruptive processes which accompany inner-penetrating galaxy collisions. The model galaxies used in their calculations were given polytropic mass distributions, and they considered only collisions between identical $10^{11} m_\odot$ galaxies, each with radii of 10 kpc. For a collision with an impact parameter of 2 kpc, the internal energy of each individual galaxy increases by approximately 20% (another small fraction of the energy is carried away by escaping stars). The change in the galaxy internal energy E will be accompanied by a change in the galaxy potential energy U. Using the relation

$$E = T + U$$

where T is the internal kinetic energy, and also using the virial condition (which can strictly be applied only after the galaxy reaches equilibrium)

$$2T = -U$$

$$\text{so} \qquad E = \tfrac{1}{2} U$$

$$\text{and} \qquad \frac{\Delta E}{E} = \frac{\Delta U}{U}$$

Because the galaxy potential is defined as a negative quantity, an increase in E causes a decrease in U. So as a result of the collision, the galaxy potential energy decreases by 20%; taking into account the distribution of mass in the galaxy, Sastry and Alladin predict an increase in the galaxy's radius of approximately 15%. The galaxy's radius will not increase equally in all directions, but it will increase most of all in the direction in which the two galaxies collide. Because even a single collision is quite effective in altering the galaxies' internal dynamics, it is necessary to estimate the frequency of close encounters between galaxies in clusters.

The number of random two body encounters between N objects in a closed system of radius r can be estimated by using the following relation

$$N_c = \frac{3\sqrt{2}}{4} \frac{v \cdot N^2 \cdot a^2}{r^3} \tau$$

where v = mean space velocity of the N objects

a = impact parameter of each object

τ = length of time during which the N_c encounters are calculated.

Consequently the frequency of collision for an individual object is given by the relation

$$\omega = \frac{N_c}{N} = \frac{3\sqrt{2}}{4} \frac{v \cdot N \cdot a^2 \cdot \tau}{r^3} \qquad (8)$$

Aarseth (1963) made extensive N-body calculations simulating the formation and evolution of clusters of galaxies. Included in his analysis

are comparisons between the predicted collision frequency and the actual number of collisions which occurred in the models. For a model cluster with 100 galaxies Aarseth found that the collision frequency is slightly higher (by perhaps a factor of 1.5) than the value predicted by equation (8). The increase is attributed to the formation of a cluster core during the cluster collapse. This additional factor will be included in the calculations which follow. If each of the N objects are of equal mass m then

$$\frac{N}{r^3} = \frac{\frac{4}{3}\cdot\pi\cdot\rho}{m} \qquad (9)$$

and the modified equation (8) becomes

$$\omega = \frac{N_c}{N} = \frac{3\pi\sqrt{2}}{2}\ \frac{v\cdot\rho\cdot a^2\,\tau}{m} \qquad (10)$$

To estimate an upper limit to the number of collisions per galaxy, the quantities on the right hand side of equation (10) will be taken from the dense Coma Cluster. To match the Sastry and Alladin calculation take the mass for each individual galaxy to be $m = 10^{11}\,m_\odot$ and take the impact parameter to be $a = 2$ kpc. For the Coma Cluster $v = \sqrt{3}\cdot\sigma_{v_r}$ $= \sqrt{3} \times 900\ \mathrm{km\cdot s^{-1}}$ (Rood, Page, Kinter, and King 1972), and for τ use the Hubble time $\tau = \frac{1}{h} \times 10^{10}$ years. Substituting these values into equation (10) gives

$$\omega = \frac{N_c}{N} = \frac{4.2 \times 10^{25}}{h}\rho$$

The three values quoted in the previous section for the Coma Cluster density give the following three collision frequencies

$$\omega_1 = 20. \times h$$

$$\omega_2 = 5.9 \times h$$

$$\omega_3 = 2.4 \times h$$

All three values are quite large, but of course they are intended to be upper limits. The largest source of error is introduced by using equation (9) to estimate N, the number of galaxies in the cluster. This estimate is bases on the total dynamic mass of the cluster, and the assumption is made that each individual galaxy has a mass of 10^{11} solar masses. Consequently N should be over-estimated by at least a factor equal to that of the "missing" cluster mass, namely by a factor of 7 (Rood et al. 1972). Furthermore, it is generally believed that $\frac{1}{2} \leqslant h \leqslant 1$, so both of these corrections reduce the collision frequencies to a level just large enough to be significant for the cluster core.

The conclusions can be summarized as follows. If a cluster is sufficiently dense, the galaxies which are confined to the core or pass repeatedly through it will undoubtedly suffer a fair number of collisions. Consequently for the galaxies in this study, only a small percentage have suffered disruptive collisions enough times to significantly alter their ellipticity or orientation.

General Summary

None of the five mechanisms discussed in the previous sections are important in drastically changing the total internal angular momentum of most galaxies. Perhaps a few galaxies suffer disruptive collisions (e.g., central cD galaxies), but most galaxies remain unaltered.

Origin of Galaxy Angular Momentum

To explain the origin of galaxy angular momentum, it is necessary to consider the more general problem of galaxy formation. In the brief review which follows, models of galaxy formation are discussed, and special emphasis is placed on how each model explains the origin of galaxy rotation. Particular attention is given to the observationally testable predictions which might allow one model to be distinguished from the others. A total of six models are discussed. All six are based on the assumption that the universe evolved from a hot big bang era to the present time leaving the remnant $2.7^{\circ}K$ background radiation. Initial isotropy and homogeneity are assumed in all cases. The six models of galaxy formation can be divided into two sets depending upon the origin of the fluctuations which eventually cause the gravitational collapse of galaxies. In models of the first set, statistical or thermal perturbations grow in time and eventually lead to gravitational instability and Jeans collapse. In models of the second set random velocity perturbations (i.e., turbulence) produce fluctuations in the density distribution, and these density irregularities (carrying along with them their velocity irregularities) become gravitationally unstable and collapse to form galaxies. Because the first half of this chapter dealt with the details of the collapse process and the possible subsequent evolution, the discussion which follows touches only upon the "primordial" origin of angular momentum.

Jeans (1929) was the first to seriously use gravitational instability theory to explain the origin and early evolution of

galaxies, but meaningful results were not obtained until gravitational instability was combined with the hypothesis of a uniformly expanding universe (Bonner 1957). The most comprehensive modern review of galaxy formation and gravitational instability is given by Field (1968). From the contents of Field's review it is quite apparent that the gravitational instability hypothesis suffers from a number of major deficiencies. One of the most important is its failure to explain the observed mass spectrum of galaxies. In the gravitational instability models, density fluctuations are supposedly the result of statistical perturbations (i.e., adiabatic $\sqrt{N}$ fluctuations) in the early universe which are amplified as time progresses. Without introducing ad hoc assumptions it appears that the only lasting perturbations are those associated with masses greater that $10^{11}\mathcal{M}_{\odot}$. Other more recent calculations places the limit in the range of $10^{12}\mathcal{M}_{\odot}$ to $10^{14}\mathcal{M}_{\odot}$(Peebles and Yu 1970, Chibisov 1972). And consequently there is no easy way to account for the many galaxies with masses between $10^{8}\mathcal{M}_{\odot}$ and $10^{11}\mathcal{M}_{\odot}$. Statistical perturbations are not the only ones which might be considered, but it is not entirely clear what other perturbations are the most natural to consider. The simplicity of the gravitational instability approach is destroyed by requiring that the hypothesis be extended to include some other type of perturbation. In the discussion which follows note that each model has its own solution to this problem.

Tidal Acceleration of Spherical Protogalaxies

Hoyle (1949) was the first to propose that tidal interactions between protogalaxies might transfer orbital angular momentum into

rotational angular momentum. In that preliminary analysis Hoyle simply used the observed masses and densities of galaxies to estimate very roughly the importance of the mechanism. Peebles (1969, 1971a) carried the idea much further by basing his calculations on a more complete evolutionary picture. In the view adopted by Peebles, protogalaxies are aglomerations of globular cluster sized clouds. Special preference is given to the globular cluster mass scale because Peebles and Dicke (1968) found that a gaussian distribution of density and velocity perturbations which are subjected to Jeans instability at the time of recombination produce a mass spectrum which peaks at the mean mass of globular clusters. In the gravitational instability picture there is no a priori justification for introducing any perturbations at the time of recombination. Although the model looks appealing because globular clusters are naturally explained, the major downfall of this protogalaxy model seems to be its inability to explain the separation of matter on the scale of galaxies. This well recognized problem is ignored by Peebles, and the angular momentum calculations are made anyway.

Peebles calculation of the angular momentum transfer process is divided into two parts. The first is a perturbation analysis describing the situation just as the galaxies begin to separate from the background. The second part is a conventional tidal interaction calculation which is most important when the galaxies are well separated from one another. In the first paper, Peebles (1969) found analytic solutions for both cases and applied these solutions to the model of galaxy formation described above. In the second paper (Peebles 1971a), an N-body

galaxy simulation was followed through the collapse process, and this model was used to check the accuracy of the analytic solution. It was found that the N-body model and the analytic solution agreed fairly well with one another, but they both fell short by a factor of 5 in predicting the observed angular momentum of our Galaxy. As a further check of this model the analytic solution will now be used to predict how angular momentum might depend upon the mass of a galaxy or upon the mean density at its place of formation.

First the Peebles' angular momentum density perturbation analysis will be briefly explained; for more details see section IIb in Peebles (1969). To calculate the angular momentum associated with a galaxy of mass M, Peebles integrated the relation

$$L = \int \rho \cdot \vec{r} \times \vec{v} \; d^3r$$

over an arbitrarily placed spherical volume just large enough to contain the desired final mass M. The coordinate system for $\vec{r}$ and $\vec{v}$ is fixed to the center of the spherical volume. Because the density ρ and the velocity $\vec{v}$ each have a range of possible values centered around their mean values, the angular momentum can be split into two parts: (1) the angular momentum associated with the translation of the center of mass, and (2) the actual internal angular momentum associated with the developing galaxy. The quantity of interest is the second of these, and Peebles finds that its mean square value is

$$\langle L^2 \rangle^{1/2} = 0.15 \; M R^2 \; \frac{\langle \delta_s^2 \rangle}{t}$$

where the parameters of the developing protogalaxy are

L = angular momentum

M = mass associated with the perturbation

R = radius in local "Minkowski" coordinates

δ_s = fractional variance of the mean density

t = time

To estimate δ_s^2 Peebles recognized that galaxies expand with the universe until they reach a maximum extension of R_m at t_m, and then the collapse process begins, and δ_s starts to grow. So roughly

$$\langle \delta_s^2 \rangle^{1/2} = \frac{3}{5} \left(\frac{3 \cdot \pi \cdot t}{4 \cdot t_m} \right)^{2/3}$$

where $$t_m \equiv \left(\frac{\pi^2 R_m^3}{8 \cdot G \cdot M} \right)^{1/2}$$

then $$\langle \delta_s^2 \rangle = \frac{9}{25} \left(\frac{9}{2} \frac{G \cdot M}{R_m^3} \right)^{2/3} \propto \rho_m^{2/3}$$

so $$\langle L^2 \rangle^{1/2} \propto [M \cdot R^2] \cdot t^{1/3} \rho_m^{2/3} \qquad (11)$$

with ρ_m identified with the density of the protogalaxy material at the time of maximum extension. Note that the parameter ρ_m describes the local conditions at the site of galaxy formation, and equation (11) indicates that a galaxy formed in a high density region (i.e., the core of a rich cluster) should have a larger angular momentum than an

identical galaxy (one with the same $[M \cdot R^2]$) in a low density region. The other important point is the relation between a galaxy's angular momentum and its mass or radius. Equation (11) predicts that for galaxies formed under identical conditions

$$\langle L^2 \rangle^{1/2} \propto M\ R^2 \quad .$$

In order to eliminate the dependence on radius, use the relation found by Fish (1964) between (elliptical) galaxies' potential energy and mass $\Omega \propto M^{3/2}$. Because $\Omega \propto G \cdot M^2/R$ then $M \propto R^2$ and the expected relation between the angular momentum and mass should be

$$L \propto M^2 \quad .$$

Next the second part of Peebles model, tidal interactions between well separated galaxies, will be considered. Let a distant mass M apply a torque to the galaxy in question. Take

$N = \frac{dL}{dt}$ = applied torque

a = galaxy's semimajor axis

b = galaxy's semiminor axis

r = separation between the galaxy and mass M

θ = angle between galaxy's rotational axis and the direction to mass M

Also assume that all galaxies in the system have mass M , then

$$N = \frac{dL}{dt} = \frac{3}{4} \frac{G\,M}{r^3} \cdot \frac{2}{5} M\,(a^2 - b^2) \cdot \sin 2\theta$$

In the following step Peebles used this torque to calculate the ensemble average torque which a galaxy would feel if it were a member of a group of identical galaxies all at a mean separation r. With these assumptions the constant mean square average torque is

$$\langle N^2 \rangle^{1/2} = \frac{4}{25} \frac{G M^2 (a^2 - b^2)}{r^3}$$

Identifying $\rho_G = \frac{M}{\frac{4}{3} r^3}$ as the mean group density and by making the assumption that the configuration of surrounding galaxies changes very little during the collapse process then $L = N \times t$ (otherwise a changing galaxy configuration would give $L \propto \sqrt{t}$) so that

$$\langle L^2 \rangle^{1/2} = \frac{16}{75} \pi \cdot G \cdot \rho_G \cdot t \cdot M (a^2 - b^2) \qquad (12)$$

Again the angular momentum relation takes on nearly the same form as before but with a slightly stronger dependence on the density ρ_G, and equation (12) also implies that the regions of higher density should contain galaxies with large angular momentum. Separating out the dependence on galaxy mass and radius

$$L \propto M \cdot (a^2 - b^2) = M \cdot a^2 \left(1 - \frac{b^2}{a^2}\right)$$

so for a spherical galaxy no systematic angular momentum is transferred, but for flatter galaxies $L \propto M \cdot a^2$. This relation is valid only for galaxies in regions with the same ρ_G; and if the relation found by Fish (1964) between galaxy mass and potential energy is used then $\Omega \propto M^{\frac{5}{3}}$ or since $\Omega \propto G M^2/R$ then $R^2 \propto M$ and of course $a \simeq R$ so

$$L \propto M^2 \quad . \qquad (13)$$

The relation in equation (13) is an important test of the model, but nearly the same relation turns up quite often in the other models discussed below. There is one decisive prediction that this model makes: galaxies in the denser regions should feel more tidal acceleration, and consequently they should have larger mean angular momenta.

Formation of Galaxies by Gravitational Accretion

For the second model of galaxy formation consider the gravitational accretion process. A wide variety of protogalaxy models are able to produce the intermediate conditions necessary for gravitational accretion to proceed. To meet these conditions each density irregularity (which eventually will be identified with an individual galaxy) must contain a set of massive clouds, and each of these clouds must have its own peculiar velocity. The properties of the resulting galaxies depend upon the mass and velocity distributions of these clouds and also upon the exact way in which the clouds interact and finally coalesce. In testing this model with the data, it is only possible to decide whether these intermediate conditions were present at an earlier time, and very little can be said about the initial perturbations which might be responsible for producing the intermediate conditions. There are at least three models which are capable of producing these intermediate conditions. First, a gravitational perturbation scheme might provide suitable conditions. In the perturbation model of Peebles and Dicke (1968) a protogalaxy is composed of numerous globular cluster sized

clouds which quiescently fragment into stars and then merge into a galaxy. If this same system proceeds through gravitational accretion before star formation, then the discussion in this section would apply. Second, velocity induced (turbulent) perturbation schemes might produce the necessary intermediate conditions. This possibility was investigated by Silk and Ames (1972), and their results seem to indicate that decaying turbulent motions might produce suitable velocity and density perturbations. The third model which fits into this scheme was developed by Layzer (1964, 1968). Starting with an initially cold universe, Layzer followed gravitational instability through a series of "hierarchical clustering" scales attempting to identify each characteristic scale with a particular type of object (e.g., star clusters, galaxies, galaxy clusters). No further attention will be given to these protogalaxy models, since they might all lead to an indistinguishable set of intermediate conditions. The analysis will proceed under the assumption that one of these models is capable of producing the desired results.

In the context of galaxy formation, gravitational accretion models have received only cursory treatment. Silk and Lea (1973) discussed the important energy losses incurred by colliding galaxy sized clouds, but their main purpose was to trace galaxy kinetic energy loss mechanisms backwards in time starting with the presently observed state of galaxies. They briefly showed that the observed angular momentum of galaxies fits to an order of magnitude to the angular momentum produced by colliding and coalescing galaxy sized masses. Gravitational accretion models have received more attention in attempts

to explain the origin of planets in the solar system. In the most general models (cf., Alfven and Arrhenius 1970 and Marcus 1967), the situation applies equally well both to galaxies and to planets, and some interesting comparisons can be made between these two sets of objects. The transfer of angular momentum can be viewed simply as a series of successive two body collisions. To find the maximum amount of angular momentum which might be transfered, consider two sub-galaxy sized clouds each with a mass $M/2$ which fuse to form a galaxy with a total mass M. If their relative velocity is v and the impact parameter of the collision is R, then

$$L_{max} = \epsilon \cdot M \cdot v \cdot R/2$$

where ϵ is the efficiency of converting translational motion into rotational motion. If the clouds fall toward each other from infinity then their relative velocity v is simply their escape velocity

$$v_e = \left(\frac{8}{3} \pi G \rho \right)^{\frac{1}{2}} R$$

where again R = the impact radius of the last collision (or the total radius of the galaxy at the time of the collision), and with

$$\rho = \frac{M}{\frac{4}{3} \pi R^3}$$

then

$$L_{max} = \left(\frac{G}{2}\right)^{1/2} \epsilon \, M^{3/2} R^{1/2} \quad . \qquad (14)$$

If the spin-up process involves multiple collisions then the final angular momentum will be degraded by collisions which impact at any point other than the receding equatorial plane. This degradation can be expressed in terms of the angle β between the velocity vector $\vec{v}$ (of the cloud mass Δm) and the radius vector from the center of the protogalaxy to the impact point $\vec{R}$. In this case each collision adds a maximum angular momentum $\Delta\vec{L}$ where

$$\Delta\vec{L} = \Delta m \cdot \vec{R} \times \vec{v}$$

or

$$|\Delta L| = \Delta m \cdot R \cdot v \cdot \sin\beta$$

The final value of the angular momentum depends critically upon the mass distribution function of the colliding clouds. If the largest fraction of the mass is contained in a few very massive objects then the final angular momentum is determined by the peculiar geometry of each collision. But if the mass is equally divided among a large number of identical masses, then the mean value of $|\sin\beta| = \frac{1}{2}$ and $\Delta L = \frac{1}{2} L_{max}$.

Two predictions can be made from this model. First, if galaxies gain their angular momentum during the collision of a very few massive protogalaxy clouds, then the final value of L might be lower for the more massive objects (which form from 5 to 10 protogalaxy clouds) and higher for the less massive objects (which form from just a few protogalaxy clouds). Spheroidal dwarf ellipticals might be identified with protogalaxy clouds which never collided. The second prediction follows from equation (14). Using the relation found by Fish (1964) between the potential energy and mass of a galaxy $\Omega \propto G M^2/R \propto M^{5/3}$ then $R \propto M^{1/3}$

and equation (14) implies that

$$L_{max} \propto M^{7/4} .$$

This model is far from complete and many details remain to be worked out. The studies of solar system gravitational accretion indicate that large collision velocities are more likely to cause fragmentation than accretion. In fact the relative particle velocities necessary to explain planetary rotation are usually found to be too high rather than too low. For galaxy formation it is necessary to insure that the collision cross sections for galaxy sized clouds are large enough to allow a reasonable number of collisions during the period of galaxy formation. The preliminary calculations of Silk and Lea (1973) indicate that the necessary conditions for galaxy formation are at least reasonably satisfied.

Gravitational Instability of a Protocluster Disk

Sunyaev and Zeldovich (1972) proposed a model of galaxy formation in which massive protoclusters collapse to thin disks and subsequently fragment into individual galaxies. The protocluster mass scale ($M = 10^{12}$ to $10^{14}\ m_\odot$) is of special importance because it can be identified with the largest adiabatic (random $\sqrt{N}$) perturbations which remain undamped through the epoch of recombination. Even though the adiabatic perturbations are not strong enough to initiate gravitational collapse, Sunyaev and Zeldovich propose that the strongest perturbations are the ones most likely to be amplified during the recombination

process. The preference for disk-like protoclusters was obtained by Zeldovich in an analysis of gravitational instability in an expanding pressure-free medium. The collapse of the cluster into a thin disk (with "infinite" density) produces a number of interesting and involved physical effects. The Sunyaev and Zeldovich (1972) paper concentrated mainly on the thermal effects of shock waves produced during the collapse process, while two other papers by Doroshkevich (1973a, 1973b) present the general implications for galaxy formation.

Because the protocluster fragments into galaxies during the rapid collapse phase, Doroshkevich was able to make only very qualitative predictions about the mean properties of the galaxies which are produced. By relying solely upon an analysis of the growth of nonlinear gravitational instabilities (and ignoring turbulence effects), the first paper by Doroshkevich (1973a) made a number of predictions about galaxy rotation which the second paper (Doroshkevich 1973b) reversed. It seems that the turbulent velocities produced at the surface of the collapsing protocluster play an influential role in the origin of galaxy rotation. Even though no attempt was made to find a galaxy mass-angular momentum relation, a calculation of the protoclusters internal angular momentum content was made. An exact mass-angular momentum relation seems to be beyond the scope of the present analysis. Even so, a number of other interesting and testable predictions are made. First, the angular momentum vectors of all galaxies should lie (approximately) in the plane of the protocluster disk. Second, galaxies formed at the upper and lower surfaces of the cluster

should have oppositely directed angular momentum vectors. And a number of predictions are made on the basis of equation (24) in Doroshkevich (1973b):

$$\langle L^2 \rangle^{1/2} \propto L_0 \, n_1^4 \cdot r_3 \, / \, (\lambda_{11}) \qquad (15)$$

where

L = galaxy angular momentum

L_0 = angular momentum content of disk material

n_1 = distance of galaxy above plane of disk

r_3 = polar distance of galaxy from the center of the disk

λ_{11} = component of the deformation tensor in the non-linear instability calculations

$$\lambda_{11} = \sigma \nu f + \frac{3\sigma}{\sqrt{2\pi}}$$

σ = dispersion in the density perturbation

f = density autocorrelation coefficient

ν = normalized strength of the perturbation

The dependence of λ_{11} on the density of the medium implies that the value of $\langle L^2 \rangle^{1/2}$ decreases as the density of the cluster increases. This dependence implies that lower density clusters should contain galaxies with larger angular momenta, and also that among galaxies formed within a single cluster those formed in the high density central regions should have a lower mean angular momentum. The n_1 and r_3 dependences in equation (15) also demonstrate that galaxies in the outer regions of the clusters should have larger angular momenta. Finally, the angular momentum content of the disk material was calculated to be

$$L_o = 3 \times 10^{31} \Omega^{-\frac{1}{2}} (1 + z_c)^{-\frac{1}{2}} \text{ cm}^2 \cdot \text{sec}^{-1}$$

with $z_c = 4$ = redshift at the epoch of cluster formation and

Ω = density of universe / closure density ≤ 1 .

So $L_o = 1.5 \times 10^{31}$ cm$^2 \cdot$sec^{-1} and the corresponding value for our Galaxy is $L = 4 \times 10^{29}$ cm$^2 \cdot$sec^{-1} . Consequently the predicted angular momentum content is more than adequate to explain the angular momentum of individual galaxies, but of course it depends somewhat on the values of z_c and Ω .

Turbulence Models of Galaxy Formation

Whereas the three previous models of galaxy formation are based on primordial density irregularities, the next three models are based on primordial velocity irregularities (i.e., turbulence). Gamow (1951) and von Weizsacker (1951) published the first modern account of how a galaxy might form in a turbulent medium. This early work was criticized from two standpoints. First, without any reservoir of energy to supply the turbulent motions, viscous decay rapidly destroys all turbulence (Ozernoi and Chernin 1968). Second, if any turbulence survives until the recombination era, post-recombination supersonic turbulence produces density irregularities which prematurely collapse into objects bearing no resemblance to galaxies (Peebles 1971c). It now appears that Peebles' criticism might not apply if magnetic fields are produced during the pre-recombination turbulent era (Harrison 1973). There are other problems with the turbulence models which stem from a poor understanding of basic turbulence theory. First, incompressible turbulence

in an infinite medium is poorly understood (Creighton 1969). Second, the dissipation of turbulence through eddy viscosity or through the generation of density irregularities is also poorly understood (Jones 1973). And finally, supersonic turbulence is understood only in a very qualitative sense. It is necessary to understand all three of these mechanisms in order to give an adequate description of primordial turbulence. In the following paragraphs three models of galaxy formation are discussed. The first two conflict with one another on the basis of turbulence theory. And the third model is based on a cluster collapse scheme with many similarities to the Sunyaev and Zeldovich work.

Turbulence Model of Ozernoi

Ozernoi and Chernin (1968, 1969) and Ozernoi and Chibisov (1971) have presented a scheme for galaxy formation in which photon turbulence provides a reservoir of energy to counter dissipative effects. In this model the photon turbulence of the high density radiation field is linked to the ionized plasma through Thomson scattering. This energy source continues to supply turbulent energy until the epoch when the radiation and matter energy densities are equal to one another. After the radiation and matter decouple, the turbulent motions are strongly damped, but it appears that certain scales are able to maintain their rotational motions (Dallaporta and Lucchin 1972). Those turbulent eddies which survive can be associated with a density perturbation; the amplitude of this perturbation is a matter of controversy (see next model by Jones 1973), but Ozernoi and associates take its value to be

$$\frac{\delta \rho}{\rho} = \frac{v^2}{c_s^2}$$

where v = velocity of turbulence and c_s = the velocity of sound. Because the velocity of sound decreases drastically at the time of recombination, the turbulent motions become supersonic, and no present day theory adequately predicts the consequences. Ozernoi assumes that each perturbation maintains its identity during recombination, that the turbulent velocity distribution changes from the pre-recombination Kolmogorov spectrum ($v \propto r^{1/3}$) to a post-recombination state of correlated shock waves ($v \propto r$), and that the perturbations are significantly amplified.

The amplitude of the perturbations are still relatively small at the time of recombination, but they grow as the universe evolves. Eventually the mass associated with each perturbation becomes unstable and collapses to form a galaxy. Using the virial theorem as a stability criterion and the characteristics of the turbulence spectrum, Ozernoi and Chibisov (1971) find a mass versus angular momentum relation.

$$L \propto M^{5/3} \quad .$$

For galaxies as massive as our own, they find a specific angular momentum $L/M = 2 \times 10^{29} \Omega^{-1/6}\ cm^2 \cdot sec^{-1}$ where Ω = mean density of the universe / closure density. This value for the angular momentum falls short of the observed value for the Milky Way by a factor of 3 (Innanen 1966).

In this model the processes important to the origin of galaxy rotation all occur early in the history of the universe, so the density amplifications associated with clusters of galaxies are rather small. Since

$$\frac{\delta\rho}{\rho} \propto t^{2/3} \propto (1 + z)^{-2/3}$$

then the present day density contrast for clusters $\frac{\delta\rho}{\rho} \lesssim 10^3$ with $z \simeq 10^4$ at recombination implies that $\frac{\delta\rho}{\rho} \lesssim 1/3$ at the time of recombination. At earlier epochs when turbulent dissipation occurs, this density irregularity is even smaller. Even so, significant effects might be produced because the dissipative processes are strongly dependent on density. Jones (1973) finds that for the Ozernoi model the angular momentum at the largest mass scale has a density dependence

$$L \propto \Omega^{-15.3}$$

where again Ω = mean density / closure density. If this extreme relation is real, then even a 5% cluster density enhancement could lead to a 50% drop in the mean angular momentum. This might be a plausible way to explain why galaxies with low angular momentum are located in the cores of rich clusters.

Jones (1973) critically re-examined the turbulence theory of Ozernoi and found that the approximation

$$\frac{\delta\rho}{\rho} = \frac{v^2}{c_s^2}$$

does not adequately describe the perturbations associated with primordial turbulence. Using the work of Creighton (1969), Jones argues that density enhancements with $\delta\rho/\rho \simeq 1$ are associated with velocity scales of

$$v \gtrsim 0.04 \cdot (\Omega h^2)^{-2/7} \cdot c \qquad (16)$$

The Ozernoi model will work only if these extreme density enhancements are avoided. Combining equation (16) with the condition that some turbulent scales must survive until the epoch of recombination, Jones finds that $(\Omega h^2) < 0.06$. This constraint is itself a very severe test of the Ozernoi model.

Turbulence Model of Jones

Jones (1973) presented a model of galaxy formation based on the turbulence theory of Creighton (1969). This turbulence theory implies that large density irregularities with $\delta\rho/\rho \simeq 1$ are associated with all turbulent velocity scales v_* if

$$v_* \gtrsim 0.015 \cdot (\Omega h^2)^{-2/5} \cdot c$$

where Ω = mean density of universe / closure density, h = Hubble constant / 100 $km \cdot s^{-1} \cdot Mpc^{-1}$, and c = velocity of light. When these strong density irregularities are produced, Jones surmises that they initiate the formation of bound gravitational systems. Irregularities are produced on all mass scales above some minimum mass M_{min} which is determined by the value of v_*. Masses less than M_{min} have $\delta\rho/\rho < 1$, and their turbulent motions always contain more energy than their

potential motions; consequently they are not able to form gravitationally bound systems.

The choice of (Ωh^2) determines not only the minimum mass scale, but it simultaneously determines the specific angular momentum for all turbulent matter. In order to match the observed angular momentum of our Galaxy, it is necessary to take $(\Omega h^2) = 0.25$, and the corresponding value of the minimum mass is $M_{min} = 10^{12}\,\mathcal{M}_\odot$. But if M_{min} is to be identified with the lowest mass galaxies (masses $\simeq 10^8\mathcal{M}_\odot$) then $(\Omega h^2) = 0.25$ is not a suitable value. In order to account for glaxies down to $M_{min} = 3 \times 10^8\mathcal{M}_\odot$ it is necessary to take $(\Omega h^2) \simeq 3$ but in this case the predicted angular momentum for our Galaxy falls short of the observed value by a factor of 3000. Jones prefers the value $(\Omega h^2) = 0.25$ and argues that even the conventional gravitational instability model is unable to account for the small perturbations which produce low mass galaxies.

Jones' model has the advantage over the Ozernoi model in that supersonic turbulence is totally avoided. The velocity induced instabilities occur in the Jones model long before the epoch of recombination. The internal turbulent motions are damped sufficiently soon, so they are well below the velocity of sound at the epoch of recombination. In fact the turbulent velocity spectrum freezes out (i.e., $t_{damping} \gg t_{expansion}$) for all mass scales greater than M_{min}, and the velocity spectrum takes the form $v \propto r$. Jones finds that the mass versus angular momentum relation is

$$L \propto M^{5/2} ,$$

although this relation is somewhat questionable.[1] No calculations were made relating the angular momentum to the density of a specific region, but Jones finds that the angular momentum of the largest mass scale follows the relation

$$L \propto (\Omega h^2)^{-6}$$

where Ω is directly related to the mean density of the universe. This result seems to indicate that galaxies formed in high density regions will have lower mean angular momenta.

Collapse of Massive Prolate Spheroidal Protoclusters

In a model developed by Icke (1973), large scale velocity perturbations induce the collapse of massive prolate spheroids which are identified with protoclusters of galaxies (masses between 5×10^{14} and $5 \times 10^{16} \mathcal{M}_\odot$). Subsequent fragmentation of the material inside the protoclusters produces individual galaxies and residual intergalactic matter. The fragmentation into galaxies is initiated by the increasing density of the intracluster material, and the resulting characteristics of each galaxy, including the angular momentum, depend upon the hydrodynamic and thermal details of the collapse process. Clusters which are initially very nearly circular, collapse in a preferential direction because of the initial anisotropic velocity perturbation; and the

---

1. This follows from equation (52) in Jones (1973), $M \propto h^{3/3}$ where h = angular momentum per unit mass. Although no derivation is given for this relation, the inverted relation $h \propto M^{3/3}$ can be derived by combining the virial condition for galaxy collapse with the velocity spectrum relation $v \propto r$. Jones uses equation (52) in his calculations but in the following discussion implies that he has found the conventional relation $h \propto M^{3/3}$ relation.

clusters become progressively more prolate as the collapse proceeds. The overall cluster anisotropy also influences the formation process of the individual galaxies, and the model predicts that galaxies should be preferentially aligned in the direction of the prolate spheroid's major axis (i.e., the cluster's major axis). Furthermore, a galaxy's (intracluster) velocity should depend directly on its position of formation along the protocluster's major axis.

The model proceeds nicely through the protocluster collapse calculations, but as Icke states the processes involved in galaxy formation depend upon a number of critical assumptions. A linear perturbation analysis is used to follow the changing galaxy potential, density, pressure, and velocity variables. These first order solutions imply that the perturbation density and velocity grow without bounds. To avoid supersonic velocities and subsequent dissipative shocks, the maximum streaming velocity is artificially limited at the local speed of sound. This velocity limitation causes the temperature and the Jeans mass to increase as the perturbation analysis proceeds. Although the solutions obtained are realistic, it is not clear that they accurately describe the precise way in which galaxies are formed. Other numerical problems are encountered in an attempt to calculate the angular momentum for individual galaxies. A full solution to the problem of turbulence and the "kinematics of deformation" is abandoned after it leads into considerable numerical complication, and the analysis falls back on a simpler energy balance relation between the components of the deformed field. Icke finds that this rough analysis is capable of explaining

(to an order of magnitude) the total angular momentum of our Galaxy, and he also finds a mass versus angular momentum relation $L \propto M^{5/3}$. These angular momentum results apply only to protogalaxies formed from several adjacent mass elements which happen to have parallel rotation axes. The probability of this actually occurring is left undiscussed.

Icke's model is nicely divided into two parts, one relating to cluster formation and the other to galaxy formation. The section on cluster formation is very straight forward, and in many ways is similar to the Sunyaev and Zeldovich model which was described before. The collapse processes involve no special assumptions, and most of the predictions made by the model (oblate cluster shape, centrally condensed galaxy distribution, systematic galaxy velocity within a cluster) are reasonable and observationally easy to test. But the details of the galaxy formation process are less reliable, and they depend on some very special assumptions. It seems reasonable to expect that growing instabilities in the direction of cluster collapse will cause a preferential direction in the collapse of many individual galaxies, and hence will produce a galaxy alignment effect. But beyond this point, the conclusions become more and more dubious. The detailed predictions for the origin of galaxy angular momentum are especially tenuous, and perhaps is is not surprising that the mass versus angular momentum relation found by Icke is the same as in the Ozernoi and Chernin model, namely that

$$L \propto M^{5/3}.$$

Table 7. Summary of Theoretical Models

Parameter \ Model	Tidal Acceleration	Gravitational Accretion	Protocluster Disk	Ozernoi Turbulence	Jones Turbulence	Icke Prolate Spheroid
Angular Momentum vs. Galaxy Mass	$L \propto M^2$	$L \propto M^{7/4}$	?	$L \propto M^{5/3}$	$L \propto M^{5/2}$	$L \propto M^{5/3}$
Angular Momentum vs. Cluster Density	L increases when ρ increases	?	L increases when ρ decreases	L increases when ρ decreases	L increases when ρ decreases	L increases when ρ decreases
Possible Alignment	No	No	Yes	?	?	Yes
Maximum* $\frac{L_{theory}}{L_{Galaxy}}$	0.2	10	35	1	1	1

* Numbers quoted for this quantity are only approximate and in most cases depend on the redshift at the epoch of galaxy formation and also on the mean density of the universe. See the discussions of each individual model for details.

CHAPTER VI

INTERPRETATION AND CONCLUSIONS

In this final chapter the observational results are reviewed and then compared with the theoretical model predictions. The peculiar properties of the cluster A 2197 are also briefly discussed, and a few suggestions are given as to how one might find another cluster which shows galaxy alignment.

Comparison of Observational and Theoretical Results

In order to easily compare the theoretical model predictions as listed in Table 7 with the observational data, a brief summary of the observational results will now be given.

1. Galaxies in the cluster A 2197 show a significant alignment effect (χ^2 probability < 0.0002), and the preferential direction of alignment corresponds approximately to the major axis of the overall cluster elongation (see Figure 13 below). Galaxies in the cluster core are less significantly aligned than the galaxies in the cluster halo. This result can be interpreted in terms of a slow dynamic reorientation for galaxies which are confined to the dense cluster core.
2. None of the other seven clusters show any systematic position angle effects, but the ellipticity distribution of A 400 indicates that galaxies in this cluster might be preferentially

aligned with the plane of alignment nearly parallel to the plane of the sky. Besides this questionable case, the other clusters show remarkably ramdom orientation effects. This includes the cluster A 2199 for which Rood and Sastry (1972) reported a marginal alignment effect.

3. A significant fraction of the galaxies in the symmetrical Coma Cluster (A 1656) show a preferential radial alignment effect. This result was previously reported by Gainullina and Roshjakova (1967) for the two clusters A 1656 and A 2065 (Corona Borealis). Besides A 1656, none of the other clusters in this study showed any significant radial alignment trends. The effect in the two rich symmetrical clusters might be interpreted in terms of the disruption of galaxies which pass repeatedly through the dense cluster core.

4. In four clusters the spiral galaxy samples were large enough to analyze the number distribution of forward and reverse winding spirals. Very balanced distributions were found in all cases, including the sample for the cluster A 2197.

5. The distribution of intrinsic ellipticities for E galaxies is very broad and peaks at $\epsilon = 4$; there are very few E galaxies with intrinsic ellipticities equal to zero. These results agree with the analysis of Sandage, Freeman, and Stokes (1970).

6. SO galaxies appear to have a double peaked intrinsic ellipticity distribution with one peak at $\epsilon = 4$ and the other at $\epsilon = 7$. This result might be caused by the confusion of E galaxies for

SO galaxies because the classifications were obtained from low scale plate material (Palomar Sky Survey plates).

7. Spiral galaxies have a narrow intrinsic ellipticity distribution centered on $\epsilon = 7.5$.

8. Large and small spiral galaxies have identical ellipticity distributions. Using the results of King (1961) and also Ozernoi (1967), if a galaxy is a gravitationally relaxed ellipsoid with its ellipticity determined only by its total rotational energy, then the total angular momentum L follows the relation

$$L \propto M^{5/3} \rho^{-1/6} f(\epsilon)$$

where M = galaxy mass, ρ = galaxy density, and $f(\epsilon)$ is a function of the galaxy ellipticity. If ϵ is independent of galaxy mass as the data indicate, then ignoring the very weak dependence on density $L \propto M^{5/3}$.

9. Large and small E galaxies have very slight ellipticity differences so that the same $L \propto M^{5/3}$ relation should hold. If the slight ellipticity difference is significant, the the exponent should be somewhat less than $5/3$.

10. The large SO galaxies tend to be more spherical than the small SO galaxies. This again indicates that the angular momentum relation $L \propto M^{\alpha}$ should have $\alpha < 5/3$, simply because the larger SO galaxies have proportionately less angular momentum for their mass than the smaller SO galaxies, implying a less steep relation between L and the galaxy mass M . This result

depends of course on the assumption that there is no confusion in the morphological classification between E and SO galaxies.

11. A comparison between the cluster population and the halo or "field" population shows that E galaxies occur mainly within the central regions of the rich clusters, whereas spiral galaxies occur most frequently in the halo or field population.
12. The intrinsic ellipticities of E, SO, and spiral galaxies which which are found in rich clusters (this study) are identical to the intrinsic ellipticities of these same galaxies found in the "field" population (results of Sandage, Freeman, and Stokes 1970).

Concluding Remarks Relating Each Theoretical Model to the Observational Results

Tidal Accleleration Model. Although the predicted $L \propto M^2$ relation is nearly the same as the observed $L \propto M^{5/3}$, the model improperly predicts that galaxies found in the dense cores of clusters should have the largest angular momenta. Points (5), (7), and (11) show that in fact the galaxies with the lowest mean ellipticities (and hence the lowest mean angular momenta) fall in the dense regions of the cluster cores. The tidal acceleration model is not compatible with the alignment effect observed in the cluster A 2197. And there is the previously published objection that the model falls short by a factor of five in predicting the total angular momentum of our galaxy.

Gravitational Accretion Model. The predicted relation $L \propto M^{7/4}$ comes fairly close to the observed result and it might apply directly to E and SO galaxies (points 9 and 10). But the model has no satisfactory explanation for any preferential alignment effects. And the model has the inherent problem of requiring just the right number of accretion collisions to produce the various galaxy morphological types, from dwarf ellipticals to spirals.

Turbulence Models of Ozernoi and Jones. Potentially either of the turbulence models are capable of explaining all of the observational effects summarized above. The major problem is the traditional one of maintaining the turbulent motions in spite of strong dissipative effects. As the models are now formulated, they assume that the entire universe is isotropic, and no account is given for cluster formation. It seems possible that some form of systematic galaxy alignment might occur during the process of cluster formation as the models of Icke and Doroshkevich have done. And the mass versus angular momentum relation $L \propto M^{5/3}$ is accurately predicted by the Ozernoi turbulence theory.

Protocluster Disk and Prolate Spheroid Models. Among all the other models, these two are most successful in explaining all of the observational results. Even though the mechanism for forming the cluster is different for each of the two models, the galaxy formation processes within each of the protoclusters are very similar. In the denser central regions of each cluster, galaxies of low ellipticity are formed, and in the holo of the cluster galaxies of high ellipticity are

formed, consistant with point 11. Doroshkevich (1973b) even predicts point (4); that is, spiral galaxies should be evenly divided between forward and reversed winding spirals even for the cluster A 2197. Many details of this model remain to be worked out, and one of the major problems is to explain why one cluster shows alignment of galaxies while the other seven clusters do not.

Special Properties of A 2197

Because A 2197 is the only cluster which definitely shows alignment of galaxies, it is important to find what other special characteristics this cluster possesses. Knowing these special characteristics, it might be possible to predict which other clusters might also show preferential alignment effects. A 2197 has two outstanding properties which might be related to the galaxy alignment effect. First, Rood and Sastry (1971) classified this cluster as "L", meaning that it is dominated by a linear distribution of bright galaxies. And the position angle orientation of this linear distribution coincides approximately with the direction of preferential alignment. The second outstanding feature of A 2197 is its close proximity to the cluster A 2199. The overall geometry of the field containing both A 2197 and A 2199 is presented in Figure 13. The contours are drawn approximately at levels of constant surface brightness. Because the redshifts of both clusters are very similar, it is quite likely that the two clusters are near neighbors of one another. This close relationship might be an important factor in explaining the galaxy alignment effect, but it is logical to ask why A 2197 shows galaxy alignment but A 2199 does not. To check the

possibility that the close pairing causes the alignment effect, there are other close cluster pairs which might be analyzed (e.g., the pair A 399 and A 401). The other possibility is to check for galaxy alignment in the clusters which Rood and Sastry (1971) have classified as "L". If galaxies in "L" clusters are found to be predominately aligned in the direction of the cluster elongation, then it will be necessary to conclude that the origin of galaxy angular momentum is intrinsically related to the cluster collapse process.

Figure 13. Luminosity Map of A 2197 and A 2199 Cluster Area

Adjoining cluster areas of A 2197 (top) and A 2199 (bottom) shown at contour intervals of 25, 26, and 27 magnitudes per square second of arc. The individual galaxy luminosities were obtained from a diameter versus luminosity relation, and the luminosity in each grid square was summed and then slightly smoothed to simulate a beam with a diameter of 4 minutes of arc. North is to the top and east is to the left.

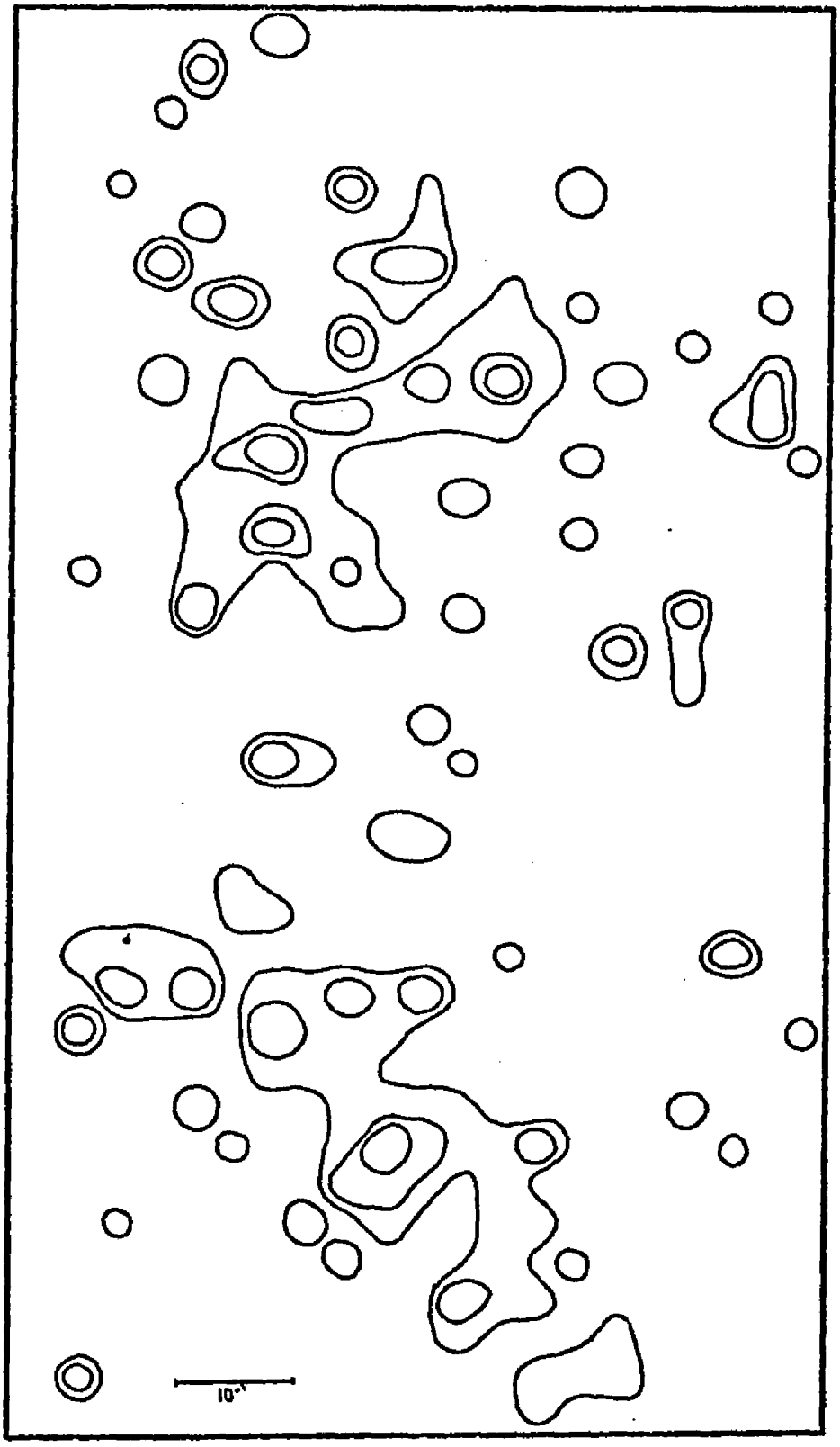

Figure 13. Luminosity Map of A 2197 and A 2199 Cluster Area

APPENDIX I

OBSERVATIONAL DATA

The following tables contain all of the basic data used in this dissertation analysis. Table 8 describes the largest portion of the data, which follows Table 8 in computer printout format. Supplementary information is given in Tables 9 through 13. The individual galaxies in the Virgo Cluster can be identified by their NGC or IC numbers listed in Table 12. Galaxies in the other seven clusters can be identified by using their polar coordinates listed in the computer printout, in conjunction with the cluster photographs in Figures 14 through 20. In each of these figures the center of the polar coordinate system is labeled with the letter "A", and the positions of reference galaxies lettered "B" through "D" are identified in Table 13.

Table 8. Description of the Following Computer Listed Galaxy Data

	Description
Column 1.	Galaxy Number. For the adjoining clusters A 2197 and A 2199, the designation "+" following the galaxy number indicates that the galaxy is also included in the other cluster's data list. An "*" implies that the corrected face-on diameter is < 7.5 kpc/h or that the mean surface brightness < 3 (i.e., image is too faint).
Column 2.	Right Ascension for epoch 1950.0
Column 3.	Declination for epoch 1950.0
Column 4.	Radial distance from the cluster center given in fractions of a degree.
Column 5.	Theta. Angular polar coordinate of galaxy position, measured in degrees north through east.
Column 6.	Type. Galaxy morphological type; a blank implies galaxy type was indeterminate; a "*" indicates a pecularity; a "+" indicates that 200" plate material was used (in part) for determining classification.
Column 7.	D(0). The corrected and final galaxy major axis diameter given to the nearest second of arc.
Column 8.	ELL. Galaxy ellipticity = $10 \times (1 - \frac{\text{minor axis}}{\text{major axis}})$
Column 9.	PA. Position angle of galaxy major axis given in degrees and measured north through east.
Column 10.	COL. Galaxy color estimated by blinking the red and blue Sky Survey plates; R+ = very red; R = red; R- = moderately red; N = neutral; B- = moderately blue; B = blue; B+ = very blue.
Column 11.	SUR.BRG. Surface brightness on a relative system from 1 to 10 . First, maximum surface brightness; second, average surface brightness; third, surface brightness gradient with 1 the flattest profile and 10 the steepest profile.
Column 12.	AREA. Galaxy area given in square seconds of arc.
Column 13.	SW. Spiral winding direction with FWD meaning s , and REV meaning z ; ":" implies uncertainty.

CLUSTER VIRGO PAGE 1

NO	RA(1950)	DEC(1950)	R	THETA	TYPE	D(0)	ELL	PA	COL	SUR.BRG	AREA	SW
1	12 5 36.0	10 39 0	5.7124	244.0	S/SO	152	5.5	107	B-	10 8 3	1.07E4	
2	12 10 18.0	11 8 0	4.4657	242.9	SB	188	6.0	27	B+	10 7 3	1.51E4	REV
3	12 11 12.0	15 10 0	4.1974	298.4	SB	246	5.8	151	R-	10 8 2	3.94E4	FWD
4	12 12 42.0	13 18 0	3.3596	272.1	S	194	7.0	176	B-	10 7 3	1.33E4	FWD
5*	12 13 6.0	14 11 0	3.4000	287.2	S	118	3.3	66	B-	10 8 3	8.64E3	FWD
6	12 13 24.0	13 26 0	3.1954	274.6	S	284	6.8	16	N	10 8 3	2.92E4	FWD
7	12 14 36.0	7 28 0	6.4365	207.3	S/SO	179	7.0	44	R+	10 7 3	1.15E4	FWD
8*	12 15 24.0	7 28 0	6.3496	205.7	S	127	4.8	76	R-	9 7 2	8.54E3	FWD
9	12 16 18.0	14 42 0	2.8938	301.5	S	208	1.5	70	B-	10 6 4	3.10E4	REV
10	12 17 12.0	13 5 0	2.2671	267.3	SBO	146	.9	0	N	10 5 2	1.63E4	
11	12 18 42.0	18 40 0	5.7790	341.3	SB/SBO	212	3.8	62	N	10 6 1	2.59E4	
12*	12 19 0.0	14 53 0	2.4783	313.0	SB	125	5.0	134	N	10 8 4	7.98E3	FWD
13	12 19 12.0	14 53 0	2.4429	313.8	S	187	7.2	173	B+	10 7 3	1.16E4	
14*	12 19 36.0	9 19 0	4.2357	203.7	S	121	7.3	19	N	10 7 4	4.99E3	
15	12 20 0.0	15 49 0	3.0531	329.2	S/SO	152	6.0	163	R-	10 7 2	9.82E3	
16	12 20 6.0	12 5 0	1.9194	234.6	S	152	6.7	137	R-	9 7 3	8.83E3	
17	12 20 24.0	16 6 0	3.2537	333.2	S	273	1.3	32	N	10 7 2	5.38E4	FWD
18	12 20 42.0	11 39 0	2.0994	222.6	S*	174	7.2	54	B-	9 6 3	1.04E4	
19	12 21 54.0	7 35 0	5.7293	191.5	E	239	2.8	37	R-	10 7 2	3.65E4	
20	12 22 24.0	11 59 0	1.5751	219.5	SBO	185	4.7	86	R-	10 6 2	1.79E4	
21	12 22 30.0	13 10 0	.9742	268.2	E/SO	261	1.2	120	R-	10 7 1	5.00E4	
22	12 22 48.0	10 17 0	3.0540	197.3	S	158	4.1	151	N	10 6 3	1.41E4	
23	12 22 54.0	18 28 0	5.3373	350.8	SBO*	239	2.7	3	R-	10 7 2	3.65E4	
24	12 23 6.0	7 30 0	5.7610	188.4	S	156	7.2	151	N	9 7 3	8.21E3	
25	12 23 18.0	12 56 0	.8236	251.2	S	245	5.8	83	B-	9 6 2	2.65E4	REV

CLUSTER VIRGO PAGE 2

NO	RA(1950)	DEC(1950)	R	THETA	TYPE	D(0)	ELL	PA	COL	SUR.BRG	AREA	SW
26	12 23 36.0	13 23 0	.7290	284.6	S*	148	6.8	83	R-	9 6 4	8.27E3	FWD
27	12 23 2.0	13 14 0	.6823	272.9	E/SO	362	2.8	119	R-	10 6 1	8.34E4	
28*	12 24 12.0	9 51 0	3.3970	189.6	SO	124	5.9	43	N	10 7 3	6.87E3	
29	12 24 18.0	9 9 0	4.0858	187.6	S	160	0.0	0	B	9 4 1	2.08E4	REV
30	12 24 36.0	7 32 0	5.6859	184.8	S	138	0.0	0	B	7 4 2	1.55E4	
31	12 24 42.0	9 42 0	3.5277	187.2	SB/SBO	140	3.9	86	B-	10 7 3	1.13E4	FWD
32	12 24 54.0	11 23 0	1.8582	192.2	S/SO	200	5.1	92	R	10 8 3	1.97E4	
33	12 25 12.0	13 17 0	.3272	284.8	S/SO*	146	4.8	16	R-	10 8 3	1.11E4	
34	12 25 30.0	10 5 0	3.1263	184.5	SBO	172	5.2	79	R-	10 7 2	1.45E4	
35	12 25 54.0	17 21 0	4.1525	358.0	S	189	3.2	168	R	10 7 2	2.20E4	REV
36	12 26 30.0	13 28 0	.2667	0.0	S/SO	151	5.9	1	R-	10 6 3	9.98E3	
37	12 26 30.0	14 15 0	1.0500	0.0	E/SO	157	2.5	100	N	10 8 2	1.64E4	
38	12 26 54.0	9 1 0	4.1845	178.6	SB/SBO*	161	6.1	82	R	10 8 3	1.10E4	
39	12 27 12.0	8 16 0	4.9363	178.0	E/SO	474	2.5	152	R+	10 7 1	1.75E5	
40	12 27 18.0	13 42 0	.5365	21.2	E	168	3.5	87	N	10 7 2	1.71E4	
41	12 27 30.0	13 55 0	.7568	18.7	SBO	168	1.4	13	R-	10 7 3	2.06E4	
42	12 28 18.0	12 40 0	.6905	140.5	E	303	1.9	144	R	10 7 1	6.33E4	
43	12 29 24.0	14 42 0	1.6568	25.0	S	229	4.4	135	B-	10 8 2	2.81E4	FWD
44	12 29 36.0	11 27 0	1.9068	156.5	SB/SBO	154	4.7	5	R	10 7 2	1.25E4	REV
45	12 31 0.0	8 55 0	4.4233	165.4	SB	145	2.9	135	B+	10 5 2	1.35E4	REV
46	12 31 6.0	9 26 0	3.9318	163.2	S	138	6.1	29	B	9 6 3	8.11E3	FWD
47	12 31 30.0	7 58 0	5.3755	166.7	SBO	325	4.4	105	R	10 7 1	5.60E4	
48*	12 31 48.0	6 45 0	6.5805	168.4	IRR	124	5.5	157	B+	10 8 2	7.32E3	
49	12 31 48.0	8 28 0	4.9089	164.5	S	317	2.3	5	B+	10 5 2	6.72E4	FWD
50	12 31 48.0	13 21 0	1.2983	83.2	S/SO	146	2.8	149	N	9 6 3	1.38E4	FWD

CLUSTER VIRGO PAGE 3

NO	RA(1950)	DEC(1950)	R	THETA	TYPE	D(0)	ELL	PA	COL	SUR.BRG	AREA	SW
51	12 32 54.0	14 46 0	2.2056	44.6	SB	219	2.1	145	R-	10 7 2	3.26E4	REV
52*	12 33 0.0	12 30 0	1.7320	113.7	SO*	125	6.9	172	N	9 7 4	5.81E3	
53	12 33 6.0	12 50 0	1.6489	102.7	E	148	.7	0	R-	10 8 2	1.70E4	
54	12 34 0.0	11 31 0	2.4876	132.4	SB	180	5.5	21	B-	10 7 4	1.51E4	REV
55	12 34 18.0	7 31 0	5.9980	161.2	SO	157	6.2	153	R	10 8 3	1.03E4	
56	12 34 18.0	13 26 0	1.9119	82.8	S	278	4.6	11	B	10 7 3	4.04E4	FWD
57	12 34 24.0	14 29 0	2.3074	56.0	S	197	1.4	41	B-	9 5 2	2.81E4	REV
58	12 35 0.0	9 50 0	3.9584	148.0	SO	157	2.7	27	N	10 6 3	1.59E4	
59	12 35 12.0	12 5 0	2.3981	117.5	SB	269	1.9	123	N	10 6 3	5.04E4	FWD
60	12 36 6.0	10 45 0	3.3932	136.0	S	173	4.8	86	N	9 4 1	1.55E4	
61	12 37 24.0	10 27 0	3.8308	135.6	SBO	220	1.4	115	N	10 5 2	3.50E4	
62	12 38 42.0	10 25 0	4.0814	132.7	SBO	148	1.1	110	N	10 4 2	1.64E4	
63	12 39 30.0	11 55 0	3.4219	111.7	E/SO	185	3.8	154	N	10 7 2	2.00E4	
64	12 40 24.0	13 32 0	3.3972	84.0	S	138	3.5	105	B-	9 7 4	1.15E4	REV
65	12 41 6.0	11 50 0	3.8162	110.6	E	248	1.6	87	R-	10 8 1	4.37E4	
66*	12 41 18.0	16 40 0	4.9793	45.4	S	133	3.2	71	B-	10 7 2	1.10E4	FWD
67	12 41 24.0	13 25 0	3.6314	86.2	S	200	4.2	111	B-	9 7 4	2.20E4	FWD
68	12 45 18.0	14 2 0	4.6432	79.1	S	154	1.6	156	B-	10 8 2	1.68E4	REV
69	12 45 54.0	8 45 0	6.5161	132.6	S	162	4.1	161	R	9 7 4	1.46E4	
70	12 47 12.0	15 26 0	5.4887	65.4	SO*	192	6.4	21	R-	10 8 3	1.47E4	
71	12 49 48.0	11 35 0	5.9142	105.2	SBO	160	4.5	220	R	10 8 2	1.37E4	
72	12 50 12.0	16 7 0	6.4307	62.3	IRR*	139	6.6	150	N	9 7 3	7.55E3	
73	12 50 24.0	11 30 0	6.0789	105.6	SBO*	242	6.1	26	R	10 8 2	2.44E4	

CLUSTER A 119 PAGE 1

NO	RA(1950)	DEC(1950)	R	THETA	TYPE	D(0)	ELL	PA	COL	SUR.BRG	AREA	SW
1	0 51 14.7	- 1 31 49	.6165	269.6	S	14	5.1	169	N	9 6 3	1.45E2	
2	0 51 25.7	- 1 32 22	.5708	268.6	S/SO	14	4.4	128	N	9 8 2	1.57E2	
3	0 51 25.7	- 1 43 27	.6041	250.8	S	17	3.6	113	N	9 5 2	2.22E2	
4	0 51 30.2	- 1 21 47	.5754	286.4	S	16	0.0	0	N	9 7 2	2.55E2	
5	0 51 38.8	- 1 41 59	.5446	251.4	SO*	27	2.3	7	R-	10 8 3	5.80E2	
6	0 51 42.5	- 1 30 38	.5009	271.7	SO	29	3.6	73	N	10 5 1	5.97E2	
7	0 51 52.7	- 1 11 58	.5626	305.5	S/SO	22	5.7	44	N	9 7 3	2.92E2	
8*	0 52 .2	- 1 40 56	.4547	249.9	IRR	13	5.6	8	B	5 3 2	1.26E2	
9	0 52 5.4	- 1 50 43	.5160	231.7	SO*	26	1.7	148	N	10 6 3	5.68E2	
10	0 52 7.7	- 1 50 45	.5089	231.0	E	17	0.0	0	N	9 7 4	3.14E2	
11	0 52 8.6	- 1 23 40	.4134	288.5	S*	16	3.0	108	B+	9 8 3	2.09E2	
12	0 52 8.8	- 1 45 37	.4560	239.1	S	35	6.9	6	N	10 7 4	5.20E2	
13	0 52 16.0	- 1 39 35	.3851	249.7	SO	17	2.8	70	N	9 7 3	2.48E2	
14	0 52 17.3	- 1 45 2	.4207	237.7	S/SO	17	5.3	89	N	9 6 3	1.90E2	
15	0 52 20.1	- 1 50 51	.4710	226.9	S	42	7.4	116	N	10 8 4	6.74E2	
16*	0 52 27.5	- 1 54 53	.4993	218.8	S/IRR	22	6.9	62	N	7 3 3	2.32E2	
17*	0 52 30.2	- 1 35 19	.3084	258.3	S/SO	12	5.7	170	N	9 7 3	1.06E2	
18	0 52 31.6	- 1 31 25	.2962	270.4	SBO	22	2.0	24	N	10 5 2	4.15E2	
19	0 52 32.1	- 1 30 17	.2948	274.1	S	18	6.7	88	N	9 7 3	1.85E2	
20	0 52 35.5	- 1 19 2	.3491	306.7	E/SO	32	1.7	72	R-	10 6 2	8.14E2	
21	0 52 37.7	- 1 4 52	.5207	328.7	S	20	4.0	104	N	10 7 3	3.01E2	
22	0 52 40.2	- 1 20 49	.3159	304.5	S	35	6.4	8	N	9 7 4	5.84E2	
23	0 52 41.2	- 1 5 35	.5029	329.4	S/IRR	15	6.1	36	N	8 5 3	1.45E2	
24	0 52 43.4	- 1 11 20	.4178	323.8	S/SO	42	6.2	100	N	9 7 2	8.42E2	
25	0 52 45.4	- 1 32 53	.2397	264.7	E/SO	54	2.7	86	R	10 6 2	2.05E3	

NO	RA(1950)	DEC(1950)	R	THETA	TYPE	D(0)	ELL	PA	COL	SUR.BRG	AREA	SW
26	0 52 48.0	- 1 37 24	.2478	246.8	S/SO*	18	5.4	180	R-	9 8 4	2.21E2	
27	0 52 49.6	- 1 28 56	.2254	281.2	S/SO	21	4.1	61	N	9 7 2	3.16E2	
28	0 52 51.9	- 1 34 47	.2183	255.7	SO*	25	0.0	0	N	9 7 4	5.83E2	
29	0 52 52.3	- 1 0 47	.5541	337.7	S/SO	26	5.7	86	N	9 6 2	3.82E2	
30	0 52 56.1	- 1 24 13	.2294	302.2	S/SO	23	6.0	92	N	9 7 2	3.05E2	
31*	0 52 58.9	- 1 28 55	.1876	283.5	SO	13	4.7	105	N	9 7 4	1.41E2	
32	0 53 4.8	- 1 51 2	.3611	205.9	SO	31	1.2	93	N	10 6 2	7.94E2	
33	0 53 6.2	- 1 8 51	.4077	338.1	S	15	2.4	83	B+	9 6 3	1.94E2	
34	0 53 7.3	- 1 34 58	.1581	248.9	S	29	3.2	78	N	10 7 3	6.29E2	
35	0 53 7.3	- 1 57 16	.4533	199.0	S	16	0.0	0	B+	9 5 3	2.70E2	
36	0 53 9.7	- 1 18 16	.2606	328.2	E	21	4.8	75	N	10 6 2	2.84E2	
37	0 53 12.3	- 1 26 2	.1565	306.0	S	14	5.1	144	N	9 7 3	1.45E2	
38	0 53 12.4	- 1 2 8	.5063	345.6	S/IRR	15	4.5	23	R-	9 7 1	1.65E2	
39*	0 53 12.4	- 1 53 14	.3828	199.2	S/IRR	12	6.6	139	N	6 3 3	.95E2	
40	0 53 13.4	- 1 33 22	.1257	256.1	SO*	16	3.9	73	R+	8 6 3	1.94E2	
41	0 53 17.7	- 1 26 7	.1380	311.0	E/SO	19	4.4	166	N	9 8 4	2.61E2	
42	0 53 18.1	- 1 30 19	.1045	281.3	S	16	2.5	14	N	9 6 3	2.38E2	
43	0 53 21.0	- 1 11 27	.3470	344.9	SO*	44	2.0	12	N	10 7 2	1.46E3	
44	0 53 22.3	- 1 31 4	.0854	275.4	S/SO	27	5.8	94	N	10 8 2	3.98E2	
45*	0 53 26.8	- 2 2 30	.5201	187.3		14	3.7	74	R+	6 3 1	1.62E2	
46	0 53 29.0	- 1 46 1	.2478	193.3	SO	14	6.1	32	B	9 6 2	1.31E2	
47	0 53 29.3	- 1 36 18	.0969	215.2	E/SO	32	0.0	0	N	10 7 3	9.12E2	
48	0 53 29.8	- 1 5 55	.4306	352.8	S/SO	18	5.4	137	N	10 8 4	2.03E2	
49	0 53 32.6	- 1 19 40	.2025	348.0	SO*	15	6.3	115	N	10 7 3	1.39E2	
50	0 53 33.7	- 1 36 50	.0957	203.1	SO	21	2.9	115	N	10 7 3	3.42E2	

NO	RA(1950)	DEC(1950)	R	THETA	TYPE	D(0)	ELL	PA	COL	SUR.BRG	AREA	SW
51	0 53 37.2	- 1 23 15	.1402	350.6	E/SO	30	3.1	56	N	10 8 3	6.51E2	
52	0 53 39.0	- 0 56 14	.5888	358.5	IRR*	16	4.3	33	B+	7 5 2	1.90E2	
53	0 53 40.9	- 1 24 53	.1114	356.1	S/SO	15	5.4	153	N	10 8 2	1.51E2	
54	0 53 42.7	- 1 31 33	0.0000	0.0	SO	77	2.6	36	R-	10 7 1	4.06E3	
55	0 53 42.9	- 1 35 4	.0586	179.2	SO	16	0.0	0	B	10 7 2	2.70E2	
56	0 53 44.7	- 1 30 45	.0157	32.0	E	16	2.5	149	N	10 8 4	2.24E2	
57*	0 53 44.8	- 1 53 47	.3707	178.6	S	13	3.9	149	N	10 7 3	1.50E2	FWD
58	0 53 47.6	- 1 26 50	.0812	14.6	SO	19	5.4	33	N	10 8 3	2.37E2	
59	0 53 48.3	- 0 58 53	.5449	2.5	SO	19	6.2	70	N	10 7 3	2.05E2	
60	0 53 49.4	- 1 28 49	.0534	31.5	E/SO*	28	4.5	118	N	10 8 3	4.92E2	
61	0 53 50.1	- 1 15 27	.2701	6.6	E	22	4.5	150	N	10 8 4	3.23E2	
62	0 53 50.6	- 1 56 51	.4229	175.5	S/IRR	24	5.8	97	B	8 5 2	3.19E2	
63	0 53 51.1	- 1 24 50	.1173	17.4	S	23	7.3	46	N	10 9 4	2.41E2	
64	0 53 52.2	- 1 31 59	.0402	100.3	SO	47	1.4	122	R-	10 7 2	1.73E3	
65	0 53 52.2	- 2 5 4	.5600	175.9	S/SO	21	5.7	22	N	10 7 3	2.73E2	
66	0 53 52.5	- 1 32 44	.0453	115.8	E	21	0.0	0	N	10 8 2	4.31E2	
67	0 53 53.2	- 1 53 48	.3734	173.3	S	15	4.6	122	N	10 8 3	1.73E2	
68	0 53 53.9	- 1 3 47	.4651	5.8	SO	25	5.0	94	N	10 7 2	3.89E2	
69	0 53 56.3	- 2 9 21	.6325	174.9	S/SO	14	6.1	64	B-	9 7 3	1.26E2	
70	0 53 57.1	- 1 48 16	.2850	167.9	S	20	3.6	138	N	10 7 2	2.95E2	
71	0 53 57.3	- 1 26 36	.1025	36.4	SO	21	5.0	5	N	10 7 2	2.90E2	
72	0 53 58.1	- 1 53 14	.3670	169.9	S	19	5.5	28	N	9 7 3	2.24E2	
73	0 53 59.3	- 2 2 33	.5213	172.4	S	69	5.7	83	N	10 8 3	2.27E3	
74	0 54 5.0	- 1 23 47	.1593	35.7	S/SO	18	6.0	60	N	10 7 2	2.00E2	
75	0 54 5.2	- 1 39 40	.1646	145.3	S/SO	19	1.4	160	N	10 7 4	3.36E2	

NO	RA(1950)	DEC(1950)	R	THETA	TYPE	D(0)	ELL	PA	COL	SUR.BRG	AREA	SW
76	0 54 5.6	- 1 33 56	.1033	112.6	S	23	6.2	98	N	10 8 5	2.78E2	
77	0 54 7.4	- 1 18 18	.2436	25.0	E*	16	2.5	63	N	10 7 3	2.25E2	
78	0 54 11.0	- 1 8 42	.3987	17.2	SO	22	2.7	146	N	10 7 2	3.94E2	
79	0 54 13.3	- 1 52 1	.3641	159.5	S	25	4.4	131	N	10 7 3	4.23E2	
80	0 54 13.6	- 1 8 54	.3988	18.8	SO	14	6.1	96	N	10 9 4	1.28E2	
81	0 54 18.1	- 1 32 34	.1484	96.6	S/SO	29	6.1	89	N	10 8 2	4.33E2	
82	0 54 23.0	- 1 12 50	.3542	28.3	S/SO	19	0.0	0	B-	10 7 2	3.61E2	
83	0 54 23.5	- 1 28 55	.1755	75.5	S*	51	1.8	92	B	10 5 1	1.97E3	
84	0 54 23.7	- 1 39 34	.2168	128.0	S	25	6.4	56	N	10 7 2	3.23E2	
85	0 54 26.8	- 1 5 44	.4679	23.1	SO	25	3.3	142	N	10 7 2	4.60E2	
86	0 54 28.6	- 1 8 43	.4259	26.7	SO	51	1.8	39	R-	10 7 3	1.95E3	
87	0 54 33.6	- 1 40 4	.2551	123.8	SO	36	0.0	0	N	10 6 1	1.19E3	
88	0 54 36.3	- 1 39 2	.2557	119.2	SO	18	3.6	151	N	10 7 1	1.92E2	
89	0 54 37.2	- 1 17 20	.3281	43.8	S/SO	18	4.6	59	R-	10 7 2	2.24E2	
90	0 54 37.8	- 1 39 2	.2612	118.5	S	16	6.5	26	N	10 7 4	1.52E2	
91	0 54 38.3	- 1 53 23	.4313	147.5	S	14	6.9	144	R-	10 7 4	1.17E2	
92	0 54 40.3	- 1 16 57	.3417	44.6	E/SO*	21	2.1	42	R-	10 8 2	3.64E2	
93	0 54 41.2	- 1 33 22	.2455	97.1		24	3.5	20	N	10 8 5	4.30E2	
94	0 54 43.4	- 0 56 22	.6386	23.3	SO	36	1.6	11	R-	10 7 3	1.06E3	
95	0 54 51.3	- 1 0 37	.5895	29.0	S/SO	18	1.1	95	N	10 7 3	3.07E2	
96	0 55 1.5	- 1 39 40	.3550	112.4	E	51	0.0	0	R-	10 7 2	2.25E3	
97	0 55 8.2	- 1 34 58	.3606	99.1	S	18	3.7	2	N	10 8 4	2.48E2	FWD
98	0 55 18.3	- 1 24 21	.4159	73.2	SB	30	3.1	124	N	10 7 2	6.45E2	
99	0 55 20.2	- 1 5 4	.5998	42.6	E	19	0.0	0	N	10 8 4	3.61E2	
100	0 55 26.6	- 1 41 21	.4625	110.7	S	20	6.8	90	B	8 7 3	2.06E2	

CLUSTER A 119 PAGE 5

NO	RA(1950)	DEC(1950)	R	THETA	TYPE	D(0)	ELL	PA	COL	SUR.BRG	AREA	SW
101	0 55 31.9	- 1 58 30	.6392	134.7	S	18	6.9	4	N	7 5 2	1.70E2	
102	0 55 41.9	- 1 25 39	.5061	78.8	S/IRR	14	6.5	42	R-	8 6 2	1.21E2	
103	0 55 44.6	- 1 25 7	.5189	78.1	SO	27	0.0	0	R-	10 7 3	6.70E2	

CLUSTER A 400 PAGE 1

NO	RA(1950)	DEC(1950)	R	THETA	TYPE	D(0)	ELL	PA	COL	SUR.BRG	AREA	SW
1*	2 50 35.6	5 49 33	1.1084	270.1	S/SO	21	5.0	139	N	8 5 3	2.61E2	
2	2 50 52.3	6 16 12	1.1303	293.3	S/SO	35	2.6	171	R-	9 6 2	8.79E2	
3	2 50 59.3	5 51 28	1.0107	271.9	S/SO	33	6.3	72	R-	9 7 4	5.03E2	
4	2 51 2.5	6 3 42	1.0245	283.4	SO*	112	5.6	144	R+	9 6 2	5.89E3	
5	2 51 20.4	5 47 4	.9236	267.6	S	57	2.5	20	B-	8 6 2	2.22E3	FWD
6	2 51 24.9	6 3 15	.9326	284.3	SO	48	6.5	115	R-	9 7 3	1.01E3	
7	2 51 54.5	5 20 55	.9151	238.7	SO	30	2.8	6	R-	7 5 3	6.40E2	
8	2 51 56.6	5 2 57	1.0949	225.0	S	28	4.4	42	R-	9 7 3	4.93E2	
9	2 52 10.7	6 11 47	.8050	297.6	S/IRR	28	1.9	52	N	7 5 2	6.06E2	
10	2 52 23.3	5 24 33	.7817	237.9	S/IRR	23	2.8	54	N	8 5 3	3.95E2	REV
11	2 52 36.3	5 58 31	.6264	284.0	SO	34	3.0	80	R-	9 7 2	7.98E2	
12	2 52 39.0	6 0 31	.6246	287.2	S	26	5.6	45	R-	7 6 2	3.74E2	
13*	2 52 41.0	6 1 28	.6216	288.8	S	22	6.0	28	N	7 6 3	2.51E2	
14	2 52 41.3	5 55 20	.5954	279.5	S*	38	2.6	64	N	9 7 3	1.95E3	
15*	2 52 43.6	6 4 50	.6319	293.9	SO	22	5.8	58	R-	6 4 2	2.72E2	
16	2 53 .8	5 37 23	.5452	248.3	SO	46	0.0	0	R-	8 5 2	1.78E3	
17	2 53 4.0	6 8 48	.5891	303.2	S	24	5.9	9	R-	9 8 5	3.08E2	
18	2 53 8.3	6 0 57	.5124	292.0	S	78	1.1	148	B-	9 6 1	4.62E3	FWD
19	2 53 18.7	6 17 36	.6377	317.4	S	80	6.0	165	N	9 7 2	2.87E3	
20	2 53 27.9	6 10 29	.5273	311.7	SO	29	0.0	0	R	9 7 3	7.64E2	
21	2 53 36.8	5 11 30	.7268	209.5	S	28	7.2	172	N	7 7 3	3.22E2	
22	2 53 39.2	5 45 48	.3527	260.0	S/SO	25	4.6	83	R-	9 7 3	3.99E2	
23	2 53 44.1	5 57 14	.3517	291.6	SB	42	6.1	10	N	9 7 2	8.39E2	FWD
24	2 53 50.1	6 6 59	.4201	314.0	S/SO	30	5.3	45	R	9 8 4	5.08E2	
25*	2 53 50.4	5 59 37	.3452	299.4	SO	22	4.0	45	R-	9 8 4	3.32E2	

CLUSTER A 400 PAGE 2

NO	RA(1950)	DEC(1950)	R	THETA	TYPE	D(0)	ELL	PA	COL	SUR.	BRG	AREA	SW
26	2 53 53.1	6 4 42	.3852	311.2	S	31	6.9	159	N	8	6 3	4.17E2	
27	2 54 2.1	5 42 43	.2764	246.0	SO*	46	3.8	18	R+	9	6 2	1.30E3	
28	2 54 7.3	5 51 13	.2327	277.2	S/SO*	29	5.1	153	B	8	7 3	4.68E2	
29	2 54 9.2	4 46 35	1.0716	192.0	S	62	5.5	143	R	9	7 2	1.91E3	FWD:
30	2 54 14.9	5 40 18	.2512	232.6	E	29	1.7	31	R	9	7 3	6.57E2	
31	2 54 17.9	6 0 17	.2597	314.0	E*	25	3.6	44	R-	9	8 4	4.37E2	
32	2 54 18.0	5 37 28	.2735	223.0	S/SO	23	5.3	170	R	7	5 2	3.15E2	
33	2 54 20.9	6 19 59	.5377	341.1	SO	27	6.1	43	R-	9	7 2	3.75E2	
34	2 54 31.2	5 7 14	.7161	190.6	S/SO	46	2.8	65	R-	9	7 3	1.48E3	
35	2 54 39.2	5 46 45	.1086	245.4	SO	25	4.1	133	R	9	8 2	4.15E2	
36*	2 54 40.9	4 48 13	1.0249	185.1	S/SO	21	6.3	66	N	8	7 3	2.20E2	
37	2 54 44.5	5 44 46	.1096	224.4	SO	23	5.6	19	R	9	8 3	2.86E2	
38	2 54 49.0	5 48 45	.0592	258.4	SO	24	4.3	77	R-	9	7 3	3.68E2	
39	2 54 50.5	5 1 20	.8039	183.7	S	32	3.7	104	N	8	6 3	6.56E2	REV
40	2 54 55.2	5 46 36	.0577	214.1	E/SO	30	3.0	158	R	9	8 3	6.20E2	
41	2 54 57.2	6 54 16	1.0803	358.7	SO	33	3.8	87	R+	9	7 3	7.21E2	
42	2 55 3.0	5 49 35	.0019	0.0	E	23	0.0	0	R+	10	8 3	5.02E2	
43	2 55 3.1	5 49 20	.0023	169.4	E	23	0.0	0	R+	10	8 3	5.02E2	
44	2 55 4.1	5 13 55	.5925	179.6	SO*	38	4.2	162	R-	9	7 2	8.96E2	
45	2 55 5.1	5 39 56	.1591	176.9	SO	23	4.2	80	R	9	7 3	3.57E2	
46	2 55 5.4	6 22 24	.5490	1.0	S/SO	34	2.1	6	N	9	5 2	8.66E2	
47	2 55 6.3	5 28 19	.3528	177.8	SO	27	2.8	165	R	9	7 2	5.35E2	
48	2 55 6.7	5 37 35	.1986	175.6	SO	24	5.2	76	R-	9	7 3	3.44E2	
49	2 55 7.5	5 45 1	.0765	165.9	IRR*	35	5.6	146	R-	8	7 2	6.27E2	
50	2 55 12.1	5 51 8	.0468	53.6	SO	25	3.9	41	R	9	7 3	4.34E2	

NO	RA(1950)	DEC(1950)	R	THETA	TYPE	D(0)	ELL	PA	COL	SUR.BRG	AREA	SW
51*	2 55 13.1	6 9 36	.3382	7.1	SO	20	5.4	92	R-	9 8 2	2.40E2	
52	2 55 16.0	6 38 54	.8256	3.7	S	47	2.5	91	B-	9 6 2	1.55E3	FWD
53	2 55 19.2	5 35 14	.2465	164.2	SO	32	3.7	59	R-	9 7 2	6.85E2	
54*	2 55 20.0	5 34 59	.2515	163.7	SO*	21	5.3	139	N	9 8 3	2.58E2	
55	2 55 33.3	5 38 12	.2259	146.2	S/SO	44	5.8	119	R-	9 7 2	9.50E2	
56*	2 55 35.3	5 42 17	.1796	131.8	SO	20	5.6	144	N	9 7 2	2.31E2	
57	2 55 35.7	5 46 20	.1453	111.1	E	26	1.1	87	R+	9 8 5	5.52E2	
58	2 55 35.7	6 53 59	1.0838	7.2	S/SO	28	4.2	99	N	8 6 2	4.96E2	
59	2 55 39.3	6 54 48	1.0992	7.9	SB	24	3.9	96	N	9 7 4	3.93E2	FWD
60	2 55 42.4	5 53 43	.1780	66.5	E/SO	44	1.3	6	R+	10 7 2	1.53E3	
61	2 55 45.6	6 23 32	.5946	17.3	E/SO	44	3.0	11	R+	10 7 2	1.32E3	
62	2 55 49.8	6 0 23	.2659	46.8	S/SO	32	6.3	53	R-	9 7 3	4.85E2	
63	2 55 50.9	6 6 25	.3453	35.1	S	38	2.3	44	N	10 7 3	1.06E3	
64	2 55 55.6	6 8 41	.3874	34.2	SO	40	2.3	6	R-	9 7 2	1.17E3	
65	2 55 59.1	5 58 35	.2778	56.8	SO	27	3.5	117	R	10 7 4	5.05E2	
66	2 56 5.8	6 13 26	.4767	33.1	SB	25	4.3	123	N	9 7 3	4.03E2	REV
67*	2 56 6.3	5 11 55	.6787	157.2	IRR	32	0.0	0	R-	5 3 2	9.18E2	
68	2 56 10.6	6 6 20	.3969	44.9	S	23	6.2	128	B-	7 6 2	2.73E2	
69*	2 56 11.0	6 3 32	.3666	50.2	S	22	6.5	114	R	8 7 3	2.45E2	
70	2 56 12.2	6 10 29	.4527	39.3	S	26	3.7	146	R-	9 8 4	4.47E2	REV
71	2 56 14.8	5 57 32	.3265	65.7	S	24	3.0	136	R-	9 6 4	4.31E2	FWD
72	2 56 16.5	5 59 38	.3486	60.9	S	34	6.2	45	R+	9 7 4	5.46E2	FWD:
73*	2 56 19.2	6 52 19	1.0940	16.7		23	.6	0	B-	4 2 1	4.69E2	
74	2 56 22.1	6 4 9	.4091	53.2	SO	28	2.2	69	R-	10 7 3	5.86E2	
75	2 56 25.4	5 47 20	.3434	95.9	SO	26	4.2	108	R	9 7 3	4.29E2	

NO	RA(1950)	DEC(1950)	R	THETA	TYPE	D(0)	ELL	PA	COL	SUR.BRG	AREA	SW
76	2 56 37.4	5 56 5	.4065	74.2	E	30	0.0	0	N	9 7 4	8.05E2	
77*	2 56 42.0	5 5 15	.8436	150.9	S/IRR	42	2.5	113	N	6 3 2	1.26E3	
78*	2 56 46.7	5 50 1	.4299	88.8	IRR	35	0.0	0	B+	6 3 2	1.09E2	
79	2 56 55.6	5 8 9	.8320	145.8	S	28	6.2	4	N	8 7 2	3.91E2	
80	2 57 3.3	5 13 25	.7810	140.3	S/IRR	25	4.1	100	B-	8 7 2	4.15E2	
81	2 57 7.6	5 44 48	.5223	98.5	SO	24	4.4	74	R-	9 7 3	3.78E2	
82	2 57 13.2	6 20 5	.7426	46.6	S	27	2.0	156	R-	9 8 4	5.71E2	
83	2 57 14.3	6 18 57	.7331	47.9	S	26	2.8	110	N	8 5 4	5.15E2	
84*	2 57 16.1	5 32 27	.6205	117.2	S	21	7.1	11	N	8 7 4	2.06E2	
85	2 57 21.4	5 46 11	.5763	95.4	S	28	2.0	67	N	9 6 3	6.04E2	
86	2 57 30.2	5 36 24	.6480	109.6	SO	42	1.0	161	R-	9 6 2	1.39E3	
87	2 57 31.3	5 30 50	.6889	116.8	S	30	1.4	166	N	9 6 3	7.12E2	FWD
88	2 57 34.2	5 24 51	.7493	123.2	SO	62	3.5	118	R	10 7 2	2.42E3	
89	2 57 42.2	5 30 53	.7291	115.1	SO*	60	2.1	35	R+	10 7 2	2.58E3	
90*	2 57 49.8	5 7 17	.9864	135.4	S*	43	6.6	157	R	4 3 2	7.92E2	
91*	2 57 55.3	5 41 4	.7279	101.1	IRR	22	4.2	172	B	5 3 2	3.18E2	
92	2 58 11.9	5 35 7	.8189	106.9	SO*	34	3.2	89	R	9 6 2	7.94E2	
93	2 58 57.6	6 1 51	.9939	78.0	S/SO	23	6.0	13	R-	8 7 2	2.72E2	
94*	2 59 2.2	5 16 40	1.1326	118.8	S/SO*	21	4.9	84	R-	9 7 3	2.82E2	
95	2 59 2.9	5 30 18	1.0447	107.8	S*	26	4.2	15	B-	7 5 3	4.29E2	
96	2 59 27.0	6 5 13	1.1251	76.5	E/SO	32	0.0	0	R	9 6 2	9.18E2	

CLUSTER A1656 PAGE 1

NO	RA(1950)	DEC(1950)	R	THETA	TYPE	D(0)	ELL	PA	COL	SUR.BRG	AREA	SW
1*	12 52 54.5	28 8 14	1.0061	264.6	SO*	23	3.6	146	B-	10 7 5	4.04E2	
2	12 52 57.3	28 44 18	1.1079	297.2	S/SO	28	5.6	143	B-	10 7 5	4.54E2	FWD
3	12 52 59.5	28 4 7	.9974	260.5	SO	52	2.0	160	B-	10 7 3	2.04E3	
4	12 53 2.2	27 55 37	1.0220	252.6	S*	37	7.2	179	N	10 6 4	5.94E2	FWD
5	12 53 3.5	27 47 30	1.0671	245.6	E	38	3.0	35	B-	10 7 4	1.03E3	
6	12 53 20.4	27 38 3	1.0901	236.7	S	24	8.0	164	B	8 4 5	2.43E2	
7	12 53 22.5	28 31 36	.9422	288.1	S	33	7.1	79	B-	10 5 3	4.94E2	
8	12 53 30.8	27 52 48	.9394	247.9	S/IRR	28	7.1	81	N	8 5 3	3.67E2	
9	12 53 44.6	28 6 53	.8264	261.7	SB/SBO	34	2.7	175	B-	10 5 3	8.80E2	FWD
10	12 53 46.8	28 0 56	.8393	254.9	E	71	1.1	91	B-	10 5 2	4.01E3	
11	12 53 51.2	27 42 58	.9501	236.9	SO	29	4.7	5	N	10 5 2	5.32E2	
12	12 54 3.1	27 33 42	1.0103	228.2	S/SO	39	3.6	66	B+	10 5 3	1.06E3	
13	12 54 17.6	28 17 26	.6975	274.6	SO	44	.6	0	N	10 6 3	1.70E3	
14	12 54 18.0	27 26 55	1.0523	221.6	E	54	1.9	52	B-	10 7 3	2.18E3	
15	12 54 24.1	27 21 49	1.1037	217.8	S	30	6.6	151	N	10 7 5	4.62E2	FWD
16	12 54 31.6	28 53 36	.9181	315.8	SO	25	6.4	99	N	10 7 3	3.31E2	
17*	12 54 36.2	27 38 32	.8659	226.8	S/SO	22	6.1	101	N	10 6 4	2.90E2	
18	12 54 44.1	27 44 11	.7814	230.3	E/SO	29	3.3	169	N	10 8 4	6.42E2	
19*	12 54 46.5	27 22 24	1.0472	214.6	S	23	6.7	13	B-	9 6 3	2.78E2	FWD
20	12 54 58.3	28 2 10	.5825	250.0	SBO	30	1.4	65	B-	10 5 3	7.96E2	
21	12 54 59.2	27 46 4	.7186	229.4	E/SO	120	2.5	62	N	10 5 2	9.84E3	
22*	12 55 3.3	28 26 47	.5673	291.8	S/SO	21	5.4	132	N	10 8 5	2.99E2	
23	12 55 5.0	28 27 29	.5659	293.1	S	38	6.1	161	N	10 7 4	7.23E2	FWD
24	12 55 5.3	27 38 29	.7921	221.4	S	35	7.6	166	B-	8 5 3	4.90E2	
25	12 55 7.0	28 44 49	.7232	315.0	E	77	2.2	119	N	10 6 2	4.22E3	

NO	RA(1950)	DEC(1950)	R	THETA	TYPE	D(0)	ELL	PA	COL	SUR.BRG	AREA	SW
26	12 55 7.6	27 52 49	.6249	235.3	E	31	1.0	114	B-	10 7 4	8.66E2	
27	12 55 8.9	28 45 8	.7220	315.6	E	37	.8	0	N	10 7 3	1.20E3	
28	12 55 11.1	27 18 4	1.0619	208.3	S/SO	28	3.4	121	N	10 7 3	5.72E2	REV
29	12 55 21.0	28 1 37	.5088	245.7	S	37	7.2	115	B-	10 7 3	5.83E2	
30	12 55 22.2	28 6 11	.4780	253.8	SO	25	6.5	91	N	10 6 4	3.43E2	
31*	12 55 23.0	28 9 10	.4635	259.6	SO	23	3.8	74	N	9 6 3	3.92E2	
32	12 55 29.2	27 45 38	.6445	222.4	SB	26	1.5	0	N	10 6 3	5.96E2	FWD
33	12 55 36.3	27 45 35	.6278	220.6	SO	33	3.3	81	B-	10 7 3	8.02E2	
34	12 55 37.7	27 11 8	1.1264	201.1	SO	26	4.4	129	B-	10 6 4	4.69E2	
35	12 55 38.1	28 14 25	.4001	270.5	SB	30	.8	68	B-	10 6 3	8.01E2	FWD
36	12 55 40.7	28 30 45	.4774	305.3	S	85	8.1	155	B	10 7 3	2.11E3	REV
37	12 55 40.9	29 17 14	1.1194	339.8	S	28	7.4	121	B	9 5 3	3.48E2	
38	12 55 44.7	28 58 42	.8304	333.3	S	46	6.5	84	B+	10 6 3	9.98E2	
39	12 55 48.7	29 13 4	1.0444	340.0	S	50	7.6	14	N	10 8 4	9.18E2	
40	12 55 48.9	28 27 9	.4196	301.0	S	34	4.9	58	B-	10 6 3	7.28E2	
41*	12 55 52.5	27 24 22	.9013	202.8	E	23	2.3	18	R-	10 7 4	4.52E2	
42	12 55 56.9	28 14 15	.3311	270.1	SO	38	0.0	0	N	10 6 2	1.34E3	
43	12 56 3.3	29 14 38	1.0522	343.2	SO*	35	4.4	47	B-	10 7 1	7.97E2	
44	12 56 5.3	28 17 4	.3039	279.0	+E/SO	44	3.2	94	N	10 6 3	1.33E3	
45	12 56 5.6	29 7 43	.9399	341.6	SBO	36	0.0	0	N	10 5 3	1.17E3	
46	12 56 10.1	27 51 57	.4670	217.4	E*	45	2.2	81	N	10 9 5	1.51E3	
47	12 56 11.2	27 22 24	.9080	198.0	SO	55	2.4	137	N	10 5 2	2.21E3	
48	12 56 11.5	28 22 60	.3135	297.9	S	39	7.1	60	N	10 7 4	6.61E2	
49*	12 56 12.7	27 44 1	.5732	208.6	S	20	7.3	155	B-	10 6 4	2.07E2	
50	12 56 18.7	29 10 47	.9751	345.2	SO	24	1.4	0	B	10 6 4	5.08E2	

NO	RA(1950)	DEC(1950)	R	THETA	TYPE	D(0)	ELL	PA	COL	SUR.BRG	AREA	SW
51	12 56 22.4	27 56 39	.3774	219.1	+E/SO	49	2.2	52	B-	10 4 3	1.81E3	
52	12 56 23.7	28 4 48	.2810	236.0	+SO	36	6.3	75	N	10 6 3	6.67E2	
53	12 56 25.9	28 21 13	.2529	297.5	+SO	42	7.6	166	N	10 6 4	6.76E2	
54	12 56 31.2	28 6 11	.2453	236.9	S/SO	49	7.8	73	N	10 8 5	8.29E2	
55	12 56 36.6	27 48 23	.4692	203.4	S	30	0.0	0	B-	9 5 3	8.79E2	
56	12 56 37.0	28 29 41	.3163	324.5	S/SO	40	6.6	110	N	10 6 4	7.52E2	
57	12 56 39.1	28 23 35	.2351	311.6	E	50	3.0	125	N	10 6 2	1.75E3	
58*	12 56 39.4	27 13 39	1.0249	189.9	S/SO	22	6.5	103	B	9 4 2	2.74E2	
59	12 56 40.3	27 54 50	.3663	208.1	+SB	35	.7	0	B+	10 5 3	1.08E3	
60	12 56 41.2	28 15 59	.1710	279.9	+SO	31	2.9	25	N	10 6 3	7.49E2	
61	12 56 48.2	28 14 47	.1431	273.7	+E	31	2.0	62	N	10 6 3	7.65E2	
62	12 56 48.7	27 40 19	.5827	194.1	E	34	3.1	137	N	10 5 3	8.27E2	
63	12 56 48.7	28 2 38	.2393	216.2	+SO	25	5.8	76	N	10 7 5	3.78E2	
64	12 56 49.1	28 20 44	.1766	307.9	+SO	56	1.4	112	B-	9 6 2	2.47E3	
65	12 56 53.5	27 46 58	.4710	195.2	S	24	6.6	18	B-	8 4 3	3.14E2	
66	12 56 55.1	28 21 13	.1653	314.8	+E/SO	40	5.7	117	N	10 6 3	8.59E2	
67	12 56 58.5	28 10 51	.1192	241.8	+E	47	0.0	0	B-	10 6 3	1.95E3	
68*	12 57 0.0	28 0 30	.2496	203.5	+SO	22	6.1	7	N	9 5 4	2.90E2	
69*	12 57 4.5	28 7 10	.1441	215.2	+E/SO	23	5.8	154	N	9 6 3	3.26E2	
70	12 57 5.2	28 13 32	.0812	261.8	+SO	38	2.9	177	B-	10 5 3	1.08E3	
71	12 57 6.0	28 9 13	.1140	222.8	+SBO	49	3.4	132	N	9 6 3	1.60E3	
72	12 57 8.0	28 15 10	.0718	282.5	+E/SO	27	3.7	102	N	10 6 3	5.49E2	
73	12 57 9.3	28 12 58	.0687	252.1	+SBO	34	4.7	109	N	10 8 2	7.16E2	
74	12 57 10.8	28 13 43	.0605	261.8	+SO	168	1.2	50	N	10 5 1	2.09E4	
75*	12 57 11.1	28 49 14	.5863	354.3	S	22	4.6	136	N	10 6 3	3.29E2	

CLUSTER A1656 PAGE 4

NO	RA(1950)	DEC(1950)	R	THETA	TYPE	D(0)	ELL	PA	COL	SUR.BRG	AREA	SW
76*	12 57 13.0	28 2 46	.1980	195.2	S/SO	23	5.8	98	B-	9 5 2	3.22E2	
77	12 57 14.8	29 9 55	.9291	357.2	S/SO	43	6.9	29	N	10 8 5	7.99E2	
78	12 57 15.4	29 11 45	.9596	357.5	SO	43	5.6	67	N	10 5 3	9.68E2	
79	12 57 15.7	28 54 1	.6644	356.4	S	26	0.0	0	B+	10 6 3	6.70E2	FWD
80	12 57 16.4	27 55 45	.3106	187.3	S	30	3.8	111	B-	9 4 2	6.48E2	FWD
81	12 57 16.7	28 46 35	.5405	356.0	E	27	1.2	121	N	10 6 4	6.54E2	
82	12 57 19.6	28 10 54	.0620	206.4	+E	27	4.6	24	N	10 7 2	2.96E2	
83	12 57 21.3	28 7 35	.1129	190.9	+SO	30	6.7	155	N	9 5 3	4.33E2	
84	12 57 22.0	28 14 35	.0196	287.3	+E/SBO	26	4.0	4	N	10 7 4	4.78E2	
85	12 57 22.3	27 58 46	.2584	183.9	S	45	7.2	167	B-	9 5 4	8.17E2	
86	12 57 31.3	28 0 57	.2219	176.0	S	35	6.6	43	B	9 4 2	5.82E2	
87	12 57 31.3	28 18 14	.0684	13.0	+SBO	30	2.3	104	N	10 6 3	7.39E2	
88	12 57 33.1	28 30 57	.2795	4.5	+E/SO	54	0.0	0	N	10 6 3	2.60E3	
89	12 57 33.4	27 28 7	.7690	178.3	SBO	29	1.6	0	N	10 6 3	7.30E2	
90	12 57 38.5	27 10 1	1.0711	177.7	S	71	7.0	13	B-	10 7 3	1.96E3	
91	12 57 39.8	28 15 24	.0505	67.3	+E	44	0.0	0	B-	10 7 3	1.75E3	
92	12 57 40.8	28 4 37	.1680	162.6	S	29	7.0	8	N	10 6 4	4.04E2	REV
93	12 57 41.3	27 34 11	.6695	175.5	S/SO	27	6.4	36	B-	9 5 4	3.82E2	
94*	12 57 41.3	28 14 53	.0532	78.2	SO	23	6.3	131	N	10 7 5	2.92E2	
95	12 57 41.5	28 2 42	.1994	164.6	S	37	6.5	145	N	10 5 3	6.80E2	
96	12 57 43.4	28 14 45	.0604	81.8	+E	199	2.6	78	B-	10 4 1	2.60E4	
97	12 57 49.5	27 32 59	.6924	173.1	S	27	6.7	22	B+	9 5 3	3.61E2	REV
98	12 57 49.6	29 5 52	.8645	5.4	SO	34	5.2	1	B-	10 6 3	6.83E2	
99	12 57 51.9	28 14 12	.0910	90.3	S/SO*	25	6.2	31	N	10 7 4	3.60E2	
100	12 57 53.0	28 13 27	.0960	97.8	+E*	28	4.0	90	N	10 8 5	5.56E2	

NO	RA(1950)	DEC(1950)	R	THETA	TYPE	D(0)	ELL	PA	COL	SUR.BRG	AREA	SW
101	12 57 53.4	28 28 17	.2532	22.4	+S/SO	100	6.4	154	N	10 6 3	4.23E3	
102	12 57 58.3	28 50 38	.6173	10.6	IRR	34	1.2	0	B+	9 4 3	9.77E2	
103	12 58 1.0	27 43 47	.5226	166.2	IRR*	26	4.7	133	B+	5 4 1	4.45E2	
104	12 58 1.4	29 8 13	.9084	7.9	E/SO	35	1.4	169	N	10 6 3	1.05E3	
105	12 58 3.8	28 14 29	.1348	88.2	+SO	25	5.6	95	N	10 5 2	3.90E2	
106	12 58 4.4	27 36 9	.6494	167.8	S/IRR	31	4.6	14	B+	8 4 3	6.21E2	REV
107	12 58 6.2	28 36 56	.4046	20.7	SO	39	3.9	9	N	10 6 3	1.01E3	
108	12 58 7.0	29 13 10	.9930	8.4	S	32	6.8	120	B+	8 5 2	4.81E2	
109	12 58 11.0	27 50 36	.4257	157.7	S	29	6.9	57	B	10 7 3	4.13E2	
110	12 58 11.0	28 24 55	.2401	42.1	SO	32	7.3	170	N	10 7 4	4.42E2	
111	12 58 13.3	28 19 35	.1915	62.2	+S/SO	30	6.7	151	B+	10 7 4	4.55E2	
112*	12 58 14.1	28 17 0	.1785	75.0	+SBO	23	5.5	82	N	10 6 3	3.44E2	
113	12 58 15.1	28 11 34	.1818	104.1	+E	31	.6	0	N	10 7 4	8.74E2	
114	12 58 15.4	29 17 20	1.0664	9.5	S	58	4.8	56	B+	10 6 3	1.89E3	REV
115	12 58 16.2	28 15 56	.1824	81.0	+E/SO	26	3.6	46	N	10 7 3	5.02E2	
116	12 58 16.2	28 47 18	.5797	18.0	S/SO*	28	7.6	6	B+	9 7 4	3.30E2	
117	12 58 18.1	28 14 25	.1872	89.0	+SBO	33	0.0	0	B-	10 7 2	1.02E3	
118	12 58 18.2	28 13 55	.1877	91.6	+SBO	29	3.4	102	N	10 6 3	6.09E2	
119	12 58 19.4	28 41 7	.4873	23.1	SO*	26	4.4	42	N	9 5 1	4.52E2	
120	12 58 19.7	28 36 22	.4162	27.5	E	25	4.5	53	N	10 7 4	4.37E2	
121*	12 58 20.6	28 0 58	.2959	138.3	S/IRR	22	7.1	6	B	5 3 3	2.41E2	
122	12 58 24.1	28 21 35	.2424	59.6	+E	27	2.8	112	N	10 7 3	5.63E2	
123	12 58 24.2	28 25 39	.2830	47.7	SB	50	1.0	0	B	10 6 2	2.05E3	REV
124	12 58 25.1	27 40 28	.6019	159.2	SBO	47	3.4	160	B-	10 7 4	1.48E3	
125	12 58 27.0	28 18 42	.2321	71.2	+E/SO	40	3.7	55	N	10 6 2	1.10E3	

NO	RA(1950)	DEC(1950)	R	THETA	TYPE	D(0)	ELL	PA	COL	SUR.BRG	AREA	SW
126	12 58 27.6	28 38 6	.4554	29.1	E/SO	33	4.8	27	N	10 7 4	6.79E2	
127*	12 58 29.4	28 3 10	.2940	128.8	SO	23	5.6	53	N	10 7 4	3.34E2	
128	12 58 29.8	28 16 35	.2334	80.3	+E	57	2.6	103	N	10 5 2	2.34E3	
129	12 58 31.5	28 3 34	.2959	126.9	S	61	2.1	123	B	10 7 3	2.73E3	FWD
130	12 58 33.6	27 55 16	.3996	142.2	SO	31	3.7	9	B-	9 6 3	6.96E2	
131	12 58 34.6	28 10 8	.2571	105.3	+S/SO*	32	7.0	173	N	9 7 4	4.85E2	
132	12 58 44.6	28 37 44	.4838	35.9	SO	25	3.7	157	B-	9 6 3	4.67E2	
133	12 58 45.4	29 20 4	1.1339	14.5	S/IRR	24	5.9	59	B+	7 4 2	3.49E2	
134	12 58 47.6	27 52 24	.4691	140.8	S/SO	26	7.2	134	N	10 7 4	3.21E2	
135*	12 58 51.6	29 8 28	.9552	18.8	S/SO	19	7.8	8	N	9 6 5	1.78E2	
136	12 58 53.0	28 4 40	.3536	116.7	E/SO	57	3.5	146	N	10 7 1	2.13E3	
137	12 58 58.3	28 27 54	.4046	55.7	SO	29	3.4	110	N	10 7 3	6.10E2	
138	12 59 .9	28 56 47	.7878	25.7	S	30	2.3	103	B+	10 6 3	7.39E2	FWD
139	12 59 1.5	28 9 17	.3563	103.3	+SB	132	1.4	164	B	10 7 1	1.30E4	REV
140	12 59 7.3	28 6 58	.3874	108.1	SO	34	1.2	83	N	10 6 2	9.79E2	
141	12 59 19.9	29 16 6	1.1104	21.7	S	30	6.5	24	N	10 7 3	4.50E2	
142	12 59 22.7	28 21 49	.4425	73.3	S/SO	46	6.3	87	N	10 7 2	9.85E2	
143	12 59 23.8	27 52 21	.5632	130.2	S/SO	26	6.9	37	N	9 7 3	3.35E2	
144	12 59 29.1	27 53 35	.5654	127.4	E	71	1.5	0	R-	10 7 2	3.82E3	
145	12 59 33.2	28 16 28	.4643	85.3	E/SO	40	2.0	14	N	10 6 3	1.23E3	
146	12 59 43.4	27 55 1	.5947	122.5	SO*	28	4.3	80	B-	10 7 3	5.26E2	
147	12 59 44.4	28 39 21	.6544	50.1	E/SO	31	2.0	57	N	10 7 2	8.10E2	
148	12 59 45.9	28 27 38	.5558	66.2	SO*	33	0.0	0	N	9 4 2	1.02E3	
149	12 59 47.4	28 26 30	.5537	68.2	SB*	28	4.4	12	B+	9 5 4	5.18E2	FWD
150	12 59 50.0	28 37 16	.6493	53.6	SO	24	3.9	101	B-	10 6 3	4.34E2	

NO	RA(1950)	DEC(1950)	R	THETA	TYPE	D(0)	ELL	PA	COL	SUR.BRG	AREA	SW
151	12 59 57.2	28 29 57	.6095	64.4	SO	26	6.5	59	N	10 8 4	3.54E2	
152	12 59 57.4	28 31 29	.6215	62.3	E	25	4.9	61	N	10 7 3	4.09E2	
153	13 0 10.4	28 13 3	.5998	91.7	S/SO	28	6.0	6	B-	10 6 3	4.32E2	FWD
154	13 0 14.0	28 46 13	.8109	48.7	S/IRR	27	6.7	36	B-	9 5 3	3.61E2	
155	13 0 14.2	28 23 0	.6301	76.4	S/IRR	37	3.5	158	B-	10 6 3	9.52E2	FWD
156	13 0 16.6	28 38 23	.7401	56.9	SO	48	7.0	124	B-	10 7 3	9.43E2	
157	13 0 20.1	28 18 49	.6394	83.0	SO	50	2.3	40	N	10 6 3	1.83E3	
158*	13 0 28.4	28 8 6	.6736	98.5	E/SO	21	5.6	136	N	10 8 4	2.86E2	
159	13 0 29.3	28 34 45	.7502	62.7	SB/IRR	29	4.0	63	B+	8 6 3	5.80E2	
160	13 0 32.3	28 20 19	.6870	81.3	S/SO	27	5.9	137	B-	9 7 4	4.10E2	
161	13 0 36.5	28 18 3	.6979	84.6	SO	71	5.5	76	B	10 6 2	2.55E3	
162	13 0 45.7	28 51 7	.9520	49.6	S	33	6.3	38	N	10 8 4	5.60E2	FWD
163	13 0 48.4	28 26 27	.7658	74.4	S/IRR	25	6.3	62	B-	9 5 2	3.52E2	
164*	13 0 49.3	27 38 15	.9559	128.7	S/SO	22	6.4	101	N	9 5 3	2.81E2	
165	13 0 52.1	28 17 55	.7548	85.1	S	53	6.5	103	B	10 7 2	1.25E3	
166	13 0 52.2	27 36 6	.9870	129.9	S*	24	6.0	9	B+	10 6 4	3.27E2	REV
167*	13 1 20.8	28 21 8	.8651	82.1	E*	23	4.1	107	B-	10 7 4	4.00E2	
168	13 1 25.9	28 27 13	.9020	75.9	S	86	6.0	86	B-	10 8 2	3.38E3	REV
169	13 1 46.1	28 30 57	.9895	73.4	SO	44	2.6	40	N	10 7 2	1.41E3	
170	13 1 48.8	28 27 42	.9855	76.6	S	26	6.8	141	N	10 7 4	3.47E2	
171	13 1 54.5	28 44 10	1.0990	62.7	S/SO	26	5.8	179	N	10 7 3	3.49E2	
172	13 2 25.4	28 32 15	1.1339	74.3	SO	28	0.0	0	B-	9 6 4	7.49E2	

CLUSTER A2147 PAGE 1

NO	RA(1950)	DEC(1950)	R	THETA	TYPE	D(0)	ELL	PA	COL	SUR.BRG	AREA	SW
1	15 57 40.1	15 58 6	.5781	255.6	SBO	20	3.0	139	R-	9 6 3	3.59E2	
2	15 57 41.1	15 43 53	.6742	235.7	S	40	6.4	96	R-	10 8 3	8.04E2	FWD
3	15 57 56.1	16 33 5	.6616	311.6	E*	18	4.0	85	N	9 7 5	2.66E2	
4	15 57 58.3	15 54 32	.5279	247.4	SB	23	2.2	80	B	8 4 2	4.63E2	REV
5	15 57 58.4	16 23 1	.5565	299.2	S/SO	15	6.0	94	B-	9 5 3	1.72E2	
6	15 57 59.3	16 17 1	.5120	289.6	S/SO	15	6.6	162	N	9 7 4	1.62E2	
7	15 57 59.6	16 17 6	.5113	289.8	S	29	6.5	125	R-	10 7 4	4.43E2	
8	15 58 .4	15 53 46	.5253	245.7	S	31	5.8	48	R-	10 8 3	5.53E2	FWD:
9	15 58 1.7	16 33 54	.6543	313.8	S/SO	21	5.5	135	N	9 7 2	3.07E2	
10	15 58 18.4	15 49 30	.4980	234.8	SB	49	1.7	160	B	10 6 2	1.95E3	FWD
11	15 58 28.6	15 54 52	.4158	241.6	S*	19	4.3	96	N	9 6 4	2.83E2	
12	15 58 36.9	16 28 29	.4913	317.5	S/SO	32	3.8	118	N	10 7 3	7.38E2	
13	15 58 37.7	16 29 7	.4970	318.6	SB	36	3.0	93	N	9 6 3	9.84E2	FWD
14	15 58 38.6	15 39 57	.5529	216.2	S	32	5.8	132	R-	10 7 4	6.01E2	
15	15 58 38.9	15 53 39	.3910	236.1	SO	19	5.6	74	R-	9 6 2	2.50E2	
16	15 58 41.0	16 25 21	.4424	314.5	SO	15	4.1	22	B	9 6 3	2.06E2	
17	15 58 43.7	15 33 32	.6323	208.9	SBO	34	3.3	35	R+	10 6 3	8.81E2	
18	15 58 44.9	15 38 2	.5652	212.2	S/SO*	31	2.6	136	R-	9 7 3	7.62E2	
19	15 58 55.1	15 53 41	.3388	230.0	S	38	6.6	176	N	9 6 2	7.21E2	
20*	15 58 56.2	16 36 41	.5601	333.0	S	14	7.4	144	N	8 6 4	1.29E2	
21	15 58 57.1	15 49 41	.3797	221.5	S	39	7.3	83	N	9 7 3	6.65E2	
22	15 58 59.4	15 47 3	.4081	216.5	E	33	.4	0	R+	10 7 3	9.93E2	
23	15 59 1.1	15 43 53	.4481	211.8	IRR	20	2.8	128	B+	9 6 5	3.69E2	
24	15 59 4.5	16 26 45	.4003	326.4	SB	58	2.4	115	N	10 6 2	2.48E3	REV
25	15 59 6.3	16 21 25	.3252	318.8	S/IRR*	17	3.6	77	B	10 8 6	2.50E2	

CLUSTER A2147 PAGE 2

NO	RA(1950)	DEC(1950)	R	THETA	TYPE	D(0)	ELL	PA	COL	SUR.BRG	AREA	SW
26	15 59 12.5	15 58 15	.2368	233.3	S	18	5.3	45	R-	8 5 3	2.40E2	
27	15 59 12.9	15 38 33	.5063	201.9	E	74	0.0	0	R	10 6 2	4.72E3	
28	15 59 14.7	15 58 10	.2307	231.7	S/SO	29	5.8	96	N	10 6 3	5.11E2	
29	15 59 14.9	15 36 38	.5334	199.8	S/IRR	18	6.9	178	B-	9 6 3	1.94E2	
30	15 59 20.2	16 34 10	.4837	340.9	SB/SBO	60	3.5	36	N	10 7 2	2.40E3	
31	15 59 22.2	16 9 11	.1563	285.1	S/SO*	26	4.0	180	R	9 6 4	5.15E2	
32	15 59 22.7	16 26 56	.3678	336.2	S	27	7.0	63	N	9 7 4	3.64E2	
33	15 59 25.9	16 4 25	.1416	254.1	S/SO	23	6.8	23	R-	9 6 3	2.87E2	
34	15 59 27.9	15 58 32	.1875	223.1	S/IRR	17	5.9	150	R-	9 7 4	2.06E2	
35	15 59 28.4	16 1 47	.1509	236.7	S/SO	22	7.0	168	N	9 7 3	2.75E2	
36	15 59 29.3	15 29 34	.6317	191.2		21	7.0	40	R-	6 4 2	2.47E2	
37	15 59 29.5	15 57 39	.1945	218.8	SO	29	5.9	111	R-	9 7 2	4.82E2	
38	15 59 29.7	16 17 45	.2196	326.6	S/SO	17	6.6	126	R-	9 8 5	1.87E2	
39	15 59 34.5	16 22 29	.2812	338.8	S	19	6.8	100	N	9 6 4	2.26E2	
40	15 59 34.7	15 55 50	.2081	209.0	SB	55	2.0	131	R-	10 5 2	2.35E3	FWD
41	15 59 35.2	16 23 14	.2919	340.2	S/SO	25	0.0	0	R-	10 6 2	6.51E2	
42	15 59 38.3	15 50 41	.2814	197.9	IRR	17	2.2	10	B+	9 7 5	2.99E2	
43	15 59 38.3	16 35 34	.4880	349.8	E	28	1.6	70	R-	10 8 4	7.10E2	
44*	15 59 41.0	16 26 20	.3350	347.0	IRR	14	2.6	68	B	4 2 2	2.05E2	
45	15 59 42.9	15 37 45	.4881	188.0	E*	15	2.5	108	R-	9 7 5	2.21E2	
46	15 59 45.2	16 34 25	.4648	352.7	E	20	5.0	110	N	9 8 4	2.95E2	
47	15 59 46.7	16 40 3	.5575	354.6	S	26	6.8	161	N	9 7 3	3.54E2	
48	15 59 48.1	16 29 42	.3854	353.0	IRR*	20	7.7	154	R-	5 5 3	2.07E2	
49	15 59 48.1	16 29 57	.3895	353.0	SO	17	2.9	150	N	9 7 4	2.75E2	
50	15 59 50.7	15 50 4	.2805	187.6	SO	38	0.0	0	R	9 7 3	1.33E3	

NO	RA(1950)	DEC(1950)	R	THETA	TYPE	D(0)	ELL	PA	COL	SUR.BRG	AREA	SW
51	15 59 51.3	15 49 51	.2838	187.0	S*	19	3.1	153	R	10 8 3	3.35E2	REV
52	15 59 51.7	16 28 49	.3692	354.9	S/SO	15	5.4	54	R-	9 7 4	1.79E2	
53	15 59 51.8	15 38 22	.4742	183.9	S/SO*	16	6.4	38	N	9 7 3	1.75E2	
54	15 59 51.9	15 50 57	.2653	186.9	S/SO	20	6.8	91	R-	9 5 3	2.43E2	
55	15 59 52.0	16 1 33	.0923	200.1	S	35	6.7	102	N	10 8 2	6.05E2	
56*	15 59 54.2	16 25 20	.3106	355.8	S/SO	14	6.5	131	R	8 6 3	1.46E2	
57*	15 59 54.9	15 31 58	.5801	182.0	S	15	7.3	113	R+	6 3 2	1.49E2	
58*	15 59 55.2	15 32 9	.5770	181.9	S	18	7.0	95	N	4 2 2	2.01E2	
59	15 59 55.7	16 2 44	.0690	194.1	E	71	1.8	27	R	10 7 2	3.80E3	
60	15 59 56.2	16 4 31	.0401	201.7	E/SO	35	2.0	176	N	10 7 3	1.02E3	
61	15 59 56.5	16 33 51	.4519	358.3	SB	65	0.0	0	N	10 7 5	3.69E3	
62	15 59 57.7	16 9 44	.0505	350.0	SO*	34	6.0	20	R+	9 5 3	6.40E2	
63*	15 59 58.5	16 17 21	.1768	358.2	S/IRR	25	1.3	0	N	7 3 3	5.95E2	
64	15 59 59.6	16 12 53	.1022	359.3	SB	28	3.9	111	R	8 4 2	5.84E2	FWD
65	15 59 59.9	16 6 45	0.0000	0.0	E/SO	105	2.8	15	R+	10 6 1	7.44E3	
66	16 0 1.4	16 30 14	.3914	.9	E/SO	56	2.2	179	R	10 7 3	2.38E3	
67	16 0 1.8	16 24 33	.2968	1.5	S/SO	18	4.4	158	R-	9 7 3	2.66E2	
68	16 0 3.2	16 29 2	.3716	2.0	E/SO	94	1.5	178	R+	10 6 2	6.66E3	
69	16 0 3.5	15 36 8	.5105	178.4	SBO	41	2.1	111	R-	10 7 2	1.33E3	
70*	16 0 3.5	15 37 26	.4888	178.3	S/SO	14	6.1	31	R-	9 7 5	1.52E2	
71	16 0 4.7	16 17 49	.1854	5.9	S	41	7.3	176	N	9 8 3	7.20E2	
72	16 0 9.1	16 33 34	.4485	4.7	SO	15	4.9	96	R-	9 6 4	1.84E2	
73	16 0 11.1	15 59 2	.1362	160.8	S/SO	20	5.9	136	R	9 7 3	2.71E2	
74	16 0 13.2	16 32 26	.4313	7.1	SBO	48	3.6	76	R	9 6 3	1.54E3	
75	16 0 16.6	16 3 42	.0840	127.2	S	24	3.9	107	R	9 7 3	4.42E2	

NO	RA(1950)	DEC(1950)	R	THETA	TYPE	D(0)	ELL	PA	COL	SUR.BRG	AREA	SW
76*	16 0 17.2	15 25 14	.6954	174.3	S	14	6.3	115	R	4 2 2	1.44E2	
77	16 0 19.7	16 37 6	.5120	8.9	SO	37	.7	0	R-	9 6 2	1.23E3	
78	16 0 23.1	15 53 36	.2381	157.0	SO*	47	.7	0	N	10 6 3	1.91E2	
79	16 0 23.5	16 7 14	.0948	85.1	SO	17	6.1	64	R-	9 7 3	2.08E2	
80	16 0 25.9	16 41 33	.5892	10.1	S/SO	17	6.6	130	N	9 7 4	1.99E2	
81	16 0 27.4	16 25 22	.3292	19.5	S	15	5.9	34	R	9 7 4	1.76E2	REV
82	16 0 28.4	16 23 8	.2959	22.6	SO	45	2.0	134	R-	10 6 2	1.62E3	
83	16 0 31.7	16 15 24	.1923	41.4	E/SO	39	2.9	54	R	10 7 3	1.16E3	
84	16 0 33.9	16 5 54	.1368	95.9	SBO	40	0.0	0	N	9 4 1	1.47E3	
85	16 0 34.0	16 42 27	.6104	12.9	S/SO	44	6.1	177	N	10 7 3	1.00E3	
86	16 0 34.4	15 40 2	.4662	162.7	E	18	0.0	0	N	9 8 4	3.54E2	
87	16 0 37.0	15 28 22	.6568	166.9	E*	19	2.4	21	N	9 8 5	3.29E2	
88	16 0 41.6	15 58 47	.2133	128.5	S/SO	69	3.4	152	R	10 5 2	3.11E3	
89	16 0 43.7	16 15 25	.2271	50.5	S	31	5.7	159	N	9 7 2	5.75E2	FWD
90	16 0 44.2	16 14 0	.2145	55.7	S	37	7.2	7	R-	9 7 3	6.00E2	
91	16 0 44.7	16 30 29	.4342	24.3	S/SO	22	3.2	68	N	9 7 2	4.06E2	
92	16 0 45.5	16 10 13	.1914	72.4	SO	21	7.1	119	N	9 7 3	2.39E2	
93	16 0 45.9	15 34 49	.5633	160.9	S/SO	15	6.6	69	N	8 6 3	1.53E2	
94	16 0 46.1	15 35 48	.5481	160.2	S	36	6.0	158	N	9 6 2	6.96E2	
95	16 0 48.6	16 24 14	.3505	33.7	SO	20	4.7	155	R	9 7 4	3.08E2	
96	16 0 51.1	16 19 22	.2936	44.2	S	16	7.0	51	R-	7 4 3	1.71E2	
97	16 0 53.0	16 16 33	.2680	52.4	S/SO	26	4.0	77	R-	9 6 3	4.92E2	
98	16 0 55.6	15 59 8	.2566	119.6	S*	30	5.3	164	B+	9 7 4	5.53E2	
99	16 0 56.4	16 13 18	.2511	64.2	SO	23	3.1	54	R-	8 4 4	4.50E2	
100	16 0 57.4	16 29 32	.4439	31.2	S	24	7.2	43	R-	8 6 3	2.89E2	

NO	RA(1950)	DEC(1950)	R	THETA	TYPE	D(0)	ELL	PA	COL	SUR.BRG	AREA	SW
101	16 0 58.2	16 32 22	.4864	28.6	E	53	4.2	150	R-	10 7 3	1.79E3	
102	16 1 4.7	16 43 38	.6671	22.8	IRR	25	6.6	93	N	9 6 3	3.39E2	
103	16 1 8.5	15 46 60	.4288	140.1	S	26	7.1	59	B	9 6 3	3.38E2	
104	16 1 14.6	15 42 18	.5056	143.7	S	29	6.3	110	N	10 7 3	4.77E2	
105	16 1 16.3	16 27 34	.4623	41.3	E/SO*	58	1.7	71	R	10 6 2	2.60E3	
106	16 1 17.4	16 0 41	.3264	108.0	S	25	2.3	38	B+	9 5 3	5.26E2	
107	16 1 20.2	15 48 47	.4395	132.9	SO	24	0.0	0	R+	9 5 4	5.92E2	
108	16 1 20.4	16 7 36	.3225	87.4	SO	29	1.9	36	N	9 7 2	7.41E2	
109	16 1 21.0	16 2 13	.3334	103.1	E	29	2.8	146	R+	9 6 3	6.64E2	
110	16 1 21.3	15 46 54	.4645	135.4	S*	19	2.0	120	N	9 7 3	3.42E2	
111	16 1 25.2	16 36 43	.6048	34.3	S/SO	27	6.2	41	R-	9 7 4	4.30E2	
112	16 1 26.4	15 55 34	.3934	118.2	S/SO	24	3.4	58	N	9 5 3	4.74E2	
113	16 1 27.0	16 27 51	.4950	44.7	E	31	2.0	96	R+	10 7 3	8.22E2	
114	16 1 27.4	16 12 40	.3638	74.2	S	21	3.1	123	N	8 6 4	3.89E2	
115	16 1 27.8	16 27 29	.4929	45.4	E*	16	0.0	0	N	9 8 5	3.11E2	
116	16 1 28.4	16 24 37	.4626	49.9	E/SO	17	3.3	142	N	9 7 5	2.62E2	
117	16 1 29.2	16 28 29	.5087	44.5	E	25	0.0	0	R	10 7 4	6.51E2	
118	16 1 31.5	16 19 55	.4271	59.0	S	18	7.3	28	N	9 7 3	1.89E2	
119	16 1 33.1	16 4 54	.3744	94.7	E	33	3.2	127	R	9 7 3	8.33E2	
120	16 1 33.2	15 53 4	.4378	121.3	S	26	5.6	175	N	9 7 3	4.32E2	
121	16 1 36.7	15 55 34	.4302	115.6	SO*	27	3.4	3	R-	9 5 3	5.79E2	
122	16 1 38.2	16 15 36	.4201	69.4	S	29	6.4	114	B	9 6 3	4.51E2	
123*	16 1 40.7	16 11 13	.4102	79.5	S/SO	14	7.1	101	N	8 6 3	1.37E2	
124	16 1 40.7	16 29 52	.5576	46.2	E	23	3.2	173	N	10 7 4	4.24E2	
125	16 1 41.1	16 8 11	.4058	86.6	S/SO*	38	0.0	0	R-	10 7 3	1.33E3	

NO	RA(1950)	DEC(1950)	R	THETA	TYPE	D(0)	ELL	PA	COL	SUR.BRG	AREA	SW
126	16 1 41.7	16 6 10	.4076	91.3	E	15	4.1	78	N	9 6 3	2.06E2	
127	16 1 47.2	16 30 28	.5834	47.3	SO	15	4.6	147	B-	8 6 4	1.93E2	
128	16 1 48.0	16 36 57	.6634	40.6	S/SO	16	3.6	10	N	9 8 3	2.34E2	
129	16 1 53.6	16 13 24	.4683	76.2	S/SO	31	3.0	147	N	9 6 3	7.69E2	
130	16 1 56.5	16 17 58	.5026	68.1	SO*	21	2.1	179	R	9 7 4	4.24E2	
131	16 1 59.5	16 35 46	.6801	44.6	S	29	7.0	132	R-	9 7 3	4.25E2	
132	16 2 .1	16 13 50	.4953	76.1	S	27	6.5	83	N	10 7 3	3.92E2	
133	16 2 4.3	16 1 30	.5057	99.9	S	16	4.8	142	N	9 7 3	2.10E2	
134	16 2 8.6	16 0 30	.5257	101.4	S	19	7.2	43	N	8 6 3	2.06E2	
135*	16 2 26.2	16 6 46	.5856	89.9	IRR	14	6.3	98	R-	5 3 2	1.44E2	
136	16 2 34.4	15 51 30	.6690	112.2	SBO	43	2.3	56	R-	10 7 2	1.41E3	
137	16 2 35.6	15 59 45	.6343	100.5	S/SO	18	2.4	171	N	9 6 4	3.07E2	
138	16 2 47.5	15 59 38	.6815	99.9	S	27	5.3	98	N	9 5 3	4.61E2	

CLUSTER A2151 PAGE 1

NO	RA(1950)	DEC(1950)	R	THETA	TYPE	D(0)	ELL	PA	COL	SUR.BRG	AREA	SW
1	15 59 53.1	18 2 6	.7275	281.4	S	16	5.7	125	N	10 7 3	1.86E2	REV
2	15 59 59.5	17 38 38	.7324	250.2	S/IRR	19	6.0	125	B+	8 4 2	2.37E2	
3	16 0 16.0	17 47 22	.6316	260.7	S	15	6.3	67	B-	9 4 2	1.63E2	
4	16 0 25.5	18 8 40	.6367	293.4	SO	21	6.7	95	R	10 6 3	2.69E2	
5	16 0 29.5	17 26 29	.7272	231.7	S	23	5.0	39	B	10 6 3	3.61E2	FWD
6	16 0 37.2	18 6 34	.5805	292.0	S	21	5.6	119	B	9 5 2	3.06E2	REV
7	16 0 39.7	17 52 18	.5294	267.8	S	28	3.4	36	B	9 5 3	5.98E2	
8	16 0 51.4	17 39 49	.5345	244.7	S/IRR	26	3.7	65	N	9 5 2	5.05E2	
9*	16 0 52.3	17 25 33	.6694	225.8	S	14	7.0	11	R	9 4 3	1.29E2	
10	16 0 54.3	18 12 50	.5697	304.4	SB	21	2.7	98	B-	10 7 4	3.82E2	FWD
11	16 0 58.6	17 30 16	.5978	229.6	S	32	6.8	175	R-	10 7 3	5.02E2	
12	16 1 1.3	17 56 1	.4451	275.3	S	26	0.0	0	N	10 8 3	6.70E2	
13	16 1 7.1	17 43 19	.4539	248.0	S/IRR	39	2.6	17	B+	9 5 2	1.17E3	FWD
14	16 1 12.6	17 34 11	.5133	231.1	E/SO*	18	2.5	123	R	10 7 4	2.95E2	
15	16 1 16.4	17 20 7	.6770	214.6	E/SO	91	2.0	49	R-	10 6 2	6.08E3	
16	16 1 17.3	17 36 57	.4703	234.0	SB	41	2.2	140	N	10 6 2	1.34E3	REV
17	16 1 25.1	17 28 27	.5452	219.9	S	22	2.3	87	B-	10 5 3	4.47E2	REV
18*	16 1 25.8	17 57 46	.3531	281.5	S/IRR	14	7.1	148	N	9 4 3	1.41E2	
19	16 1 32.7	17 22 38	.6064	211.8	SB	70	5.5	56	N	10 7 2	2.52E3	REV
20	16 1 41.1	17 26 29	.5343	212.4	SO	25	1.1	13	N	10 6 3	5.97E2	
21	16 1 41.4	18 25 51	.6083	332.2	S	22	7.4	137	R-	10 7 4	2.53E2	FWD
22	16 1 45.1	17 41 28	.3368	233.3	S	18	2.1	84	R-	10 5 3	3.09E2	
23	16 1 47.3	17 25 7	.5414	208.9	E/SO	34	4.7	45	R	10 7 3	7.40E2	
24	16 1 51.5	17 22 20	.5752	205.2	S/IRR	36	3.8	164	N	8 4 2	8.95E2	
25	16 1 52.2	17 43 6	.2980	234.2	S	24	7.2	139	R-	9 6 3	3.00E2	

NO	RA(1950)	DEC(1950)	R	THETA	TYPE	D(0)	ELL	PA	COL	SUR.BRG	AREA	SW
26	16 1 54.7	17 20 26	.5989	202.8	S	20	7.3	157	N	9 6 4	2.24E2	
27	16 1 55.5	18 7 0	.3197	314.5	S/SO	20	4.3	150	R-	10 7 4	3.22E2	
28	16 2 .4	18 15 55	.4270	330.8	S/SO	18	5.4	72	N	9 6 4	2.43E2	
29	16 2 3.9	17 18 58	.6089	198.7	S*	19	1.7	81	R-	10 8 5	3.66E2	
30	16 2 4.9	17 34 20	.3733	210.9	S	25	7.4	105	N	10 8 4	3.12E2	
31	16 2 7.2	18 16 29	.4230	334.6	S	29	7.5	111	B	9 7 4	3.73E2	
32	16 2 8.0	17 40 1	.2881	218.4	S	25	7.2	2	N	9 5 3	3.18E2	
33	16 2 8.2	18 0 49	.2151	304.2	SBO	32	1.8	143	R	10 7 3	8.68E2	
34	16 2 8.7	18 27 44	.5960	342.9	S/SO	30	3.1	50	N	10 5 2	7.00E2	
35	16 2 11.5	17 52 39	.1657	264.7	S/SO	30	0.0	0	B-	10 7 3	8.79E2	
36	16 2 11.5	18 7 23	.2832	324.4	S	21	5.3	25	N	10 7 5	3.18E2	REV
37	16 2 11.7	17 53 9	.1643	267.6	S*	72	6.2	43	N	10 7 3	2.42E3	FWD
38	16 2 13.7	17 47 4	.1902	235.3	E	15	3.3	60	R-	10 8 5	2.23E2	
39	16 2 15.1	17 36 17	.3251	207.7	SB	38	4.1	10	B+	10 6 3	9.62E2	FWD
40	16 2 15.2	18 35 42	.7181	348.0	S	20	7.5	138	N	9 7 5	2.14E2	
41	16 2 16.7	17 51 25	.1487	256.1	E/SO	25	5.8	89	N	10 8 3	3.82E2	
42	16 2 19.8	17 51 11	.1379	253.3	E	21	3.6	86	R-	10 8 3	3.76E2	
43	16 2 20.6	17 51 24	.1338	254.4	E/SO	94	2.7	32	R	10 6 2	5.99E3	
44	16 2 22.9	17 58 18	.1434	303.4	S	29	0.0	0	R-	10 7 3	8.42E2	REV
45	16 2 23.6	17 29 8	.4237	196.1	SO	19	3.8	158	N	10 7 5	2.95E2	
46	16 2 24.5	17 50 10	.1268	243.5	E	93	1.8	67	R	10 6 2	6.37E2	
47	16 2 25.1	17 56 44	.1229	295.4	S	18	7.1	71	N	10 7 4	1.89E2	
48	16 2 25.3	18 10 4	.2962	338.2	S/SO	17	6.9	88	N	10 8 5	1.81E2	
49	16 2 27.1	17 49 9	.1267	234.5	SO	17	6.3	107	N	10 6 3	2.05E2	
50	16 2 27.7	17 46 27	.1556	220.4	SBO	22	1.0	0	R-	10 6 2	4.73E2	

NO	RA(1950)	DEC(1950)	R	THETA	TYPE	D(0)	ELL	PA	COL	SUR.BRG	AREA	SW
51	16 2 30.1	17 35 2	.3221	196.5	SB	41	.5	0	B	10 6 3	1.47E3	FWD
52	16 2 32.2	17 28 59	.4180	191.5	S	23	5.7	30	B-	10 7 4	3.33E2	FWD
53*	16 2 35.6	17 24 24	.4911	188.1	S/IRR	14	6.4	52	N	9 6 3	1.46E2	
54	16 2 44.0	18 19 20	.4310	355.2	S	18	7.1	78	N	10 7 3	1.90E2	
55	16 2 44.8	18 0 20	.1175	343.7	+S/SO	35	0.0	0	N	10 7 4	1.15E3	FWD
56	16 2 46.4	17 54 39	.0321	304.2	+E/SO	38	0.0	0	R-	10 6 3	1.32E3	
57	16 2 46.7	17 57 59	.0779	341.0	+S	16	6.1	18	R-	10 8 5	1.91E2	
58*	16 2 49.0	17 42 56	.1780	185.2	S	14	7.1	61	B	9 6 3	1.34E2	
59	16 2 51.4	17 53 32	.0067	264.7	+S*	20	4.5	78	B-	9 6 3	3.13E2	REV
60	16 2 53.1	17 53 34	0.0000	0.0	+S*	37	6.9	72	N	10 8 5	6.51E2	REV
61	16 2 54.0	17 51 53	.0283	172.7	+SO	70	1.7	123	R-	10 6 2	3.74E3	
62	16 2 55.6	17 59 22	.0972	5.9	+IRR*	22	4.3	105	B	9 6 3	3.58E2	
63	16 2 57.3	17 44 1	.1600	174.0	S*	17	0.0	0	B+	9 5 3	3.21E2	
64	16 2 57.4	17 33 30	.3349	177.1	SB	71	5.0	63	N	10 7 3	2.79E3	REV
65*	16 2 57.7	17 29 21	.4040	177.4	IRR	14	6.0	116	B-	8 5 3	1.47E2	
66	16 2 59.5	18 1 8	.1286	11.4	+S	42	2.4	118	B-	8 5 3	1.40E3	
67	16 2 59.6	17 56 8	.0499	31.1	+S*	16	5.5	180	R	10 6 5	2.07E2	
68	16 3 .2	17 40 29	.2199	172.6	S	39	7.3	160	N	9 7 3	6.55E2	REV
69	16 3 .8	17 50 33	.0588	148.7	+E/SO	21	6.7	82	N	10 8 3	2.69E2	
70	16 3 1.0	17 44 22	.1565	168.4	S/SO	20	7.0	32	N	10 8 5	2.55E2	
71	16 3 5.4	18 27 1	.5596	5.0	SBO	22	0.0	0	R-	10 7 2	4.94E2	
72	16 3 7.2	17 53 20	.0560	94.0	+SB	36	4.4	152	B	10 5 3	8.65E2	REV
73	16 3 7.6	17 59 24	.1129	30.6	+SB	25	1.3	147	R-	10 7 3	5.81E2	FWD
74	16 3 8.4	17 53 31	.0607	90.8	+S	46	4.4	132	B-	10 7 3	1.33E3	FWD
75	16 3 11.0	18 18 33	.4224	9.7	SO	26	0.0	0	N	9 7 4	6.70E2	

CLUSTER A2151 PAGE 4

NO	RA(1950)	DEC(1950)	R	THETA	TYPE	D(0)	ELL	PA	COL	SUR.BRG	AREA	SW
76	16 3 11.2	17 49 53	.0945	130.5	+S	29	7.3	157	N	9 6 3	3.87E2	FWD
77	16 3 11.8	18 2 40	.1688	26.0	SB	35	5.4	177	R-	10 7 3	7.39E2	REV
78	16 3 12.7	17 57 54	.1061	47.1	+S	15	6.8	119	R-	10 8 4	1.52E2	
79	16 3 13.1	18 28 32	.5881	7.7	S	24	5.7	142	B-	10 7 3	3.62E2	
80*	16 3 13.4	17 57 48	.1061	47.5	+S	13	6.8	113	R-	10 8 4	1.20E2	
81	16 3 14.7	17 48 55	.1155	132.1	+S	31	0.0	0	N	10 6 3	9.52E2	FWD
82	16 3 14.7	18 3 47	.1906	26.7	S/SO	23	5.2	149	R-	10 7 4	3.53E2	
83	16 3 15.7	17 54 12	.0902	83.3	+SB	42	4.0	176	B-	10 6 2	1.16E3	REV
84	16 3 16.6	18 5 54	.2257	24.4	S/SO	53	4.8	59	R-	10 7 3	1.64E3	
85	16 3 17.7	18 12 52	.3361	16.8	S/SO	18	5.1	16	N	10 7 5	2.44E2	
86	16 3 18.0	17 44 9	.1854	147.8	+SO*	28	1.2	83	R-	10 7 3	7.39E2	
87	16 3 18.0	18 17 38	.4131	13.8	SB/SBO	78	2.5	55	R+	10 6 2	4.33E3	
88	16 3 18.4	17 49 23	.1222	124.8	+SB	19	5.6	85	N	10 7 4	2.57E2	REV
89	16 3 18.7	17 43 43	.1930	148.2	SB/SBO*	21	4.8	62	R	10 7 5	3.14E2	
90	16 3 20.8	17 51 55	.1132	104.0	+S	20	4.9	180	N	9 6 3	3.09E2	FWD
91	16 3 21.9	17 56 12	.1223	69.0	+SO*	51	2.5	67	R	10 6 2	1.92E3	
92	16 3 22.1	18 24 27	.5274	12.6	E	31	2.4	117	B-	10 7 3	7.70E2	
93	16 3 23.2	17 54 8	.1197	85.5	+SO	47	2.6	73	R	10 7 2	1.63E3	
94	16 3 25.1	18 17 56	.4254	17.3	E	32	1.2	0	R	10 7 3	8.94E2	
95	16 3 25.4	18 11 25	.3239	23.3	S	79	3.6	160	R	10 6 2	3.95E3	FWD
96	16 3 26.3	18 14 31	.3731	20.6	SO	33	0.0	0	R-	10 7 4	1.03E3	
97*	16 3 27.7	18 29 34	.6154	12.8	S	13	5.1	154	R	10 7 4	1.50E2	REV
98	16 3 28.8	17 29 47	.4210	160.3	SB	39	4.0	3	N	10 8 3	1.04E3	REV
99	16 3 29.7	17 51 4	.1510	106.0	+S	43	2.7	9	N	10 7 3	1.41E3	REV
100	16 3 30.4	17 43 1	.2298	139.9	S	39	0.0	0	B-	9 5 2	1.42E3	REV

NO	RA(1950)	DEC(1950)	R	THETA	TYPE	D(0)	ELL	PA	COL	SUR.BRG	AREA	SW
101	16 3 31.7	18 9 4	.3002	30.6	SB	30	2.9	121	R	10 7 4	6.96E2	
102	16 3 33.1	18 31 9	.6461	14.2	S/IRR	17	7.5	100	B	9 5 3	1.64E2	
103	16 3 37.9	18 21 17	.4948	21.0	SB	60	5.8	117	N	10 6 3	1.83E3	REV
104	16 3 38.1	18 35 57	.7285	14.1	S/IRR	17	4.1	114	B	10 6 4	2.55E2	
105	16 3 38.6	17 28 30	.4552	156.6	S	19	5.6	4	N	10 7 4	2.57E2	
106	16 3 40.5	18 26 46	.5843	18.7	S	18	6.6	63	N	10 8 4	2.04E2	REV
107	16 3 45.7	18 19 48	.4843	25.4	SB	55	5.0	82	N	10 6 3	1.75E3	REV
108	16 3 47.4	18 14 47	.4139	31.3	S	24	0.0	0	B-	10 6 3	5.79E2	FWD
109	16 3 50.6	18 10 13	.3590	39.3	S	23	5.5	118	R-	10 6 4	3.48E2	FWD
110*	16 3 51.2	18 17 22	.4586	30.1	IRR*	17	3.7	159	B-	4 3 2	2.53E2	
111	16 3 52.1	17 35 42	.3788	141.8	S	28	4.3	5	R	10 8 4	5.66E2	REV
112	16 3 54.2	18 0 39	.2694	64.0	+IRR*	31	0.0	0	B-	7 4 3	9.52E2	
113	16 3 55.4	17 50 10	.2535	102.9	+S	20	6.9	133	N	9 6 3	2.24E2	REV
114	16 3 56.7	17 26 9	.5221	151.0	S	27	6.2	114	N	10 8 3	4.21E2	FWD
115	16 3 57.3	18 27 47	.6243	24.0	S	21	7.7	176	N	10 9 5	2.14E2	
116	16 3 59.0	18 5 18	.3263	53.1	+S	24	1.9	36	B+	10 6 4	5.17E2	REV
117	16 4 .1	18 32 55	.7074	22.0	S/SO	42	3.4	2	N	10 6 3	1.24E3	
118	16 4 .4	18 19 0	.5007	32.1	S	28	3.1	175	R-	10 7 3	6.03E2	FWD
119	16 4 1.7	18 18 18	.4937	33.3	SO	17	5.6	30	N	10 7 3	2.11E2	
120	16 4 1.7	18 23 1	.5610	28.9	SO	72	2.3	99	R	10 6 2	3.77E3	
121	16 4 3.3	18 29 44	.6637	24.7	SO*	16	5.3	145	N	10 8 5	1.99E2	
122	16 4 5.6	17 55 19	.2889	84.2	+SO	18	6.6	126	N	10 7 3	2.02E2	
123	16 4 6.4	17 25 13	.5549	148.3	IRR	18	4.6	117	B-	8 4 3	2.61E2	
124	16 4 7.7	18 3 47	.3412	60.0	+SO	25	6.7	68	N	10 7 3	3.36E2	
125*	16 4 10.9	17 23 16	.5920	148.5	S/SO	13	7.3	100	R-	10 5 4	1.22E2	

CLUSTER A2151 PAGE 6

NO	RA(1950)	DEC(1950)	R	THETA	TYPE	D(0)	ELL	PA	COL	SUR.BRG	AREA	SW
126	16 4 14.6	18 24 8	.6030	32.3	S	20	7.3	172	N	10 9 5	2.25E2	
127	16 4 15.4	18 24 5	.6040	32.6	S/SO	15	6.4	156	N	10 8 4	1.54E2	
128	16 4 17.2	17 50 50	.3366	97.7	E/SO*	51	2.1	9	R+	10 7 3	1.98E3	
129	16 4 18.2	17 54 34	.3378	87.1	+S	40	6.6	119	R-	10 6 3	7.91E2	
130	16 4 18.9	17 25 51	.5740	143.5	S	23	5.0	142	R	10 6 3	3.61E2	FWD
131	16 4 20.5	18 1 34	.3712	68.9	S/SO	23	5.3	149	N	8 4 3	3.63E2	
132	16 4 20.8	17 51 20	.3498	96.1	S/SO	22	6.5	113	R-	10 7 3	2.90E2	
133*	16 4 20.9	17 49 46	.3539	100.3	S/SO	14	6.7	173	N	10 8 4	1.46E2	
134	16 4 23.7	17 55 1	.3600	86.1	E/SO	20	3.1	24	R-	10 7 4	3.45E2	
135	16 4 24.4	17 53 39	.3620	89.7	E	28	2.1	23	R	10 7 4	6.61E2	
136	16 4 25.0	18 3 47	.4021	64.9	IRR	23	2.9	68	B	8 4 3	4.56E2	
137	16 4 25.3	17 19 31	.6754	147.1	S	28	3.1	17	N	10 7 4	6.29E2	
138	16 4 28.7	17 34 30	.4949	129.9	SB	24	2.8	10	B-	9 5 3	4.80E2	
139	16 4 30.2	18 22 45	.6200	38.3	S	17	7.7	152	B-	8 6 3	1.56E2	
140	16 4 33.1	17 37 33	.4782	123.9	S	28	0.0	0	B-	10 7 3	7.69E2	
141	16 4 33.2	17 46 52	.4124	105.6	S	26	7.8	17	N	10 8 5	2.99E2	
142	16 4 38.5	18 21 22	.6236	41.9	SO	50	2.6	169	R-	10 6 3	1.85E3	
143	16 4 42.2	17 59 24	.4433	77.3	S	31	7.0	158	B	9 6 3	4.63E2	
144	16 4 44.9	18 22 43	.6573	42.3	SO	44	1.5	6	R-	10 6 2	1.57E3	
145	16 4 45.5	17 41 60	.4858	113.3	S	16	5.0	128	B+	10 6 3	1.98E2	
146*	16 4 46.0	17 18 31	.7364	142.4	IRR	14	6.4	85	B-	8 5 3	1.46E2	
147	16 4 46.9	17 59 6	.4604	78.4	SO	18	6.8	102	R-	10 7 4	1.93E2	
148	16 4 47.0	18 9 20	.5222	59.7	S	45	4.4	74	N	9 7 2	1.28E3	
149*	16 4 48.2	17 25 14	.6571	135.9	S	14	6.8	58	R+	8 4 2	1.41E2	
150	16 4 51.2	17 58 56	.4766	79.1	S	25	2.5	24	R-	10 6 4	5.24E2	FWD

NO	RA(1950)	DEC(1950)	R	THETA	TYPE	D(0)	ELL	PA	COL	SUR.BRG	AREA	SW
151	16 5 1.9	17 49 44	.5148	97.0	SO	20	6.6	166	R-	9 8 4	2.52E2	
152	16 5 3.9	17 56 8	.5203	85.2	E*	18	0.0	0	B-	10 6 5	3.65E2	
153	16 5 4.8	17 27 40	.6780	129.5	S/IRR	15	7.6	177	R-	10 5 3	1.43E2	
154	16 5 9.3	17 47 39	.5491	100.3	S	45	4.8	124	N	10 7 3	1.23E3	
155	16 5 16.7	18 10 23	.6342	63.7	S/SO*	34	6.5	28	R-	10 7 3	6.00E2	
156	16 5 18.0	17 46 24	.5870	101.6	S	30	6.3	124	R	10 8 3	5.01E2	FWD
157	16 5 24.5	17 40 4	.6415	110.4	S	18	6.8	165	N	9 6 3	1.94E2	
158	16 5 35.9	17 57 41	.6490	83.8	IRR	18	5.8	82	B+	7 4 3	2.27E2	
159	16 5 43.3	18 10 53	.7335	66.7	IRR	19	7.1	136	B-	7 6 3	2.06E2	

CLUSTER A2197 PAGE 1

NO	RA(1950)	DEC(1950)	R	THETA	TYPE	D(0)	ELL	PA	COL	SUR.BRG	AREA	SW
1*	16 22 29.3	40 57 25	.8598	269.0	S	30	4.2	154	B	7 3 2	5.61E2	FWD
2	16 22 39.1	40 58 43	.8286	270.4	S	35	6.0	81	B-	8 6 2	6.06E2	
3*	16 22 39.5	41 12 46	.8585	286.2	SO	18	2.2	42	B-	7 3 2	2.65E2	
4*	16 22 40.6	41 16 7	.8719	289.8	IRR	19	4.2	87	B-	5 3 2	2.57E2	
5	16 22 50.6	40 52 45	.7991	263.2	S/SO	20	2.9	82	N	9 6 3	3.14E2	
6*	16 22 59.0	41 7 59	.7806	281.8	S*	16	4.7	25	B	9 7 3	1.83E2	
7	16 23 13.7	41 9 50	.7423	284.8	S	48	6.8	104	N	9 8 4	9.60E2	
8	16 23 20.2	40 38 21	.7787	244.5	S	31	6.8	94	B-	9 8 3	4.14E2	
9*	16 23 20.9	40 38 40	.7744	244.8	S/SO	16	6.2	154	N	9 8 4	1.44E2	
10	16 23 21.6	41 3 35	.6992	277.0	S	46	4.3	178	N	10 9 4	1.23E3	REV
11	16 23 25.1	41 2 29	.6865	275.6	S	28	1.8	9	N	9 8 5	6.27E2	
12	16 23 29.5	41 0 21	.6705	272.7	E	121	3.0	74	R	10 7 1	9.32E3	
13	16 23 31.6	40 58 47	.6634	270.4		24	4.9	88	N	8 5 3	3.51E2	
14	16 23 31.9	40 57 17	.6630	268.3	SO	18	5.3	84	R-	9 8 5	1.98E2	
15	16 23 32.8	41 28 7	.8201	307.0	S	20	7.4	61	B-	8 7 4	1.76E2	
16*	16 23 38.4	41 28 37	.8111	308.2	S/IRR	17	3.0	58	B-	7 4 3	2.38E2	
17	16 23 38.7	40 42 15	.6984	247.2	S/SO	18	5.7	173	R-	9 7 2	1.92E2	
18*	16 23 48.9	40 57 27	.6094	268.3	IRR	16	7.2	107	R-	7 5 4	1.22E2	
19	16 23 53.5	40 53 58	.6001	262.7	S	18	6.1	88	R-	9 7 3	1.77E2	REV
20	16 24 .5	41 8 26	.5944	286.1	SO	37	4.4	86	R-	10 8 3	8.20E2	
21	16 24 3.0	40 35 16	.6878	235.7	S/SO	41	6.7	144	R-	10 9 4	7.17E2	
22	16 24 5.4	41 32 35	.7918	315.8	S/IRR	21	6.4	176	R	7 5 3	2.31E2	
23	16 24 7.4	40 27 26	.7596	227.0	S*	32	0.0	0	B	9 7 3	8.85E2	
24	16 24 7.7	41 38 52	.8647	321.0	S/IRR*	26	0.0	0	B	7 5 2	6.33E2	
25	16 24 8.4	40 36 3	.6663	235.8	SO	70	3.7	72	R-	10 7 2	2.97E3	

NO	RA(1950)	DEC(1950)	R	THETA	TYPE	D(0)	ELL	PA	COL	SUR.BRG	AREA	SW
26*	16 24 11.7	41 10 11	.5697	289.9	E/SO	16	3.8	149	R-	9 7 3	1.97E2	
27	16 24 14.4	40 53 27	.5363	260.9	S	18	6.3	167	B-	9 8 5	1.82E2	
28*	16 24 16.6	40 27 31	.7378	225.5	S	15	6.2	74	B-	9 8 3	1.35E2	
29	16 24 20.8	40 51 18	.5238	256.6	SO	26	4.2	88	N	9 7 3	4.35E2	
30	16 24 24.8	41 9 43	.5284	290.6	S	24	3.7	70	B-	9 8 5	3.92E2	FWD
31	16 24 27.2	41 27 29	.6836	314.8	SBO	28	2.7	117	R-	9 7 2	5.74E2	
32	16 24 41.2	41 1 24	.4466	276.0	SO*	50	1.1	115	R-	10 7 2	1.93E3	
33	16 24 53.6	40 52 3	.4206	254.9	S	18	5.6	60	N	9 8 5	1.87E2	
34*	16 24 55.2	41 0 17	.4012	274.0	IRR	17	4.5	106	B+	8 5 3	2.00E2	
35*	16 24 57.5	40 58 39	.3932	269.9	S*	16	5.2	2	N	9 9 5	1.67E2	
36	16 24 58.5	40 35 21	.5516	225.3	SB	62	0.0	0	B	10 8 3	3.17E3	REV
37	16 24 58.5	41 12 26	.4518	300.6	S	25	5.4	29	B-	9 7 3	3.61E2	FWD
38+	16 24 59.1	40 17 30	.7895	209.8	S	20	3.8	176	B-	9 8 5	2.87E2	
39	16 25 4.1	40 47 43	.4153	244.1	E/SO	34	.4	123	R-	10 7 1	9.62E2	
40*	16 25 7.0	41 40 54	.7910	333.0	S/IRR	16	3.8	126	R+	9 7 3	1.97E2	
41*	16 25 9.5	41 1 43	.3589	278.3	S/SO	17	5.3	179	B	9 7 3	1.87E2	
42	16 25 9.7	41 6 39	.3785	290.7	S	22	6.8	70	B-	9 7 3	2.24E2	
43*	16 25 12.0	41 4 53	.3624	286.7	IRR	24	4.9	39	B	7 3 3	3.51E2	
44	16 25 13.1	41 21 53	.5170	318.6	S	59	1.1	90	B	10 7 3	2.72E3	REV
45	16 25 17.2	40 54 33	.3385	258.4		18	6.3	93	N	8 6 3	1.72E2	
46	16 25 18.6	41 10 58	.3852	302.2	S	23	6.1	72	R-	8 6 3	2.71E2	
47	16 25 19.1	41 44 48	.8339	337.3	S	23	6.5	147	B-	9 7 3	2.66E2	
48	16 25 19.6	41 12 35	.3976	305.8	E*	18	3.5	141	R-	9 9 5	2.52E2	
49	16 25 20.0	40 55 17	.3275	260.2	S/SO	35	4.6	70	R-	9 8 4	7.17E2	
50	16 25 30.7	41 1 2	.2913	277.9	SO	25	6.1	147	R-	10 9 4	3.13E2	

NO	RA(1950)	DEC(1950)	R	THETA	TYPE	D(0)	ELL	PA	COL	SUR.BRG	AREA	SW
51	16 25 36.1	41 1 30	.2757	279.9	E	22	0.0	0	N	9 6 2	4.50E2	
52	16 25 37.4	41 21 22	.4628	324.9	S/SO	21	0.0	0	R-	10 8 3	4.23E2	
53	16 25 42.8	40 47 17	.3149	233.0	E	26	2.6	100	N	10 9 6	5.06E2	
54	16 25 52.9	41 14 55	.3478	321.2	E*	24	3.6	109	N	9 6 2	3.97E2	
55	16 25 55.9	40 46 52	.2878	226.9	E	33	3.6	11	N	9 8 5	7.09E2	
56*	16 25 56.0	41 16 26	.3620	324.9		17	4.5	173	N	9 7 2	1.92E2	
57	16 25 59.3	40 19 31	.6827	197.1	S*	33	3.7	42	R-	10 8 4	6.92E2	
58*	16 25 59.5	41 1 28	.2035	283.3	S/SO	16	5.8	24	R	9 7 4	1.49E2	
59	16 26 .5	40 59 7	.1952	272.2	E	23	0.0	0	R-	9 8 4	5.06E2	
60	16 26 .5	41 2 13	.2036	286.9	E/SO	148	3.0	60	R+	10 7 1	1.38E4	
61*	16 26 3.1	40 14 4	.7670	194.3	S/IRR	23	4.5	97	B+	6 3 2	3.49E2	
62	16 26 3.7	41 25 3	.4765	337.3	S/SO	22	5.0	108	B	9 8 3	2.95E2	
63	16 26 5.4	41 10 58	.2722	318.9	SO	49	4.4	101	R	9 7 2	1.42E3	
64	16 26 9.5	41 5 45	.2040	305.3		20	5.4	66	R-	8 5 2	2.43E2	
65	16 26 9.9	41 2 50	.1793	292.8	E	20	0.0	0	R	9 8 3	3.93E2	
66	16 26 12.9	41 17 27	.3494	333.6	S/SO	21	5.8	49	B-	8 6 2	2.35E2	
67	16 26 13.9	40 42 57	.3037	210.4	E/SO	19	0.0	0	R-	9 8 3	3.44E2	
68	16 26 18.0	40 36 25	.3968	200.8	SO	41	6.8	74	R-	9 8 4	6.83E2	
69	16 26 19.0	41 4 40	.1692	306.2	S/SO	28	4.6	69	R	9 7 3	4.83E2	
70	16 26 21.4	40 30 58	.4798	195.7	S/SO	24	6.1	127	R	9 9 5	2.88E2	
71	16 26 24.6	40 51 51	.1650	226.4		19	5.2	103	N	9 7 3	2.28E2	
72	16 26 29.0	40 48 18	.2027	211.4	S	45	6.1	17	R	9 8 3	9.20E2	
73	16 26 32.5	40 25 24	.5628	189.7	SB	50	0.0	0	B-	9 8 3	2.15E3	REV
74+	16 26 34.2	40 13 31	.7581	186.8	SO	43	0.0	0	R-	9 6 2	1.56E3	
75	16 26 37.2	40 35 58	.3869	191.9	IRR	21	5.0	39	B-	6 4 3	2.64E2	

NO	RA(1950)	DEC(1950)	R	THETA	TYPE	D(0)	ELL	PA	COL	SUR.BRG	AREA	SW
76	16 26 37.3	41 4 35	.1263	321.2	E/SO	25	0.0	0	R	9 8 4	5.70E2	
77	16 26 39.7	41 2 33	.0964	312.0	SB	49	5.0	114	B-	9 7 2	1.32E3	FWD
78*	16 26 39.8	41 15 33	.2900	345.8	S	15	7.4	3	N	7 7 3	1.14E2	
79	16 26 41.1	41 0 58	.0773	299.5	SO	40	3.4	56	N	9 8 3	1.04E3	
80	16 26 44.6	40 58 3	.0573	259.4	S	25	4.9	115	R-	9 9 5	3.65E2	
81	16 26 44.9	41 16 39	.3045	349.6	SB	52	0.0	0	R	9 7 2	2.27E3	
82	16 26 47.6	41 16 12	.2957	350.9	E	20	3.1	93	R-	9 9 5	2.89E2	
83	16 26 47.9	40 49 47	.1553	197.2	S/SO	21	0.0	0	B-	9 7 4	4.23E2	
84	16 26 48.2	41 19 46	.3542	352.7	PEC	19	3.4	124	B-	10 9 5	2.74E2	
85*	16 26 48.8	41 19 29	.3493	353.0	S/SO	17	4.6	93	B-	9 8 4	1.97E2	
86	16 26 51.1	41 24 53	.4381	355.3	S/SO*	27	0.0	0	N	9 7 2	6.66E2	
87	16 26 51.4	41 0 17	.0439	307.4	S	28	7.5	117	R-	8 7 4	2.97E2	
88*	16 26 52.3	41 43 46	.7521	357.6	S/SO	14	4.7	104	N	9 7 3	1.36E2	
89	16 26 53.7	40 59 43	.0326	301.9	SBO	23	2.3	104	R-	9 7 4	4.30E2	
90	16 26 54.3	41 50 33	.8648	358.3	S	21	5.0	136	B-	7 6 3	2.79E2	
91	16 26 54.9	40 36 23	.3724	183.7	SO	27	2.6	143	R	9 7 2	5.60E2	
92+	16 26 57.5	40 13 57	.7457	181.2	S*	39	4.1	137	B-	9 8 4	9.36E2	
93	16 26 58.0	41 16 22	.2951	357.3	SO*	40	0.0	0	R	9 7 2	1.38E3	
94	16 26 59.6	41 13 11	.2418	357.8	SO	54	4.4	143	R	9 7 3	1.67E3	
95+	16 27 .3	40 13 58	.7453	180.5	S	26	2.6	102	N	9 8 4	5.02E2	
96	16 27 1.6	41 14 45	.2678	359.4	E/SO	28	1.5	84	R-	9 8 3	6.51E2	
97*	16 27 8.2	40 34 22	.4057	177.5	S/IRR	17	6.0	48	B+	8 6 3	1.62E2	
98	16 27 10.4	40 27 36	.5187	177.2	S/SO	30	6.2	94	R-	9 8 4	4.35E2	
99	16 27 13.7	40 58 30	.0354	94.9	S/SO	40	1.6	19	R	9 8 4	1.26E3	
100	16 27 17.0	41 0 29	.0546	56.6	SO*	22	1.9	60	R-	9 7 4	4.06E2	

NO	RA(1950)	DEC(1950)	R	THETA	TYPE	D(0)	ELL	PA	COL	SUR.BRG	AREA	SW
101	16 27 19.2	41 21 50	.3894	7.7		18	4.9	1	R-	9 9 6	2.01E2	
102	16 27 20.0	40 36 12	.3788	171.6	S/SO	19	5.6	148	N	9 9 5	2.16E2	
103	16 27 20.5	40 38 36	.3395	170.4	S	40	3.8	48	R	9 7 3	1.03E3	
104	16 27 20.5	41 45 50	.7878	4.1	S	30	6.9	98	B-	8 7 3	3.88E2	
105	16 27 20.7	41 23 33	.4184	7.8	S	66	2.6	148	R-	10 7 2	2.97E3	FWD
106	16 27 22.7	40 42 45	.2731	166.5	S	22	4.5	155	N	9 7 3	3.21E2	
107	16 27 23.9	40 43 34	.2608	165.0	SO*	27	5.1	168	R-	9 7 3	4.20E2	
108	16 27 24.9	40 44 2	.2542	163.8		18	0.0	0	B-	7 4 3	3.21E2	
109	16 27 26.3	40 41 58	.2885	164.9	S/SO	45	5.7	99	R	9 7 2	1.02E3	
110	16 27 27.0	40 46 24	.2188	159.3	SO	38	4.2	80	R-	9 7 3	8.81E2	
111	16 27 29.2	41 5 45	.1446	35.4	SBO	59	0.0	0	R	9 7 2	2.88E3	
112	16 27 30.7	40 57 57	.0896	97.8	S/SO*	50	5.3	109	R	9 7 3	1.31E3	
113	16 27 33.1	41 15 33	.2971	18.8	SB	28	0.0	0	R	9 8 3	6.99E2	
114	16 27 33.6	40 20 57	.6365	171.1	S/SO	22	6.0	73	N	9 9 5	2.65E2	
115	16 27 34.6	40 22 6	.6181	170.5	SB	32	5.9	31	B+	9 7 4	5.09E2	
116	16 27 40.0	40 40 13	.3297	158.9		20	3.2	79	R-	9 6 3	3.01E2	
117	16 27 43.4	40 58 59	.1288	87.7	SO	51	.6	149	R-	9 7 2	2.12E3	
118*	16 27 45.0	40 32 49	.4515	162.7	S/SO	16	5.6	8	N	9 7 3	1.54E2	
119	16 27 46.2	40 49 50	.2017	136.9	S/SO*	37	3.6	61	R	9 7 2	8.71E2	
120	16 27 50.4	40 31 14	.4818	161.6	S	20	3.3	100	R-	9 8 4	2.99E2	REV
121	16 27 56.8	40 20 35	.6578	164.8	S	24	7.1	75	N	9 8 4	2.45E2	
122*	16 27 59.7	40 39 12	.3715	150.9	S/IRR	22	3.7	40	R-	8 3 2	3.48E2	
123	16 28 .2	40 47 40	.2584	135.2	S	54	7.2	122	R+	9 8 3	1.08E3	
124	16 28 .3	40 21 22	.6482	163.6	S/SO	31	0.0	0	R-	9 7 1	8.47E2	
125	16 28 .3	40 26 29	.5669	161.1	S/SO	19	1.8	186	B	9 8 4	3.20E2	

NO	RA(1950)	DEC(1950)	R	THETA	TYPE	D(0)	ELL	PA	COL	SUR.BRG	AREA	SW
126	16 28 4.4	40 55 9	.2035	106.7	E/SO	164	2.9	140	R+	10 7 1	1.71E4	
127	16 28 6.6	40 20 47	.6634	162.1	SB	31	0.0	0	B	8 5 2	8.47E2	FWD
128	16 28 7.3	40 58 46	.2038	89.5	S/SO	28	3.0	119	R-	9 8 4	5.78E2	
129	16 28 8.0	40 19 42	.6819	162.2	S/SO*	27	4.3	55	R	9 7 3	4.46E2	
130*	16 28 13.3	40 11 17	.8212	164.1	IRR	19	5.7	24	N	8 3 2	2.02E2	
131	16 28 14.5	40 46 3	.3095	132.8	E	18	3.6	44	R	9 7 4	2.48E2	
132	16 28 15.5	41 42 43	.7686	17.2	SO*	62	5.7	56	R	9 7 2	1.81E3	
133	16 28 16.9	40 44 17	.3355	135.6	SO	74	5.5	98	R	10 8 2	2.63E3	
134	16 28 17.3	40 44 4	.3390	135.8	E/SO	78	3.0	19	R+	10 8 3	3.95E3	
135	16 28 17.3	41 39 52	.7252	18.7	S	19	6.3	100	N	9 8 4	1.89E2	
136*	16 28 25.0	40 25 19	.6141	154.8	SO	16	6.0	87	N	9 9 5	1.52E2	
137	16 28 25.0	41 29 40	.5775	26.5	E/SO	23	3.3	98	R+	9 7 2	3.74E2	
138	16 28 25.3	40 54 19	.2706	105.5	SO*	38	4.3	21	R	9 7 4	8.69E2	
139	16 28 27.0	40 59 15	.2660	87.8	SO*	31	6.9	144	N	9 9 5	4.23E2	
140	16 28 28.0	40 54 58	.2761	102.8	SO	22	5.7	85	N	9 7 3	2.66E2	
141*	16 28 32.7	41 2 59	.2925	75.7	S/IRR	16	5.9	152	N	9 6 2	1.58E2	
142	16 28 35.4	40 46 0	.3611	125.7	S/SO	34	4.9	177	R-	9 9 4	6.76E2	
143	16 28 36.9	40 42 20	.4035	132.4	SO*	32	0.0	0	B-	9 8 2	9.29E2	
144	16 28 39.1	41 12 33	.3813	52.6	S	77	1.8	128	B	9 7 2	4.25E3	FWD
145	16 28 41.9	41 1 52	.3170	80.2	S	38	1.7	112	B	9 8 4	1.13E3	REV
146	16 28 43.2	40 46 21	.3780	122.8	E	24	1.5	121	R-	9 8 4	4.81E2	
147	16 28 45.2	40 43 16	.4133	128.3	E	21	2.9	27	R+	9 8 4	3.36E2	
148	16 28 46.3	40 49 54	.3582	114.0	S	46	5.8	30	R-	10 9 3	1.04E3	FWD
149	16 28 47.6	41 35 29	.6960	28.1	SB	62	1.2	125	N	10 8 2	2.91E3	FWD
150+	16 28 49.5	40 15 48	.7908	154.5	S	25	5.3	98	N	9 7 4	3.53E2	

NO	RA(1950)	DEC(1950)	R	THETA	TYPE	D(0)	ELL	PA	COL	SUR.BRG	AREA	SW
151*	16 28 51.0	41 7 24	.3706	66.8	SO	17	5.6	77	R-	9 7 2	1.74E2	
152	16 28 51.6	41 12 4	.4088	56.8	S	23	6.6	79	N	9 7 2	2.60E2	
153+	16 28 53.0	40 17 37	.7685	152.8	S	18	4.7	25	B-	9 8 3	2.07E2	
154	16 28 53.0	40 38 46	.4813	133.5	E/SO	72	3.1	21	R	10 7 1	3.37E3	
155	16 28 54.0	41 32 43	.6661	31.5	S/SO	19	6.3	100	N	9 9 4	1.89E2	
156	16 28 54.6	40 43 49	.4315	124.9	S	27	3.6	42	B-	9 8 3	4.85E2	
157	16 28 57.4	40 48 54	.3969	114.1	S/SO*	27	5.8	62	B+	9 7 3	3.91E2	
158	16 28 58.3	41 41 58	.8072	26.5	S	23	4.3	85	N	9 9 5	3.53E2	
159	16 28 59.4	41 19 2	.4996	47.1	S	70	6.9	178	R	9 8 3	1.87E3	
160	16 29 .9	40 38 10	.5063	132.3	SO*	34	1.8	64	N	9 8 3	8.77E2	
161*	16 29 5.6	41 40 27	.7956	28.8		17	5.1	65	N	9 7 3	1.80E2	
162	16 29 7.1	40 59 53	.3924	86.9	S	28	5.5	105	R-	9 7 3	4.40E2	
163*	16 29 9.8	40 42 4	.4876	124.4	S/SO	16	5.7	151	R-	9 8 5	1.62E2	
164	16 29 11.0	41 30 32	.6662	37.0	S/SO	18	3.3	174	N	9 8 4	2.45E2	
165	16 29 12.7	40 54 31	.4156	99.4	E	18	3.9	94	R-	9 8 2	2.22E2	
166*	16 29 15.0	40 32 54	.5996	135.6	S/SO	17	6.0	170	N	9 7 3	1.70E2	
167	16 29 18.6	41 2 12	.4319	82.0	E	50	0.0	0	R	9 7 2	2.15E3	
168	16 29 18.7	40 21 14	.7582	145.2	E	18	2.8	73	N	9 8 2	2.61E2	
169	16 29 22.4	41 31 41	.7032	38.4		19	2.4	101	R-	8 5 3	2.94E2	
170	16 29 24.2	41 15 45	.5280	57.2	S	76	0.0	0	B-	10 7 2	4.83E3	REV
171	16 29 26.9	40 29 40	.6646	136.5	S/SO	24	4.4	152	N	9 7 3	3.82E2	
172	16 29 30.6	41 25 8	.6402	46.3	S	22	6.9	174	B	9 7 3	2.34E2	
173	16 29 31.1	40 31 39	.6504	133.6	S/SO	18	6.2	1	N	9 9 5	1.76E2	
174	16 29 45.9	41 24 47	.6721	49.4	SO	25	0.0	0	R-	9 7 2	5.70E2	
175	16 29 46.5	40 32 28	.6774	129.9	IRR	20	5.5	67	B	8 6 2	2.24E2	

CLUSTER A2197 PAGE 8

NO	RA(1950)	DEC(1950)	R	THETA	TYPE	D(0)	ELL	PA	COL	SUR.BRG	AREA	SW
176	16 29 53.7	40 40 17	.6208	119.4	S	37	4.4	123	N	10 9 3	8.20E2	FWD
177	16 29 58.9	41 35 58	.8313	41.4	S	47	2.5	89	N	10 8 3	1.55E3	REV
178*	16 30 3.1	40 31 56	.7237	127.8	S/SO	17	5.8	124	N	9 8 3	1.68E2	
179	16 30 10.3	40 48 40	.6146	105.5	S/IRR	20	6.2	31	N	7 5 3	2.06E2	
180*	16 30 15.5	40 39 6	.6906	117.9	S/SO	16	5.8	63	R-	8 6 3	1.49E2	
181*	16 30 15.9	40 50 56	.6225	101.7	S/IRR	17	4.0	11	B-	6 5 2	2.18E2	
182*	16 30 17.5	41 21 4	.7165	58.4		30	6.3	67	R+	6 3 3	4.24E2	
183	16 30 22.8	41 31 49	.8358	48.4	S/SO	22	6.3	89	R	8 6 2	2.45E2	
184	16 30 39.1	40 40 47	.7452	113.3	S	29	5.3	6	R-	9 9 4	4.72E2	
185	16 30 39.4	40 29 51	.8366	124.8	S	21	6.7	54	N	8 7 3	2.14E2	
186	16 30 59.7	40 57 46	.7464	90.8	S	21	6.2	25	R-	9 8 3	2.27E2	

CLUSTER A2199 PAGE 1

NO	RA(1950)	DEC(1950)	R	THETA	TYPE	D(0)	ELL	PA	COL	SUR.BRG	AREA	SW
1	16 22 47.5	39 26 8	.8283	254.5	S	18	5.6	138	N	9 8 3	1.95E2	
2	16 22 54.1	39 22 14	.8288	249.8	S	28	3.6	88	B+	9 7 2	5.41E2	
3	16 23 4.7	39 50 53	.7630	284.5	S	47	5.1	38	B	9 7 4	1.19E3	REV
4	16 23 13.9	39 38 41	.7114	269.0	S	30	2.9	123	B	9 8 5	6.31E2	FWD
5	16 23 21.7	39 52 14	.7165	287.3	S	31	7.6	41	R	9 9 5	3.54E2	
6*	16 23 26.0	39 23 23	.7261	248.4	S	16	6.4	20	N	9 8 3	1.47E2	
7	16 23 26.8	39 33 17	.6786	261.3	IRR	18	6.0	176	B	7 5 3	1.80E2	
8	16 23 38.8	39 17 25	.7334	239.9	SO	26	2.0	137	R-	9 6 2	5.40E2	
9	16 23 43.5	39 58 58	.6939	297.9	SO	77	4.0	94	R-	10 8 2	3.49E3	
10	16 23 44.7	39 39 53	.6123	270.6	SB	30	1.4	31	B-	9 7 3	7.08E2	REV
11	16 23 49.3	40 14 59	.8372	315.0	S	33	7.1	21	N	9 8 3	4.54E2	
12	16 23 52.8	39 14 49	.7118	235.7	S/SO	28	2.3	159	N	9 6 2	6.00E2	
13	16 23 53.7	39 5 39	.8151	226.2	IRR	22	2.9	130	B	7 5 3	3.68E2	
14	16 23 56.4	39 55 21	.6306	294.8	S	25	4.3	15	B+	9 7 2	4.01E2	
15	16 23 56.5	40 12 40	.7939	314.1	SB	33	5.1	115	R-	9 7 4	6.12E2	REV
16	16 23 58.8	39 42 45	.5692	275.4	E/SO	53	3.2	22	R	9 8 2	1.81E3	
17	16 24 7.9	40 0 9	.6361	302.7	S	22	6.3	173	N	9 9 4	2.55E2	
18*	16 24 15.7	39 31 55	.5293	256.1	S	16	5.6	172	N	9 8 3	1.51E2	FWD:
19	16 24 19.2	39 47 12	.5168	284.3	S/SO	20	5.9	72	N	9 7 3	2.20E2	
20	16 24 21.1	39 47 40	.5128	285.3	S	22	5.7	19	B	8 6 2	2.60E2	
21	16 24 21.5	39 44 27	.5004	279.4	S/SO	22	6.4	132	N	9 8 3	2.49E2	
22	16 24 27.4	39 20 55	.5696	237.0	SO	20	3.7	78	R	9 8 4	2.74E2	
23	16 24 31.2	39 46 45	.4777	284.5	S/SO	28	4.6	86	R-	9 8 3	4.75E2	
24*	16 24 31.3	38 57 19	.8451	213.6	S/SO	16	5.9	91	B	9 7 4	1.53E2	
25	16 24 31.8	40 4 44	.6215	312.5	PEC	27	2.5	172	B-	9 9 5	5.62E2	

CLUSTER A2199 PAGE 2

NO	RA(1950)	DEC(1950)	R	THETA	TYPE	D(0)	ELL	PA	COL	SUR. BRG	AREA	SW
26	16 24 35.9	39 30 16	.4751	251.0	S	32	6.7	174	R-	9 8 3	4.57E2	
27*	16 24 37.8	39 39 56	.4420	270.8	S/IRR	17	6.5	55	R-	7 6 3	1.61E2	
28	16 24 40.4	39 26 6	.4896	242.7	SO	31	4.1	146	R	9 7 2	6.16E2	
29	16 24 42.5	39 24 3	.5006	238.9	SO	20	0.0	0	R-	9 7 3	3.90E2	
30	16 24 45.5	39 11 37	.6274	222.0	E	27	2.8	30	R-	9 8 2	5.35E2	
31	16 24 48.9	38 54 56	.8499	208.9	S/SO*	22	4.5	102	B	9 8 4	3.19E2	
32	16 24 53.2	39 14 19	.5774	223.2	S*	55	5.3	45	N	9 8 2	1.53E3	
33	16 24 53.3	39 17 33	.5389	227.0	SO	25	0.0	0	R-	9 8 5	5.61E2	
34	16 24 54.2	39 58 11	.4964	308.6	S	18	5.8	82	N	9 9 5	1.90E2	
35	16 24 56.7	39 57 14	.4803	307.8	IRR	25	3.9	174	B+	6 4 2	4.29E2	
36	16 24 59.1	40 17 30	.7323	329.6	S	20	3.8	176	B-	9 8 5	2.87E2	
37	16 25 .7	39 43 47	.3748	280.7	SB/SBO	28	4.1	132	R-	9 7 3	4.96E2	
38	16 25 4.4	39 59 20	.4840	312.8	S	31	5.8	157	B-	9 8 3	4.93E2	
39	16 25 12.2	39 8 53	.6114	213.1	S	37	2.6	67	N	9 7 2	9.73E2	
40	16 25 13.7	39 14 19	.5346	218.0	E/SO	22	0.0	0	N	9 7 3	4.42E2	
41	16 25 14.0	39 29 38	.3665	243.0	S	19	3.9	165	B	9 7 4	2.67E2	
42	16 25 16.3	39 25 51	.3933	234.3	S	38	6.7	159	R-	9 8 3	6.09E2	
43	16 25 20.5	39 38 17	.3059	265.9	E/SO*	72	2.1	112	R	9 7 1	3.62E3	
44	16 25 20.8	39 32 39	.3259	249.2	S/SO	18	1.9	75	N	9 8 4	2.71E2	
45*	16 25 26.2	39 41 50	.2890	277.4	S	16	6.5	129	N	9 9 5	1.34E2	
46*	16 25 27.2	39 9 29	.5777	209.6	IRR	28	0.0	0	B	5 3 1	6.90E2	
47	16 25 27.5	39 24 56	.3746	229.2	SO	25	1.9	53	N	9 7 2	4.99E2	
48	16 25 31.4	39 3 53	.6549	204.6	S/SO	25	4.3	152	B	9 7 2	4.01E2	
49	16 25 33.3	39 29 41	.3122	238.0	S	39	7.0	8	R-	9 7 3	5.93E2	
50	16 25 36.9	39 22 9	.3861	221.0	S/SO	41	6.2	118	R-	9 7 2	7.87E2	

NO	RA(1950)	DEC(1950)	R	THETA	TYPE	D(0)	ELL	PA	COL	SUR.BRG	AREA	SW
51	16 25 38.3	39 13 12	.5062	209.5	S	47	2.9	147	B-	9 8 4	1.48E3	FWD
52	16 25 42.6	39 57 50	.3827	322.5	IRR	29	1.7	35	B+	8 4 1	6.78E2	
53*	16 25 44.1	39 30 26	.2762	236.3	IRR	22	6.1	40	B-	6 3 2	2.52E2	
54	16 25 44.5	38 58 46	.7189	198.7	SBO	37	0.0	0	R	9 7 3	1.17E3	
55	16 25 49.4	39 40 51	.2133	275.5	E	28	0.0	0	N	9 8 3	6.90E2	
56	16 25 52.1	39 35 36	.2147	251.8	E	32	0.0	0	R-	9 6 2	9.12E2	
57	16 25 53.1	39 0 25	.6842	197.2	S	18	6.3	164	B	9 7 3	1.77E2	
58	16 25 53.3	39 22 46	.3454	215.5	S*	38	4.2	148	B	9 7 2	8.90E2	
59	16 25 53.5	39 14 46	.4603	205.8	E	18	3.6	18	N	9 8 5	2.49E2	
60	16 25 57.6	39 29 34	.2509	228.0	E/SO	70	2.0	82	R	10 7 2	3.49E2	
61+	16 25 59.3	40 19 31	.6883	349.9	S*	33	3.7	42	R-	10 8 4	6.92E2	
62	16 25 59.4	39 29 15	.2502	226.2	SO	19	3.1	35	N	9 8 3	2.64E2	
63*	16 26 1.1	39 39 10	.1750	267.4		17	3.6	71	R-	9 8 5	2.14E2	
64	16 26 1.3	40 0 50	.3935	333.9	SO	29	0.0	0	N	9 6 2	7.69E2	
65*	16 26 2.8	39 3 12	.6309	195.7		17	2.4	128	B	9 8 4	2.37E2	
66*	16 26 3.1	40 14 4	.5976	343.8	S/IRR	23	4.5	97	B+	6 3 2	3.49E2	
67	16 26 10.3	39 20 29	.3511	204.6	IRR	23	3.0	164	B-	8 6 2	3.83E2	
68	16 26 11.5	39 50 47	.2332	322.8	E	19	2.8	5	N	9 8 3	2.78E2	
69	16 26 11.8	39 22 7	.3244	205.8	SO*	54	2.5	178	N	9 7 3	2.02E3	
70	16 26 12.6	39 23 28	.3031	207.2	E	32	0.0	0	N	9 8 3	9.12E2	
71	16 26 13.1	39 40 41	.1374	277.3	SO	35	3.4	155	R-	9 7 3	8.34E2	
72	16 26 14.1	39 21 45	.3268	204.1	S/SO	22	5.3	149	N	9 9 5	2.88E2	
73	16 26 14.8	38 49 46	.8417	189.1	S/IRR	23	4.2	114	N	8 6 2	3.50E2	
74	16 26 15.6	39 24 46	.2794	207.4	SB	25	0.0	0	N	9 7 3	5.61E2	
75	16 26 15.8	39 42 48	.1380	292.4	S/SO	28	1.3	121	R-	9 8 5	6.27E2	

NO	RA(1950)	DEC(1950)	R	THETA	TYPE	D(0)	ELL	PA	COL	SUR.BRG	AREA	SW
76+	16 26 21.4	40 30 58	.8622	352.8	S/SO	24	6.1	127	R	9 9 5	2.88E2	
77	16 26 29.1	39 55 52	.2833	342.6	SB	84	2.8	152	R-	10 7 2	4.67E3	FWD
78+	16 26 32.5	40 25 24	.7661	354.5	SB	50	0.0	0	B-	9 8 3	2.15E3	REV
79	16 26 34.2	40 13 31	.5686	353.1	SO	43	0.0	0	R-	9 6 2	1.56E3	
80	16 26 34.5	39 17 44	.3715	190.6	S	23	6.0	80	N	9 8 2	2.71E2	
81	16 26 35.9	38 55 14	.7430	184.9	E/SO	50	0.0	0	R-	9 7 1	2.12E2	
82	16 26 37.5	40 4 6	.4116	351.9		19	2.8	65	R	9 8 5	2.76E2	
83	16 26 40.4	39 40 46	.0522	290.9	E	41	1.4	69	N	9 7 3	1.32E3	
84*	16 26 40.8	39 42 52	.0716	318.5	S/SO	17	4.8	153	R-	9 8 4	1.90E2	
85	16 26 42.1	39 51 1	.1943	347.2	S	22	6.0	102	N	9 9 5	2.61E2	
86*	16 26 42.4	39 8 46	.5165	184.7	S/IRR	17	6.6	146	N	8 7 3	1.55E2	
87*	16 26 46.1	38 55 35	.7351	182.4		16	6.9	3	B-	7 5 3	1.28E2	
88	16 26 48.1	39 37 48	.0391	218.0	SO	24	4.9	118	R	9 8 4	3.47E2	
89*	16 26 48.2	39 12 45	.4490	183.1	S	17	6.6	31	B-	8 7 4	1.50E2	
90	16 26 48.6	39 50 13	.1775	352.8	SO	35	6.6	143	R-	9 7 3	5.42E2	
91	16 26 53.1	39 38 34	.0198	204.0	E/SO	22	0.0	0	N	9 7 4	4.42E2	
92	16 26 54.4	39 33 20	.1053	182.1	S/SO	21	6.0	158	R-	9 8 3	2.50E2	
93	16 26 54.6	39 48 29	.1473	358.8	S	24	2.8	120	N	9 7 5	4.43E2	FWD
94	16 26 54.9	39 11 48	.4642	180.3	S*	25	3.3	89	B	9 8 3	4.52E2	
95	16 26 55.2	39 39 23	.0046	196.1		26	6.2	83	R-	9 7 3	3.37E2	
96	16 26 55.6	39 39 39	0.0000	0.0	E/SO	174	3.4	38	R	10 6 1	1.82E4	
97	16 26 56.3	39 37 39	.0334	176.1	SBO	37	0.0	0	R-	9 7 2	1.17E3	
98	16 26 57.5	40 13 57	.5717	.6	S*	39	4.1	137	B-	9 8 4	9.36E2	
99	16 27 .3	40 13 58	.5721	1.5	S	26	2.6	102	N	9 8 4	5.02E2	
100	16 27 1.4	39 34 56	.0808	166.7	SO*	50	.9	56	R-	9 7 5	1.97E3	

NO	RA(1950)	DEC(1950)	R	THETA	TYPE	D(0)	ELL	PA	COL	SUR.BRG	AREA	SW
101	16 27 1.5	39 35 36	.0701	164.3	SO	18	5.9	134	N	9 8 3	1.84E2	
102	16 27 2.1	39 32 45	.1169	169.7	SO	27	2.9	116	R-	9 8 4	5.27E2	
103	16 27 3.2	39 34 18	.0924	164.7	S	40	6.1	164	N	9 8 2	7.72E2	
104	16 27 3.7	39 57 43	.3022	4.9	S/IRR	22	5.8	175	N	8 6 3	2.61E2	
105	16 27 7.3	39 56 34	.2844	7.6	S/SO*	40	2.2	135	N	9 8 3	1.19E3	
106	16 27 8.7	39 51 50	.2073	11.7	SO	26	2.7	153	B-	9 7 2	5.22E2	
107+	16 27 10.4	40 27 36	.8006	3.4	S/SO	30	6.2	94	R-	9 8 4	4.35E2	
108	16 27 14.4	39 7 55	.5323	173.4	S	23	6.1	165	N	9 8 3	2.77E2	
109	16 27 14.7	39 49 1	.1677	21.4	E	21	0.0	0	R-	9 8 3	4.15E2	
110	16 27 14.8	39 25 40	.2411	165.1	S	52	6.4	108	N	9 7 2	1.19E3	
111	16 27 16.5	39 54 42	.2596	14.9	SO	25	3.4	107	N	9 7 2	4.44E2	
112	16 27 17.2	39 47 33	.1488	27.7	E	19	3.2	106	R-	9 9 5	2.62E2	
113	16 27 24.2	39 15 24	.4145	167.1	S/SO	28	6.2	169	R-	9 8 3	3.97E2	
114	16 27 24.3	39 36 14	.1083	121.7	SO*	27	.5	66	N	9 7 2	6.51E2	
115	16 27 24.4	39 55 16	.2761	19.5		20	3.2	164	B	9 7 3	2.96E2	
116*	16 27 26.2	38 58 19	.6959	171.8	S/IRR	16	6.4	177	R-	8 6 4	1.38E2	
117*	16 27 27.4	39 27 27	.2276	153.3	S/IRR	17	6.2	8	B	8 6 2	1.60E2	
118	16 27 30.0	39 46 44	.1615	43.0	S	26	5.8	118	N	9 8 5	3.52E2	
119	16 27 33.5	39 30 33	.1945	141.2	S	46	6.3	15	R-	9 8 2	9.43E2	
120+	16 27 33.6	40 20 57	.6989	9.9	S/SO	22	6.0	73	N	9 9 5	2.65E2	
121+	16 27 34.6	40 22 6	.7184	9.9	SB	32	5.9	31	B+	9 7 4	5.09E2	
122	16 27 37.0	39 32 13	.1817	132.9	SBO	68	2.8	77	R-	9 7 2	3.04E3	
123	16 27 38.4	39 55 42	.3006	27.1	S	37	4.9	48	N	9 8 3	7.62E2	
124	16 27 39.3	39 43 43	.1556	64.1	SO	22	2.7	111	N	9 6 2	3.59E2	
125*	16 27 40.5	39 27 30	.2486	144.5	S	16	5.8	133	N	8 7 3	1.49E2	FWD

NO	RA(1950)	DEC(1950)	R	THETA	TYPE	D(0)	ELL	PA	COL	SUR.BRG	AREA	SW
126	16 27 45.1	38 55 13	.7576	167.8	S/SO	19	5.0	28	N	9 7 2	2.21E2	
127*	16 27 50.9	40 0 39	.3922	26.7		17	5.0	157	R-	9 8 3	1.95E2	
128*	16 27 52.0	38 57 23	.7267	165.1		17	5.6	137	B-	7 4 3	1.75E2	
129	16 27 52.8	40 5 22	.4660	23.0	S/SO*	38	6.6	123	N	9 6 3	6.28E2	
130+	16 27 56.8	40 20 35	.7096	15.9	S	24	7.1	75	N	9 8 4	2.45E2	
131	16 27 58.8	39 51 20	.2809	46.0	S	26	5.8	30	N	9 7 2	3.55E2	
132+	16 28 .3	40 21 22	.7253	16.5	S/SO	31	0.0	0	R-	9 7 1	8.47E2	
133+	16 28 .3	40 26 29	.8074	14.7	S/SO	19	1.8	186	B	9 8 4	3.20E2	
134*	16 28 1.7	40 7 26	.5090	24.4	S/SO	17	5.8	19	N	9 8 3	1.65E2	
135	16 28 2.8	39 55 5	.3353	39.8	E/SO	28	3.3	165	R-	9 8 5	5.49E2	
136	16 28 5.5	39 49 26	.2770	53.8	S/SO	28	0.0	0	B-	9 6 3	6.90E2	
137	16 28 5.7	39 20 6	.3962	145.2	E/SO	23	4.2	66	N	9 7 5	3.39E2	
138	16 28 6.2	40 5 46	.4903	27.3	S	24	6.1	32	R-	9 6 2	2.88E2	
139+	16 28 6.6	40 20 47	.7220	18.2	SB	31	0.0	0	B	8 5 2	8.47E2	FWD
140+	16 28 8.0	40 19 42	.7064	19.0	S/SO*	27	4.3	55	R	9 7 3	4.46E2	
141	16 28 8.7	39 52 25	.3164	47.6	SB	97	1.9	154	B-	9 7 1	6.61E3	FWD
142*	16 28 13.3	40 11 17	.5828	25.1	IRR	19	5.7	24	N	8 3 2	2.02E2	
143	16 28 14.5	40 3 4	.4648	32.8	E	37	0.0	0	R	9 8 3	1.17E3	
144	16 28 16.6	39 38 9	.2611	95.4	S/SO	28	6.1	83	N	9 8 2	4.07E2	
145	16 28 24.3	40 2 59	.4814	36.0	S/SO	18	6.5	81	R	8 7 3	1.68E2	
146*	16 28 24.8	40 9 31	.5736	29.7	IRR	35	5.8	71	R+	6 3 3	6.23E2	
147*	16 28 25.0	40 25 19	.8128	20.4	SO	16	6.0	87	N	9 9 5	1.52E2	
148*	16 28 28.7	39 24 18	.3937	130.4	S/SO	17	5.8	109	N	9 8 3	1.65E2	
149	16 28 28.9	39 39 29	.2993	90.4	E*	21	3.9	151	R-	9 8 3	3.00E2	
150*	16 28 33.2	38 57 42	.7667	155.6	SO*	16	4.7	2	N	9 8 3	1.79E2	

NO	RA(1950)	DEC(1950)	R	THETA	TYPE	D(0)	ELL	PA	COL	SUR.BRG	AREA	SW
151	16 28 35.2	39 59 47	.4628	43.4	SO	38	4.6	59	N	9 7 3	8.56E2	
152	16 28 37.1	39 57 8	.4364	48.0	S	18	5.5	68	B	8 5 3	2.00E2	
153	16 28 37.9	39 54 41	.4124	52.4	SBO	41	1.6	116	R-	9 6 1	1.28E3	
154*	16 28 44.5	39 56 25	.4468	51.1	S/SO	17	5.6	104	N	8 6 2	1.72E2	
155	16 28 46.2	39 43 59	.3619	78.3	S	55	5.1	158	N	9 7 2	1.59E3	
156	16 28 49.5	40 15 48	.7038	31.0	S	25	5.3	98	N	9 7 4	3.53E2	
157	16 28 49.8	39 29 27	.4042	114.7	S	36	6.1	100	N	9 8 4	6.22E2	
158*	16 28 50.7	40 7 34	.5932	38.2	S/SO*	17	2.4	33	B	9 7 4	2.37E2	
159	16 28 51.1	39 56 14	.4616	53.1	SO	63	1.1	123	B-	9 7 1	3.07E3	
160	16 28 53.0	40 17 37	.7355	30.5	S	18	4.7	25	B-	9 8 3	2.07E2	
161	16 28 58.8	39 11 23	.6158	139.7	S	22	6.0	40	B-	7 5 3	2.58E2	
162	16 29 1.9	39 44 24	.4126	78.8	SO	35	6.6	137	N	9 7 3	5.42E2	
163	16 29 2.0	39 18 6	.5424	131.3	E/SO	56	1.9	63	R-	9 6 2	2.29E3	
164	16 29 5.1	39 19 26	.5356	128.8	S	68	5.8	108	N	9 7 2	2.17E3	
165	16 29 9.5	40 5 45	.6104	44.4	S	34	7.1	56	B	9 7 3	4.59E2	
166	16 29 9.9	40 0 58	.5575	50.2	SO	24	5.7	109	B-	8 6 2	3.03E2	
167	16 29 11.8	39 57 14	.5253	55.9	SO	46	3.9	90	R-	9 8 2	1.29E3	
168+	16 29 18.7	40 21 14	.8300	33.2	E	18	2.8	73	N	9 8 2	2.61E2	
169	16 29 20.5	39 53 56	.5215	62.6	E	57	0.0	0	R	10 8 2	2.77E3	
170	16 29 20.6	39 40 5	.4651	88.9	S	41	6.4	17	R-	9 8 3	7.50E2	
171	16 29 21.3	39 56 41	.5460	58.5	SB/SBO*	60	2.7	99	R-	9 7 2	2.44E3	
172	16 29 23.8	39 18 40	.5911	126.1	IRR	23	3.0	48	B+	9 7 2	4.08E2	
173	16 29 24.1	39 32 10	.4928	104.5	S	52	7.4	68	R-	9 7 4	9.58E2	
174*	16 29 31.3	39 0 21	.8251	142.3	S/SO	17	5.8	53	R-	8 7 3	1.65E2	
175	16 29 31.3	40 14 26	.7638	40.4	S/IRR	33	2.9	9	R	8 5 2	7.79E2	

NO	RA(1950)	DEC(1950)	R	THETA	TYPE	D(0)	ELL	PA	COL	SUR.BRG	AREA	SW
176	16 29 34.3	39 58 55	.6009	57.5	E	25	2.1	5	R-	9 7 2	5.11E2	
177	16 29 35.9	39 15 24	.6552	127.9	E	45	0.0	0	R-	9 7 3	1.72E3	
178	16 29 37.0	39 50 60	.5505	69.7	SO	53	3.7	149	R-	9 7 2	1.73E3	
179	16 29 37.4	39 53 47	.5691	65.3	SB/SBO	25	2.1	94	R-	9 7 5	5.06E2	
180	16 29 39.4	39 16 25	.6539	126.1	S/SO	32	6.7	9	R-	9 8 4	4.66E2	
181*	16 29 46.6	39 47 15	.5625	76.8	IRR	23	3.4	2	B-	5 3 3	3.64E2	
182	16 29 49.2	40 5 51	.7063	51.6	S/SO	31	6.0	3	N	9 7 2	4.73E2	
183	16 29 49.7	40 0 12	.6539	58.2	SO	48	5.4	67	R	9 7 3	1.18E3	
184	16 29 53.9	40 7 35	.7360	50.5	S/IRR	25	5.4	108	R	9 6 3	3.40E2	
185	16 30 5.5	39 55 10	.6607	66.7	S/SO	20	3.4	151	N	9 6 2	2.86E2	
186	16 30 12.2	39 13 40	.7666	124.1	S	20	3.2	77	N	9 7 3	2.96E2	
187*	16 30 15.0	39 9 20	.8169	127.9	IRR	18	3.5	8	R+	6 3 3	2.52E2	
188	16 30 16.7	40 3 11	.7534	58.4	S	18	3.5	165	R+	9 7 4	2.50E2	
189	16 30 21.4	39 42 50	.6620	85.1	S/SO	18	4.4	118	B	8 7 3	2.18E2	
190	16 30 33.2	39 43 52	.7012	84.0	S	19	6.9	89	R-	7 6 3	1.68E2	
191	16 30 43.7	39 37 20	.7329	92.7	S*	28	0.0	0	R-	9 7 4	7.29E2	
192*	16 30 50.0	39 43 54	.7548	84.3	S/SO	17	6.0	123	B-	9 7 2	1.69E2	

Table 9. Basic Cluster Parameters

Notes on the individual table entries:

(1) Redshifts are from Noonan (1973), except for the Virgo redshift which is from Tammann (1972) and the A 119 redshift which is an average of the values in Noonan (1973) and Sandage (1972b).

(2) Cluster radii are given in degrees, and calculated using the equation

$$R = 1.^{\circ}5 \frac{(1+z)^2}{z}$$

(3) Lower diameter limit for the galaxy sample given in seconds of arc and calculated using the equation

$$D = 0.''50 \frac{(1+z)^2}{z}$$

(4) Seeing disk in seconds of arc for each of the Palomar Sky Survey plates.

(5) Total number of galaxies listed in Table 8 for each cluster.

(6) Percentage of each cluster sample which definitely falls within the three dimensional radius R, calculated by the ring count method of Noonan (1971); these are minimum values only.

(7) Total number of galaxies in the final statistical sample, i.e., number with face-on diameters $D(0) \geq 7.5$ kpc/h .

(8) Mean galaxy morphological type for each cluster sample, with E = 1, SO = 3, S = 5, and Irr = 7 .

(9) Magnification at which diameter measurements were made.

(10) Cluster type as defined by Rood and Sastry (1971).

(11) Cluster type as defined by Bautz and Morgan (1970).

Table 9. Basic Cluster Parameters

	Virgo	A 119	A 400	A 1656	A 2147	A 2151	A 2197	A 2199
(1) Mean Cluster Redshift	0.0381	0.0417	0.0231	0.0230	0.0377	0.0360	0.0303	0.0312
(2) Outer Cluster Radius	6.°619	0.°651	1.°133	1.°138	0.°714	0.°745	0.°876	0.°852
(3) Galaxy Diameter Limit	137″	13.″5	23.″3	23.″6	15.″0	15.″4	18.″1	17.″7
(4) Plate Seeing	3.″0	2.″5	2.″0	3.″0	3.″5	3.″5	2.″0	2.″0
(5) Total Galaxy Sample	73	103	96	172	138	159	186	192
(6) % of Galaxies in Cluster	62%	57%	70%	49%	66%	67%	66%	63%
(7) Homogeneous Galaxy Sample	65	96	79	152	128	142	152	161
(8) Average Galaxy Type	3.9	3.7	3.8	3.5	3.8	4.4	3.9	3.9
(9) Plate Measuring Magnification	13.0	36.3	23.8	20.6	25.8	25.4	23.7	23.8
(10) R & S Cluster Type	-	C	I	B	F	F	L	cD
(11) B & M Cluster Type	III	II-III	II-III	II	-	II	II	I

Table 10. Cluster Centers

Cluster	R.A.(1950)	Dec.(1950)	Description
Virgo	$12^h26^m30^s.0$	$+13^\circ12'00''$	This point appears to fall somewhere near the center of the overall galaxy distribution and near (but not exactly on) the point of maximum luminosity. Choosing an exact center is futile because the cluster is so irregular.
A 119	$00^h53^m42^s.7$	$-01^\circ31'33''$	This point corresponds to the central cD galaxy position and also to the center of the overall cluster luminosity distribution.
A 400	$02^h55^m03^s.0$	$+05^\circ49'28''$	This cluster is very clumpy with no particularly striking central maximum. The chosen cluster center corresponds to the center of the bright db galaxy.
A 1656	$12^h57^m27^s.1$	$+28^\circ14'14''$	The central point is equally spaced between the two central supergiant galaxies, and it corresponds to the center of the remarkably symmetric overall galaxy distribution.
A 2147	$15^h59^m59^s.9$	$+16^\circ06'45''$	This is the position of the brightest and largest cD galaxy in this very irregular cluster. This cD galaxy is centrally located in an extended galaxy distribution which has some semblance of being the cluster core.
A 2151	$16^h02^m53^s.1$	$+17^\circ53'34''$	This is the measured position of NGC 6045, a bright centrally located spiral galaxy. Although the cluster has many irregular sub-clumps, this position is centrally located in the largest and brightest aggregate.
A 2197	$16^h27^m02^s.5$	$+40^\circ58'41''$	This point is centrally located between the two widely separated cD galaxies. The elongated galaxy distribution is also centered near the listed position.
A 2199	$16^h26^m55^s.6$	$+39^\circ39'39''$	This is the position of the bright cD galaxy NGC 6166 which is located in a definite cluster core.

Table 11. S.A.O. Standard Position Stars

A 119	A 400	A 1656	A 2147	A 2151	A 2197	A 2199
129005	110807	063273	101841	101881	046050	046053
129013	110811	082554	101848	101890	046064	046139
129020	110819	082556	101895	101895	046086	046158
129037	110845	082557	101911	101917	046158	065261
129045	110846	082562	101914	101935	046163	065294
129049	110853	082578		101959	046165	065334
129061	110855	082581		101964		065381
129063	110869	082582				
129066	110872	082583				
	110881	082590				
	110886	082592				
	110904	082593				
	110907	082595				
	110919	082599				
	110937	082606				
		082617				
		082630				
		082631				
		082635				
		082640				
		082642				
		082645				
		082653				
		082654				

Table 12. Galaxy Identification for Virgo Cluster

Number	I.D.	Number	I.D.
1	N 4124	41	N 4477
2	N 4178	42	N 4486
3	N 4192	43	N 4501
4	N 4206	44	N 4503
5	N 4212	45	N 4519
6	N 4216	46	N 4522
7	N 4235	47	N 4526
8	N 4246	48	N 4532
9	N 4254	49	N 4535
10	N 4267	50	N 4531
11	N 4293	51	N 4548
12	N 4298	52	N 4550
13	N 4302	53	N 4552
14	N 4307	54	N 4568
15	N 4312	55	N 4570
16	N 4313	56	N 4569
17	N 4321	57	N 4571
18	N 4330	58	N 4578
19	N 4365	59	N 4576
20	N 4371	60	I 3608
21	N 4374	61	N 4596
22	N 4380	62	N 4608
23	N 4382	63	N 4621
24	Anon.	64	N 4639
25	N 4388	65	N 4649
26	N 4402	66	N 4651
27	N 4406	67	N 4654
28	N 4417	68	N 4689
29	Anon.	69	N 4698
30	Anon.	70	N 4710
31	N 4424	71	N 4754
32	N 4429	72	N 4758
33	N 4438	73	N 4762
34	N 4442		
35	N 4450		
36	N 4461		
37	N 4459		
38	N 4469		
39	N 4472		
40	N 4473		

Table 13. Galaxy Identification for Finder Charts

Cluster	I.D.		R.A.(1950)	Dec.(1950)	R	Theta
A 119	A	#54	$00^h53^m42^s.7$	$-01^\circ31'33''$	0.0	0.0
	B	12	00 52 08.8	-01 45 37	0.4560	239.1
	C	24	00 52 43.4	-01 11 20	0.4178	323.8
	D	81	00 54 18.1	-01 32 34	0.1484	96.6
A 400	A	Center	02 55 03.0	+05 49 28	0.0	0.0
	B	# 6	02 51 24.9	+06 03 15	0.9326	284.3
	C	34	02 54 31.2	+05 07 14	0.7161	190.6
	D	65	02 55 59.1	+05 58 35	0.2778	56.8
A 1656	A	Center	12 57 27.1	+28 14 14	0.0	0.0
	B	#138	12 59 00.9	+28 56 47	0.7878	25.7
	C	166	13 00 52.2	+27 36 06	0.9870	129.9
	D	36	12 55 40.7	+28 30 45	0.4774	305.3
A 2147	A	#65	15 59 59.9	+16 06 45	0.0	0.0
	B	85	16 00 34.0	+16 42 27	0.6104	12.9
	C	104	16 01 14.6	+15 42 18	0.5056	143.7
	D	19	15 58 55.1	+15 53 41	0.3388	230.0
A 2151	A	#60	16 02 53.1	+17 53 34	0.0	0.0
	B	117	16 04 00.1	+18 32 55	0.7074	22.0
	C	130	16 04 18.9	+17 25 51	0.5740	143.5
	D	27	16 01 55.5	+18 07 00	0.3197	314.5
A 2197	A	Center	16 27 02.5	+40 58 41	0.0	0.0
	B	#132	16 28 15.5	+41 42 43	0.7686	17.2
	C	176	16 29 53.7	+40 40 17	0.6208	119.4
	D	32	16 24 41.2	+41 01 24	0.4466	276.0
A 2199	A	#96	16 26 55.6	+39 39 39	0.0	0.0
	B	183	16 29 49.7	+40 00 12	0.6539	58.2
	C	180	16 29 39.4	+39 16 25	0.6539	126.1
	D	43	16 25 20.5	+38 38 17	0.3059	265.9

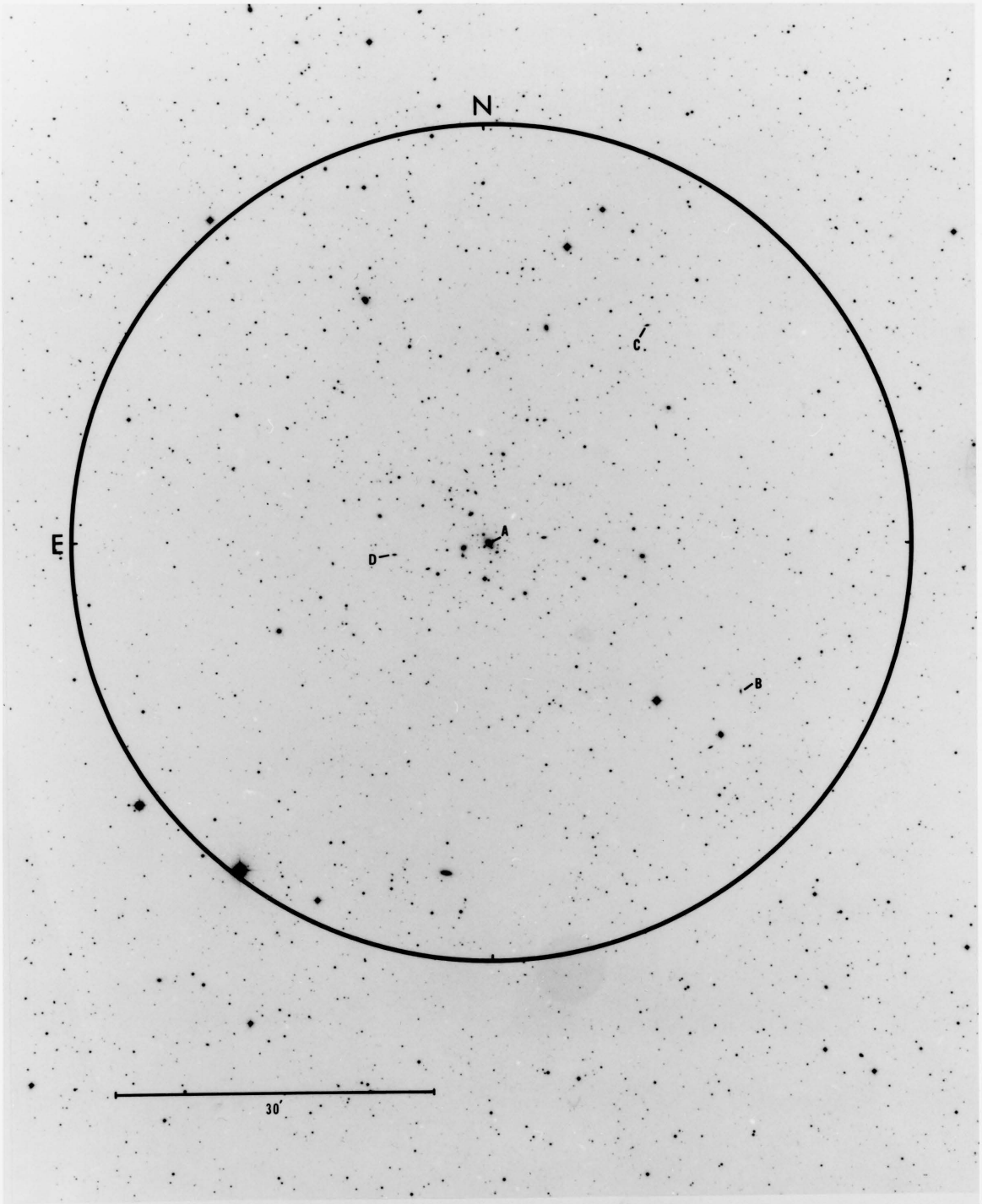

Figure 14. Cluster A 119.

Enlargement from the red Palomar Sky Survey print (copyright National Geographic Society-Palomar Observatory Sky Survey).

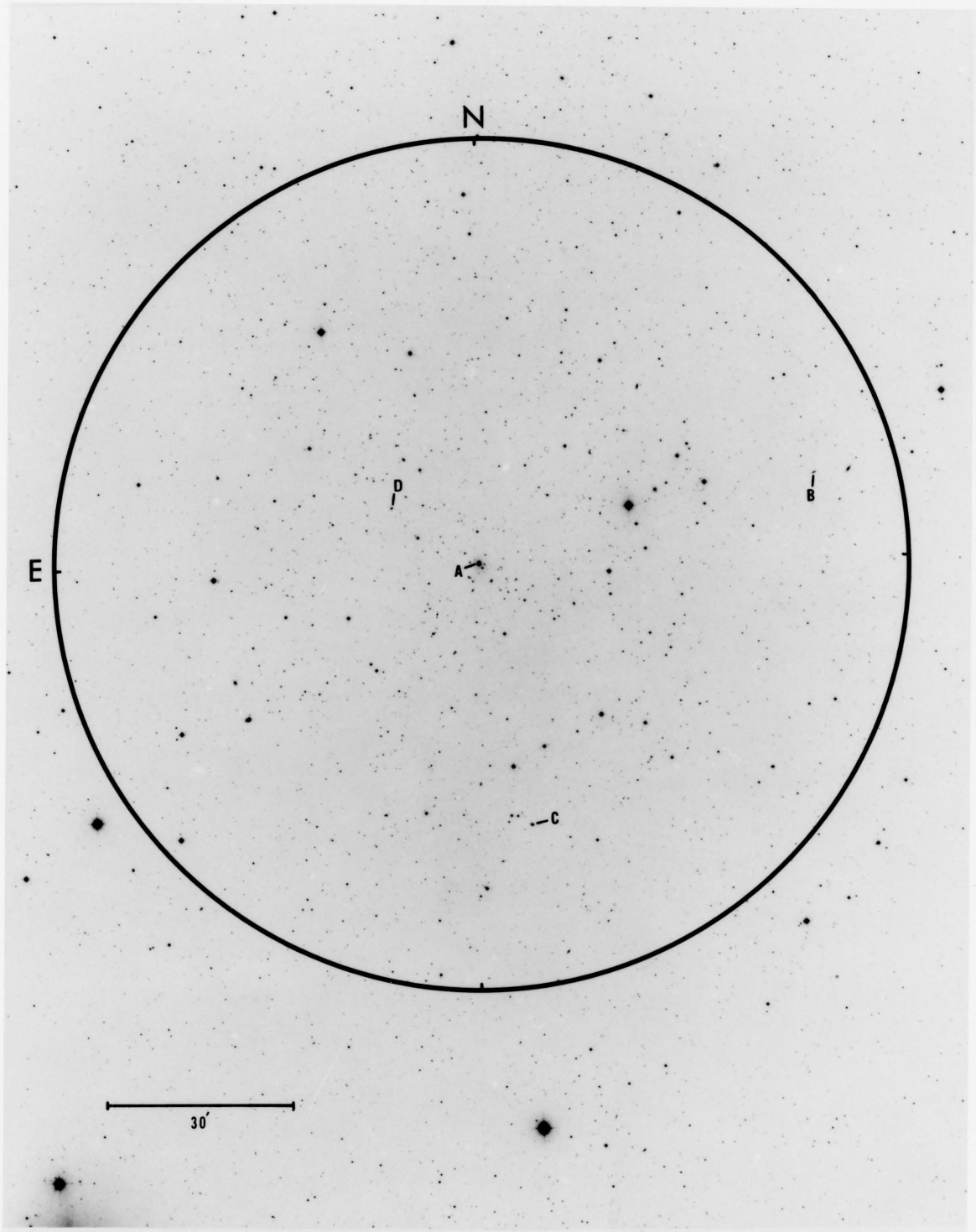

Figure 15. Cluster A 400.

Enlargement from the red Palomar Sky Survey print (copyright National Geographic Society-Palomar Observatory Sky Survey).

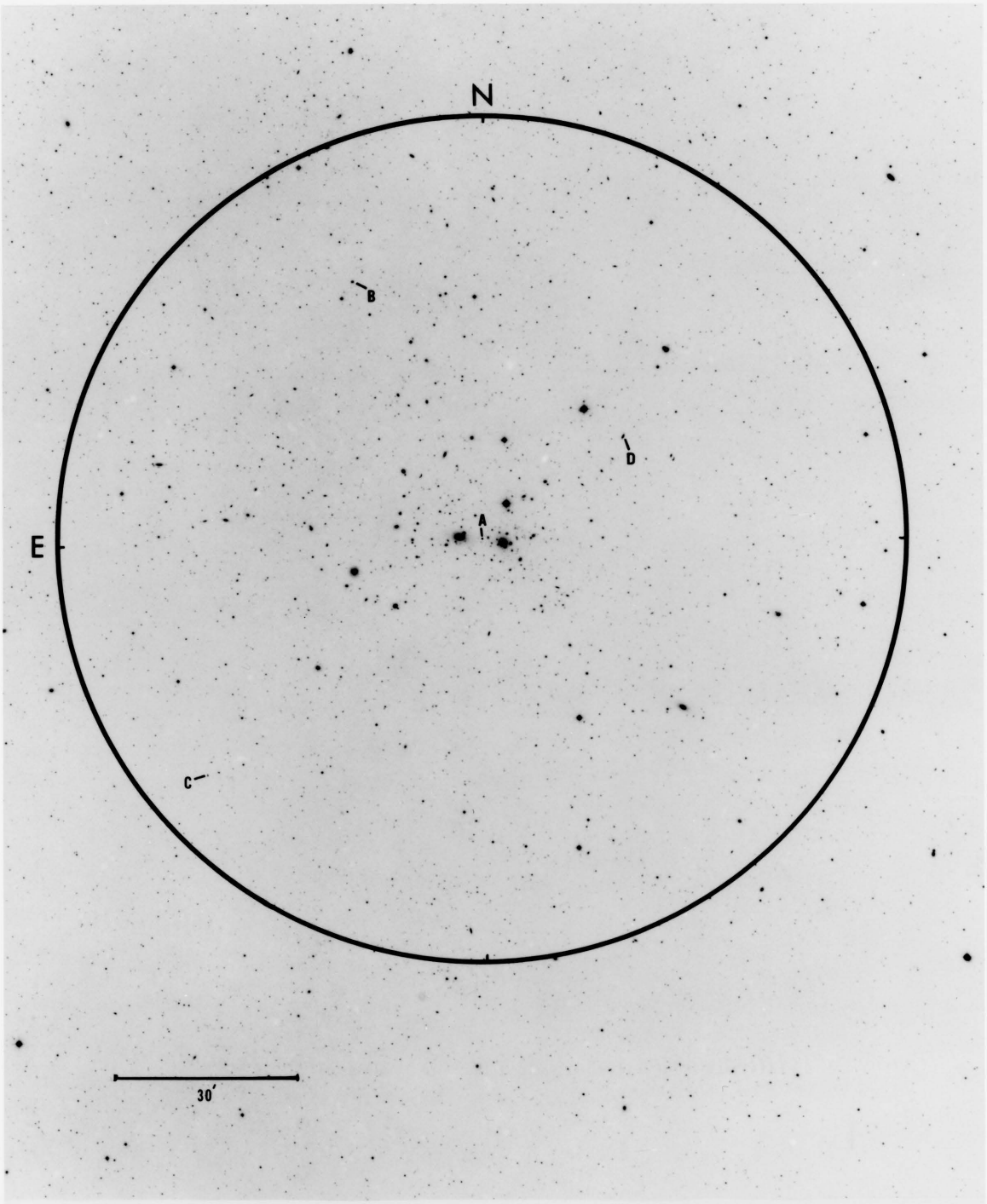

Figure 16. Cluster A 1656 (Coma).

Enlargement from the red Palomar Sky Survey print (copyright National Geographic Society-Palomar Observatory Sky Survey).

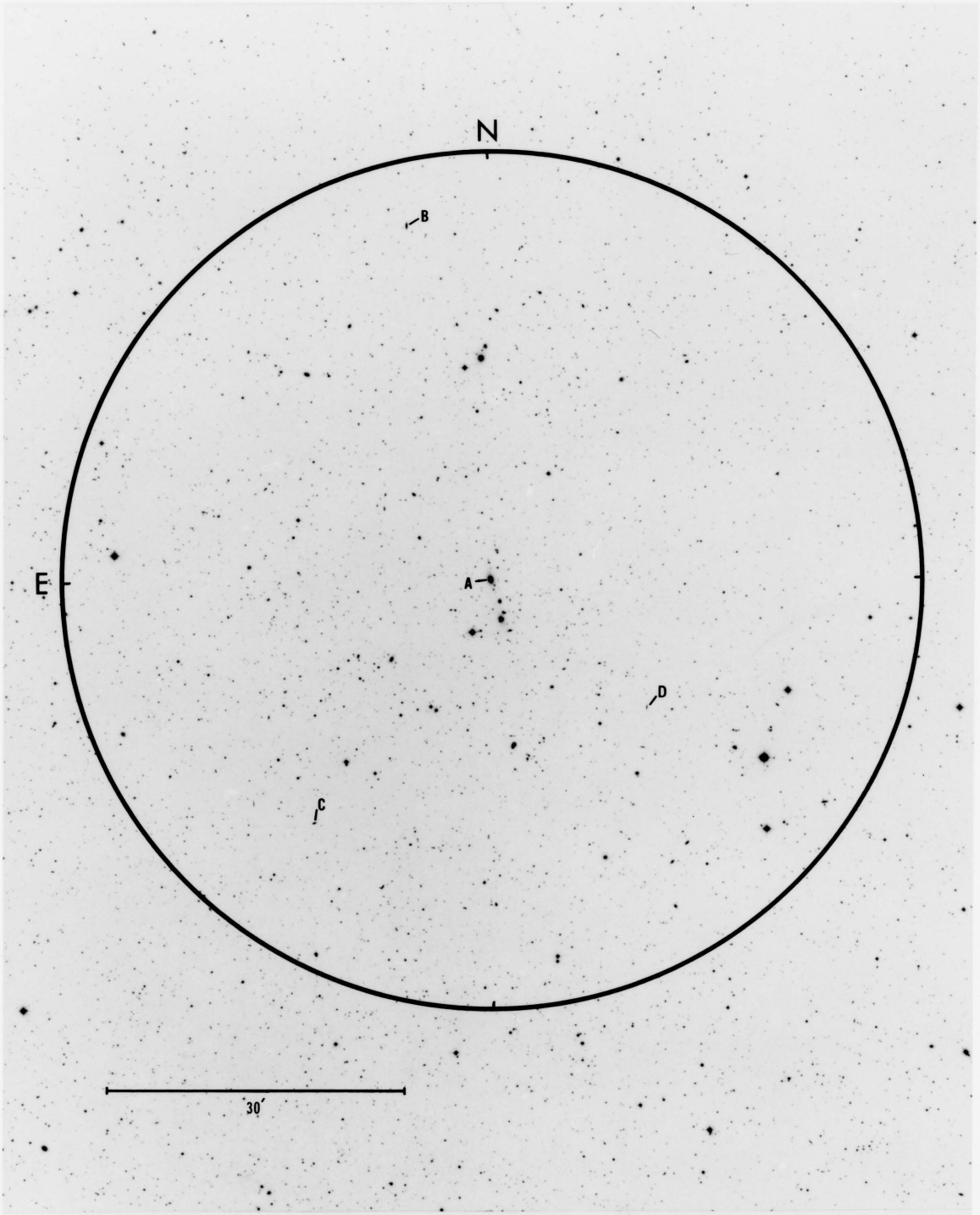

Figure 17. Cluster A 2147.

Enlargement from the red Palomar Sky Survey print (copyright National Geographic Society-Palomar Observatory Sky Survey).

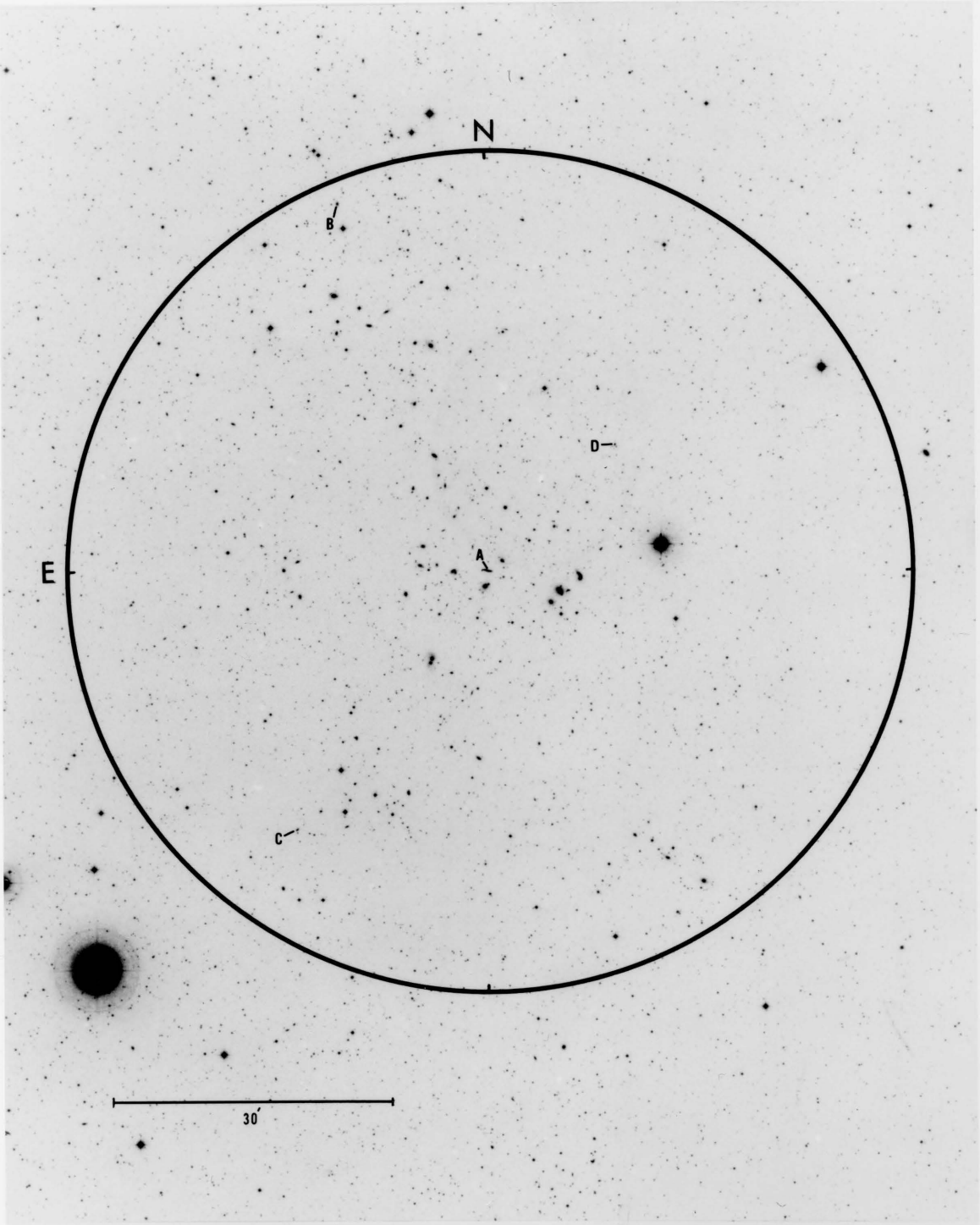

Figure 18. Cluster A 2151 (Hercules).

Enlargement from the red Palomar Sky Survey print (copyright National Geographic Society-Palomar Observatory Sky Survey).

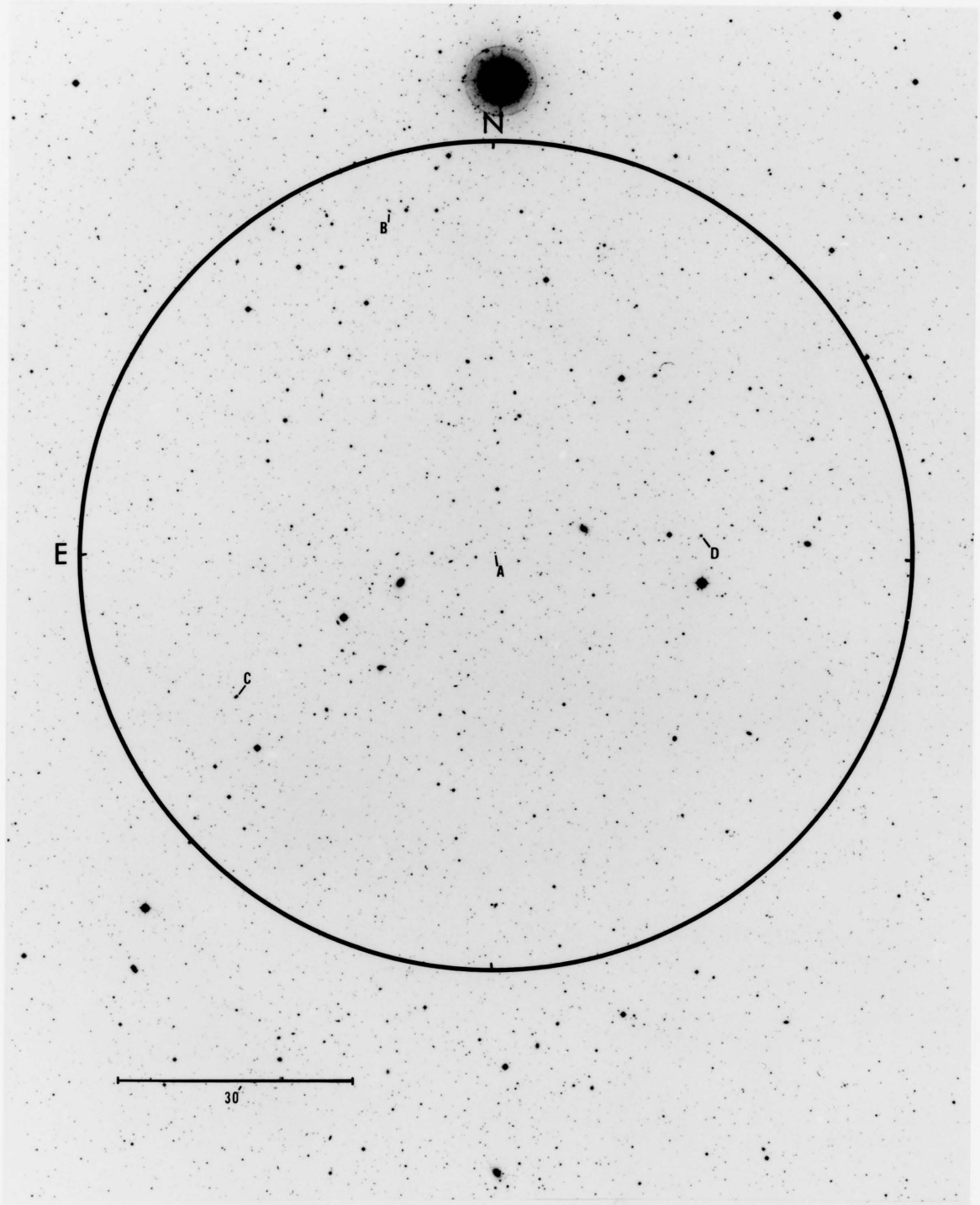

Figure 19. Cluster A 2197.

Enlargement from the red Palomar Sky Survey print (copyright National Geographic Society-Palomar Observatory Sky Survey).

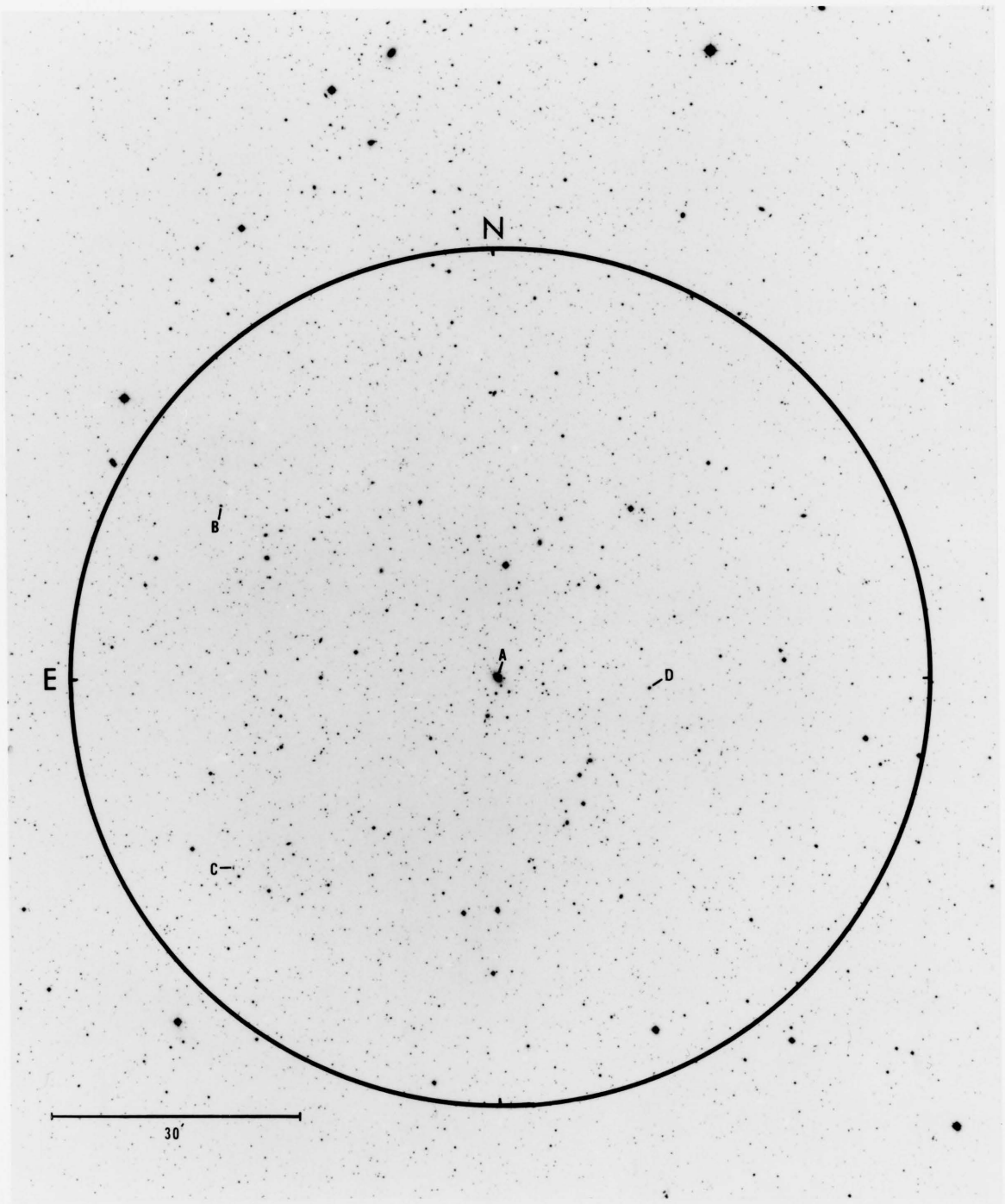

Figure 20. Cluster A 2199.

Enlargement from the red Palomar Sky Survey print (copyright National Geographic Society-Palomar Observatory Sky Survey).

APPENDIX II

DATA CORRECTION PROCEDURES

Virgo Cluster Diameter Transfer Relation

Galaxies in the Virgo Cluster are scattered over nine Palomar Sky Survey fields. The sample limited by face-on diameter 7.5 kpc/h is contained on only eight of the nine plates. The Sky Survey fields will be numbered as follows:

7	4	1	$+18^{\circ}$
8	5	2	$+12^{\circ}$
9	6	3	$+\ 6^{\circ}$
$12^{h}48^{m}$	$12^{h}24^{m}$	$12^{h}00^{m}$	

The purpose of the transfer relation will be to convert galaxy diameters from plates 1 - 4 and 6 - 8 to a system consistent with plate 5 . The transfer relation will be calibrated using those galaxies which appear on pairs of adjacent plates. Galaxy images with sharp edges (i.e. steep surface brightness gradients) require little or no diameter correction, but galaxies which fade slowly into the plate background show significant diameter differences on the adjacent plate pairs. This situation led to the following empirical diameter transfer relation:

$$D_5 = D_i \, (1 + K_i \cdot \tan (60^\circ - (10^\circ \times \mathrm{SBG})))$$

where D_5 = galaxy diameter as it would appear on plate 5

D_i = galaxy diameter measured from plate i

K_i = transfer constant to be determined

SBG = surface brightness gradient listed as the third digit in the surface brightness column of Table 8.

SBG is actually the slope of the galaxy density profile displayed on the cathode ray tube density scan of the two-coordinate Grant measuring engine. A galaxy image with sharp edges (SBG = 6) does not change diameter from plate i to plate 5 , but a galaxy image which slowly fades into the plate background (SBG = 1) changes diameter significantly.

The constants K_i were determined by measuring those galaxies which fell on adjacent plate pairs. The sign of K_i determines whether galaxy diameters must be increased or decreased. The constants are listed below, followed by numbers in parentheses giving the number of overlap galaxies used to determine the listed constant.

$K_1 = -0.45$ (8)

$K_2 = -0.27$ (6)

$K_3 = +0.13$ (4)

$K_4 = -0.25$ (3)

$K_6 = -0.07$ (5)

$K_7 = -0.09$ (4)

$K_8 = -0.41$ (9)

Holmberg Corrections

To evaluate and correct any systematic measuring errors in the galaxy diameter and ellipticity data, the analysis presented in the following paragraphs is nearly identical to the analysis presented by Holmberg (1946). For a sample of 25 Coma Cluster galaxies, both visual and isophotal dimensions were measured from the red plate copies of the Palomar Sky Survey. The visual dimensions estimates were made in the course of the general galaxy survey using the Grant two-coordinate measuring engine of Kitt Peak National Observatory (K.P.N.O.). The isophotal contour plots were recorded by the P.D.S. microphotometer of K.P.N.O., and then these plots were displayed by the photographic playback technique. Table 14 presents the list of 25 galaxies along with the data and basic calculations required in the following analysis.

Holmberg found that the visual measurements of galaxy diameter are affected by the steepness of the galaxy density profile (i.e., the surface brightness gradient, SBG) and by the galaxy ellipticity. First consider the dependence on SBG. Recognizing that "a" is the isophotal major axis and that "α" is the visual major axis; the results are as follows:

SBG	Ave a/α	# in Sample
2	1.10	6
3	1.09	8
4	1.06	8
5	1.09	3
Total Sample	1.085	25

Table 14. Holmberg Correction Data

Galaxy #	Visual α'	Visual β'	SBG n	Isophotal a'	Isophotal b'	$\epsilon=(1-\frac{\beta}{\alpha})10$	$p=\left(\frac{a}{\alpha}\right)^n$	$p=\left(\frac{b}{\beta}\right)^n$	p_α/p_β	$\frac{a}{\alpha}$
82	33.2	18.2	4	32.6	20.9	4.5	0.930	1.739	0.535	0.98
86	45.6	8.3	2	48.6	11.1	8.2	1.136	1.789	0.635	1.07
87	34.0	26.5	3	35.8	28.9	2.2	1.160	1.290	0.900	1.05
69	29.8	12.4	3	36.3	17.3	5.8	1.807	2.716	0.665	1.22
68	29.0	11.6	4	26.7	12.5	6.0	0.719	1.348	0.533	0.92
42	39.8	39.8	2	44.0	44.0	0.0	1.436	1.436	1.000	1.10
48	52.2	12.4	4	53.5	15.8	7.6	1.103	2.636	0.601	1.02
54	67.1	10.8	5	68.4	12.5	8.4	1.100	2.077	0.530	1.02
41	26.5	20.7	2	34.2	28.2	2.2	1.464	1.936	0.758	1.21
*	27.4	17.4	5	30.7	20.2	3.6	1.766	2.109	0.837	1.12
75	26.5	14.9	3	29.7	16.7	3.8	1.408	1.400	1.006	1.12
135	28.2	5.8	4	29.0	7.2	7.9	1.110	2.360	0.470	1.03
169	48.1	35.6	2	50.0	40.4	2.6	1.081	1.288	0.839	1.04
*	24.9	24.9	4	29.8	29.8	0.0	2.051	2.051	1.000	1.20
143	34.8	9.1	3	39.3	13.0	7.4	1.440	2.915	0.494	1.13
*	24.0	9.1	5	27.4	10.5	6.2	1.940	2.045	0.949	1.14
105	32.3	12.4	2	36.5	16.0	6.2	1.277	1.665	0.767	1.13
*	24.9	10.7	4	29.7	14.2	5.7	2.030	3.102	0.648	1.19
84	30.7	19.1	4	31.4	21.9	3.8	1.094	1.728	0.633	1.02
60	35.6	25.7	3	39.5	29.3	2.8	1.366	1.465	0.931	1.11
80	35.6	21.6	2	37.6	25.7	4.0	1.116	1.410	0.792	1.06
91	45.6	45.6	3	50.2	50.2	0.0	1.334	1.334	1.000	1.10
99	33.2	12.4	4	37.4	14.8	6.3	1.610	2.029	0.793	1.13
67	48.1	48.1	3	52.1	52.1	0.0	1.260	1.260	1.000	1.08
71	54.7	35.6	3	51.2	33.8	3.5	0.807	0.850	0.950	0.93

* Holmberg corrections pushed the final diameters of these galaxies below the 7.5 kpc/h limit so they are not listed in Table 8.

From the table above it appears that there are no systematic measuring effects associated with the galaxies' surface brightness gradients. Next consider the dependence on galaxy ellipticity. These results are summarized as follows:

ϵ	Ave a/α	# in Sample
0 + 1	1.12	4
2 + 3	1.08	8
4 + 5	1.11	4
6 + 7	1.07	7
8	1.05	2

The diameter ratio a/α decreases slightly as the galaxy ellipticity increases. To correct for this effect, the following correction will be adopted:

$$\alpha_{new} = \alpha_{old} (1 + 0.009 (4 - \epsilon))$$

To find the correction for galaxy ellipticity, Holmberg defined the quantity p_α / p_β as

$$\frac{p_\alpha}{p_\beta} = \left(\frac{\epsilon_{isophote}}{\epsilon_{visual}}\right)^n = \left(\frac{a/b}{\alpha/\beta}\right)^n = \left(\frac{a}{\alpha}\right)^n \left(\frac{\beta}{b}\right)^n$$

where n = surface brightness gradient. Holmberg found that for any particular value of ϵ_{visual} the value of p_α / p_β remained constant. Hence, to find the most reliable correction equation it is necessary to find the relation between ϵ_{visual} and p_α / p_β. The data from Table 14 are grouped according to ellipticity, and listed in Table 15. The

Table 15. Ellipticity Corrections

ϵ	p_α/p_β	Ave. Values by Groups
0.0	1.00	$\epsilon = 0.0$
0.0	1.00	
0.0	1.00	$\frac{p_\alpha}{p_\beta} = 1.00$
0.0	1.00	
2.2	0.90	$\epsilon = 2.45$
2.2	0.76	
2.6	0.84	$\frac{p_\alpha}{p_\beta} = 0.86$
2.8	0.93	
3.5	0.95	
3.6	0.84	$\epsilon = 3.9$
3.8	1.01	
3.8	0.63	$\frac{p_\alpha}{p_\beta} = 0.79$
4.0	0.79	
4.5	0.54	
5.7	0.65	
5.8	0.67	$\epsilon = 6.0$
6.0	0.53	
6.2	0.95	$\frac{p_\alpha}{p_\beta} = 0.73$
6.2	0.77	
6.3	0.79	
7.4	0.49	
7.6	0.60	$\epsilon = 7.9$
7.9	0.47	
8.2	0.64	$\frac{p_\alpha}{p_\beta} = 0.55$
8.4	0.53	

average values are calculated and then plotted in Figure 21. The straight line fit gives the relation

$$\frac{p_\alpha}{p_\beta} = 1 - 0.053 * \epsilon_{visual}$$

The corrected "isophotal" ellipticity is found by eliminating p_α / p_β from the two previous equations. The final result is

$$\epsilon_{isophote} = \epsilon_{visual} \ (1 - 0.053 * \epsilon_{visual})^{1/n} \ .$$

Apparent to Intrinsic Ellipticity Conversion

The following table (Table 16) contains normalized apparent ellipticity distributions for the entire range of intrinsic ellipticity from 0 to 9.0 . This table is necessary for the conversion of an apparent ellipticity distribution into an intrinsic distribution as described in Chapter IV. The entries in the table are calculated using the following equation

$$\text{frequency}(b_1, b_2, q) = \frac{(b_1^2 - q^2)^{\frac{1}{2}} - (b_2^2 - q^2)^{\frac{1}{2}}}{(1 - q^2)^{\frac{1}{2}}}$$

This frequency represents the relative number of galaxies falling between b_1 and b_2 (the upper and lower apparent ellipticity limits) where q represents the true ellipticity of the set of randomly oriented galaxies. A derivation of this relation can be found in Sandage, Freeman, and Stokes (1970).

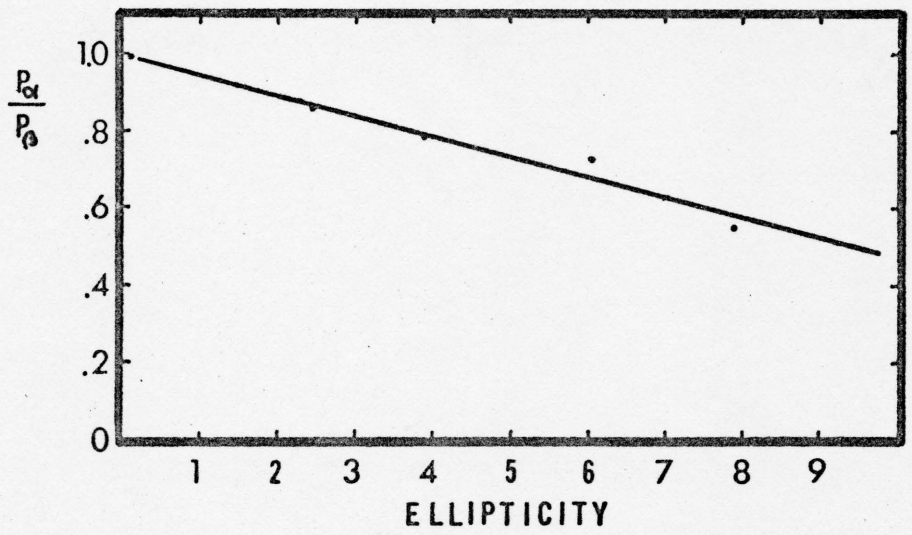

Figure 21. Holmberg Ellipticity Correction

Table 16. Frequency Distribution for Apparent to Intrinsic Ellipticity Transformation

True Ellip.	Apparent Ellipticity 0	1	2	3	4	5	6	7	8	9
9.0	.1011	.1012	.1014	.1017	.1022	.1031	.1050	.1102	.1741	
8.5	.1024	.1028	.1032	.1040	.1052	.1074	.1123	.1290	.1337	
8.0	.1044	.1050	.1059	.1073	.1096	.1142	.1253	.2282		
7.5	.1071	.1081	.1096	.1120	.1161	.1247	.1512	.1712		
7.0	.1105	.1121	.1144	.1183	.1254	.1420	.2774			
6.5	.1149	.1172	.1208	.1269	.1391	.1745	.2066			
6.0	.1203	.1237	.1291	.1388	.1609	.3273				
5.5	.1272	.1321	.1403	.1560	.2003	.2441				
5.0	.1359	.1430	.1554	.1827	.3830					
4.5	.1470	.1573	.1771	.2314	.2872					
4.0	.1615	.1771	.2107	.4507						
3.5	.1809	.2054	.2718	.3419						
3.0	.2079	.2498	.5423							
2.5	.2479	.3313	.4208							
2.0	.3128	.6872								
1.5	.4385	.5615								
1.0	1.000									
0.5	1.000									
0.0	1.000									

REFERENCES

Aarseth, S.J. 1963, M.N.R.A.S., 126, 223

Abell, G.O. 1965, Ann. Rev. Astr. and Ap., 3, 1

Alfven, H. and Arrenius, G. 1970, Ap. and Sp. Sci., 9, 3

Bautz, L.P. and Morgan, W.W. 1970, Ap. J. (Lett.), 162, L149

Bonner, W.B. 1957, M.N.R.A.S., 107, 410

Brown, F.G. 1939, M.N.R.A.S., 99, 534

Brown, F.G. 1964, M.N.R.A.S., 127, 517

Brown, F.G. 1968, M.N.R.A.S., 138, 527

Burbidge, E.M. and Burbidge, G. 1968, Stars and Stellar Systems, ed. A. and M. Sandage (Chicago: University of Chicago Press), Vol.9

Chibisov, G.W. 1972, Sov. Astron. A.J., 16, 56

Crampin, D.J. and Hoyle, F. 1964, Ap. J., 140, 99

Creighton, D.G. 1969, Proc. Cambridge Phil. Soc., 65, 557

Dallaporta, N. and Lucchin, F. 1972, Astron. and Ap., 19, 123

Danby, J.M.A. 1962, Fundamentals of Celestial Mechanics (New York: The Macmillan Company), p. 303

Denisyuk, E.K. and Tumakova, O.A. 1969, Trudy Astrofiz. Inst. Alma-Ata, 12, 125

Doroshkevich, A.G. 1973a, Astrophysics, 6, 320

Doroshkevich, A.G. 1973b, Sov. Astron. A.J., 16, 986

Edelen, D.G.B. 1965, A.J., 70, 747

Field, G.B. 1968, Stars and Stellar Systems, ed. A. and M. Sandage (Chicago: University of Chicago Press), Vol. 9

Fish, R.A. 1964, Ap. J., 139, 284

Gainullina, R.Kh. and Roshjakova, T.V. 1967, Trudy Inst. Astrofiz. Akad. Nauk. Kazaks. S.S.R., 5, 237

Gamow, G. 1952, Phys. Rev., 86, 251

Gorbachev, B.J. 1970, Sov. Astron. A.J., 14, 182

Gott, J.R. 1973, Ap. J., 186, 481

Harrison, E.R. 1973, M.N.R.A.S., 165, 185

Hawley, D.L. and Peebles, P.J.E. 1972, B.A.A.S., 4, 239

Heidmann, J. 1969, Ap. Lett., 3, 19

Heidmann, N. 1969, Ap. Lett., 3, 153

Holmberg, E. 1946, Medd. Lund Obs. (II), No. 117

Hoyle, F. 1949, Problems of Cosmical Aerodynamics (International Union of Theoretical and Applied Mechanics and International Astronomical Union), p. 195

Hubble, E. 1926, Ap. J., 64, 321

Icke, V. 1973, Astron. and Ap., 27, 1

Innanen, K. 1966, Ap. J., 143, 150

Jeans, J.H. 1929, Astronomy and Cosmogony (Cambridge: Cambridge University Press)

Jones, B.T.J. 1973, Ap. J., 181, 269

King, I. 1961, A.J., 66, 68

King, I.R. and Minkowski, R. 1966, Ap. J., 143, 1002

Kinman, T.D. 1959, M.N.R.A.S., 119, 559

Konig, A. 1962, Astronomical Techniques (Chicago: University of Chicago Press), p. 484

Kristian, J. 1967, Ap. J., 147, 864

Layzer, D. 1964, Ann. Rev. Astr. and Ap., 2, 341

Layzer, D. 1968, Astrophysics and General Relativity, Vol. 2, ed. M. Cretien, S. Deser, and J. Goldstein (New York: Gordon and Breach Science Publishers), p. 151

Liller, M.H. 1960, Ap. J., 132, 306

Liller, M.H. 1966, Ap. J., 146, 37

Marcus, A.H. 1967, Icarus, 7, 283

Mestel, L. 1963, M.N.R.A.S., 126, 553

Minkowski, R.I. and Abell, G.O. 1963, Basic Astronomical Data, ed. K. Strand (Chicago: University of Chicago Press), p. 481

Minkowski, R., Oort, J.H., van Houten, C.J., and Davis, M.M. 1971, Ap. J., 179, 64

Morton, D.C. and Chevalier, R.A. 1973, Ap. J., 179, 55

National Geographic Society and Palomar Observatory Sky Survey, 1960 (Pasadena, California: Palomar Observatory)

Noonan, T.W. 1971, A.J., 76, 182

Noonan, T.W. 1973, A.J., 78, 26

Opik, E.J. 1968, Irish A.J., 8, 229

Ozernoi, L.M. 1967, Astron. Tsirk., No. 407, p. 1

Ozernoi, L.M. and Chernin, A.D. 1968, Sov. Astron. A.J., 11, 907

Ozernoi, L.M. and Chernin, A.D. 1969, Sov. Astron. A.J., 12, 901

Ozernoi, L.M. and Chibisov, G.V. 1971, Ap. Lett., 7, 201

Pearson, E.S. and Hartley, H.O. 1966, Biometrika Tables for Statisticians (Cambridge: Cambridge University Press)

Peebles, P.J.E. 1969, Ap. J., 155, 393

Peebles, P.J.E. 1971a, Astron. and Ap., 11, 377

Peebles, P.J.E. 1971b, Physical Cosmology (Princeton, New Jersey: Princeton University Press), pp. 67-69

Peebles, P.J.E. 1971c, Ap. and Sp. Sci., 11, 443

Peebles, P.J.E. and Dicke, R.H. 1968, Ap. J., 154, 891

Peebles, P.J.E. and Yu, J.T. 1970, Ap. J., 162, 815

Piddington, J.H. 1972, Cosmic Electrodynamics, 3, 129

Prendergast, K.H. and Tomer, E. 1970, A.J., 75, 674

Reaves, G. 1958, Pub. A.S.P., 70, 461

Reinhardt, M. 1972, M.N.R.A.S., 156, 151

Reinhardt, M. and Roberts, M.S. 1972, Ap. Lett., 12, 201

Reinmuth, K. 1926, Die Herschel-Nebel (Heidelberg: Heidelberg Veroff)

Rood, H.J. and Baum, W.A. 1967, A.J., 72, 398

Rood, H.J., Page, T.L., Kintner, E.C., and King, I.R. 1972, Ap. J., 175, 627

Rood, H.J. and Sastry, G.N. 1967, A.J., 72, 223

Rood, H.J. and Sastry, G.N. 1971, Pub. A.S.P., 83, 313

Rood, H.J. and Sastry, G.N. 1972, A.J., 77, 451

Sandage, A. 1961, The Hubble Atlas of Galaxies (Washington, D.C.: Carnegie Institution of Washington)

Sandage, A. 1972a, Ap. J., 173, 485

Sandage, A. 1972b, Ap. J., 178, 1

Sandage, A., Freeman, K.C., and Stokes, N.R. 1970, Ap. J., 160, 831

Saslaw, W.C. 1970, Ap. J., 160, 11

Saslaw, W.C. 1971, M.N.R.A.S., 152, 341

Sastry, G.N. and Rood, H.J. 1971, Ap. J. Suppl., 23, 371

Sastry, K.S. and Alladin, S.M. 1970, Ap. and Sp. Sci., 7, 261

Shapley, H. and Ames, A. 1932, Harvard Ann., 88, No. 2

Silk, J. and Ames, S. 1972, Ap. J., 178, 77

Silk, J. and Lea, S. 1973, Ap. J., 180, 669

Sunyaev, R.A. and Zeldovich, Ya.B. 1972, Astron. and Ap., 20, 189

Tammann, G.A. 1972, Astron. and Ap., 21, 355

Thompson, L.A. 1973, Pub. A.S.P., 85, 528

Vaucouleurs, G. de 1956, Mem. Commonwealth Obs., No. 13

Vaucouleurs, G. de 1959a, Handbuch der Physik, 53, 275

Vaucouleurs, G. de 1959b, Handbuch der Physik, 53, 303

Vaucouleurs, G. de 1960, Sov. Astron. A.J., 3, 897

Vaucouleurs, G. de 1972, Mem. R.A.S., 76, 121

Vaucouleurs, G. de and Vaucouleurs, A. de 1964, Reference Catalogue of Bright Galaxies (Austin, Texas: University of Texas Press)

von Weizsacker, C.F. 1951, Ap. J., 114, 165

Wipple, F.L. 1966, Smithsonian Astrophysical Observatory Star Catalogue (Washington, D.C.: Smithsonian Publications)

Wyatt, S.P. and Brown, F.G. 1955, A.J., 60, 415

Yahil, A. 1974, Ap. J., 191, 623

Zwicky, F. and Herzog, E. 1963, Catalogue of Galaxies and of Clusters of Galaxies (Pasadena, California: California Institute of Technology), Vol. 2